Search for displaced leptons in $\sqrt{s} = 13$ TeV and 13.6 TeV pp collisions with the ATLAS detector

G. Aad *et al.*[*]
(ATLAS Collaboration)

(Received 23 October 2024; accepted 21 May 2025; published 17 July 2025)

A search for leptons displaced from the primary vertex is performed with the ATLAS detector at the Large Hadron Collider. The search includes the full proton-proton collision dataset collected during Run 2 at $\sqrt{s} = 13$ TeV and a partial dataset collected during Run 3 in 2022–2023 at $\sqrt{s} = 13.6$ TeV, corresponding to integrated luminosities of 140 fb^{-1} and 56.3 fb^{-1}, respectively. Final states with displaced electrons or muons are considered, and novel triggers introduced in Run 3 are employed that use large impact parameter tracking to reconstruct displaced tracks with low momentum. In addition, photon reconstruction and multivariate techniques are employed to broaden the sensitivity to channels with large background rates or highly displaced electrons, respectively. The results are consistent with the Standard Model background expectations and are used to set model-independent limits on the production of displaced electrons and muons. The analysis is also interpreted in the context of a gauge-mediated supersymmetry breaking model with pair-produced long-lived sleptons and a dark sector model with pair-produced chargino-like states. The results include 95% confidence level exclusions of selectrons with lifetimes from 4 ps to 60 ns and a mass of 150 GeV, and exclusions of selectrons, smuons, and staus with a lifetime of 0.3 ns for masses up to 740, 830, and 440 GeV, respectively. Dark charginos with masses up to 380 GeV are excluded for a mass difference with the neutral state of 40 GeV, and mass differences down to 17 GeV are excluded for dark charginos with a 100 GeV mass.

DOI: 10.1103/w8hh-xf24

I. INTRODUCTION

Long-lived particles (LLPs) occur in the Standard Model (SM) and are predicted in a wide variety of beyond-the-SM (BSM) scenarios, including both R-parity-conserving [1–7] and R-parity-violating supersymmetry (SUSY) [8,9], split-SUSY [10,11], gauge-mediated SUSY breaking (GMSB) [12–14], universal extra dimensions [15,16], and Hidden Valley models [17]. Most searches for BSM physics at the Large Hadron Collider (LHC) [18] experiments assume that BSM particles decay promptly, producing final state particles with trajectories consistent with an origin at the primary proton-proton (pp) interaction point. By contrast, LLPs with lifetimes longer than a few picoseconds travel at least hundreds of microns before decaying. Their decay products can thus be displaced from the primary vertex (PV), the vertex with the largest sum of squared track transverse momentum, or delayed with respect to the bunch crossing. Reconstruction of the decay products can pose technical challenges that could have caused them to elude detection in prior searches.

This paper presents a search for BSM physics-producing events with two displaced light leptons (electrons or muons). The search is performed with inclusive selection criteria to enable broad sensitivity to BSM models producing LLPs with lifetimes from a few ps up to the of order 100 ns that decay into electrons or muons. The sensitivity of the search is illustrated using a GMSB SUSY model [19–21] in which the lightest SUSY particle (LSP) is a nearly massless gravitino ($\tilde{G}$) and the next-to-lightest SUSY particle (NLSP) is a slepton ($\tilde{\ell}$), which can be either a selectron ($\tilde{e}$), smuon ($\tilde{\mu}$), or stau ($\tilde{\tau}$). The slepton can acquire a long lifetime due to its small gravitational coupling to the gravitino LSP. As shown in Fig. 1, the NLSP can be pair-produced, and then each decays into a charged SM lepton (ℓ) of the same flavor and a gravitino LSP, yielding events containing two displaced leptons. GMSB models often predict that staus are the NLSP [22].

Previous results setting limits on these processes include an ATLAS search using the full Run 2 dataset, consisting of 140 fb^{-1} of pp collisions collected at $\sqrt{s} = 13$ TeV, which excluded selectrons, smuons, and staus with masses of up to 720, 680, and 340 GeV, respectively, for a slepton lifetime of 0.1 ns [23], dramatically enhancing the sensitivity with respect to prior constraints from the LEP

[*]Full author list given at the end of the article.

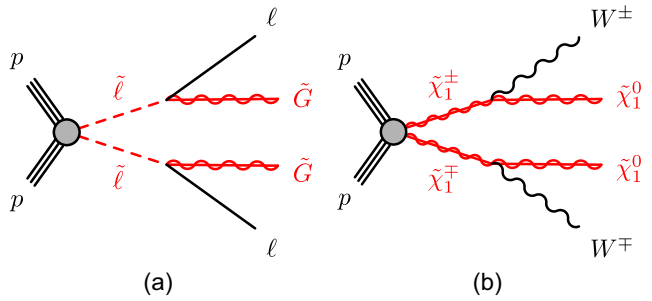

FIG. 1. Diagrams of (a) the GMSB slepton and (b) the dark sector models.

experiments [24–28]. A CMS search based on 113–118 fb^{-1} of $\sqrt{s} = 13$ TeV pp collision data extended the stau mass reach to 405 GeV for a similar lifetime [29]. A subsequent full Run 2 ATLAS search for muons with intermediate displacements in between those of the displaced and prompt lepton searches extended the sensitivity to GMSB smuons with lifetimes below about 0.01 ns [30]. Additional searches for disappearing track signatures in Run 2 data by ATLAS [31] and CMS [32], as well as a Run 2 ATLAS search for tracks with high ionization energy loss dE/dx [33], could also be sensitive to this GMSB slepton model for various lifetimes.

Interpretations are also performed using a Higgs portal model that introduces a dark sector consisting of a charged state ($\tilde{\chi}^{\pm}$) and neutral state ($\tilde{\chi}^0$) with mass difference $\Delta m \equiv m(\tilde{\chi}^{\pm}) - m(\tilde{\chi}^0)$ [34], which can produce the observed dark matter relic density for $10 \lesssim \Delta m \lesssim 40$ GeV [35]. For the signal process $\tilde{\chi}^+\tilde{\chi}^- \to W^+W^-\tilde{\chi}^0\tilde{\chi}^0$ shown in Fig. 1, the charged state can acquire a non-negligible lifetime due to the weak coupling between the dark states and the W boson. This results in events with two displaced leptons if the W bosons decay leptonically, the same final state as with the GMSB slepton model. However, with this model the leptons tend to have lower p_{T} since the lighter neutral state is massive, highlighting the need for improved low-momentum lepton acceptance. In SUSY models, as assumed here, the chargino and neutralino play the roles of the new charged and neutral states, respectively, and the chargino-pair production cross section is used for the signal model.

This result enhances the discovery reach for displaced leptons beyond that of prior searches through several novel additions. It includes data collected by the ATLAS detector at a center-of-mass energy of 13.6 TeV, new triggers introduced in Run 3 that exploit improved tracking capabilities of the high-level trigger (HLT) to enable lower lepton transverse momentum (p_{T}) thresholds, as well as improved offline tracking performance that greatly lowers the rate of incorrectly reconstructed displaced tracks [36]. Precision information from the ATLAS Liquid Argon (LAr) electromagnetic (EM) calorimeter is introduced for sensitivity to highly displaced electrons, which may fail to include reconstructed tracks and be reconstructed as photons. Finally, the analysis includes a first consideration of single displaced electron channels, which were previously inaccessible due to high background rates and are enabled using multivariate Boosted Decision Trees (BDTs).

The analysis combines two approaches with mutually exclusive selections: the "ABCD" search and the "EM-BDT" search. In both cases, backgrounds are determined with entirely data-driven methods, and Monte Carlo (MC) simulation is only used for signal models. The ABCD search targets dilepton events, requiring at least two electrons, two muons, or an electron and a muon, and uses similar techniques as the prior Run 2 ATLAS displaced leptons search [23] for the estimation of backgrounds from fake and heavy-flavor (FHF) leptons and cosmic-ray muons. The ABCD search is performed in two orthogonal sets of signal regions (SRs) with different triggers and lepton p_{T} thresholds. The "high-p_{T}" SRs use a similar selection as the prior Run 2 search [23], and the new large-radius tracking (LRT) SRs use novel Run 3 triggers that employ LRT [37] (see Sec. II B) to extend the trigger tracking to large transverse impact parameter ($|d_0|$) values, thus enabling reduced lepton thresholds with respect to Run 2. A separate EM-BDT search also exploits the new LRT trigger for electrons and leverages precision tracking and electromagnetic calorimeter information (see Sec. II C) to improve the displaced e/γ selection, building on previous ATLAS Run 2 searches for displaced photons [38,39]. The LRT channel of the ABCD search and the EM-BDT search both use 56.3 fb^{-1} of Run 3 data collected at $\sqrt{s} = 13.6$ TeV in 2022–2023, while the ABCD high-p_{T} channel also uses the full Run 2 dataset of 140 fb^{-1} collected at $\sqrt{s} = 13$ TeV.

The paper is organized as follows: Section II describes the ATLAS detector, with specific emphasis on the unique LRT and LAr reconstruction techniques employed in the analysis. Section III describes the data and simulated samples used, and selections for objects and analysis events are given in Sec. IV. Descriptions of the ABCD (Sec. V) and EM-BDT (Sec. VI) analyses follow, including detailed event selections, background estimations, and systematic uncertainties. Finally, results and interpretations are presented in Sec. VIII, followed by brief conclusions.

II. ATLAS DETECTOR

The ATLAS detector [40,41] at the LHC covers nearly the entire solid angle around the collision point.[1] It consists

[1]ATLAS uses a right-handed coordinate system with its origin at the nominal interaction point (IP) in the center of the detector and the z-axis along the beam pipe. The x-axis points from the IP to the center of the LHC ring, and the y-axis points upwards. Polar coordinates (r, ϕ) are used in the transverse plane, ϕ being the azimuthal angle around the z-axis. The pseudorapidity is defined in terms of the polar angle θ as $\eta = -\ln\tan(\theta/2)$ and is equal to the rapidity $y = \frac{1}{2}\ln(\frac{E+p_z}{E-p_z})$ in the relativistic limit. Angular distance is measured in units of $\Delta R \equiv \sqrt{(\Delta y)^2 + (\Delta\phi)^2}$.

of an inner tracking detector surrounded by a thin superconducting solenoid, electromagnetic and hadronic calorimeters, and a muon spectrometer incorporating three large superconducting air-core toroidal magnet systems.

A. Detector subsystems

The inner-detector system (ID) is immersed in a 2 T axial magnetic field and provides charged-particle tracking in the range $|\eta| < 2.5$. The high-granularity silicon pixel detector covers the interaction region and typically provides four measurements per track, with the first hit generally being in the insertable B-layer (IBL). It is followed by the SemiConductor Tracker (SCT), which usually provides eight measurements per track. These silicon detectors are complemented by the transition radiation tracker (TRT), which enables radially extended track reconstruction up to $|\eta| = 2.0$. The TRT also provides electron identification information based on the fraction of hits (typically 30 in total) above a higher energy-deposit threshold corresponding to transition radiation.

The calorimeter system covers the pseudorapidity range $|\eta| < 4.9$. Within the region $|\eta| < 3.2$, EM calorimetry is provided by barrel and endcap high-granularity lead/LAr calorimeters, with an additional thin LAr presampler covering $|\eta| < 1.8$ to correct for energy loss in material upstream of the calorimeters. Hadronic calorimetry is provided by the steel/scintillator-tile calorimeter, segmented into three barrel structures within $|\eta| < 1.7$, and two copper/LAr hadronic endcap calorimeters. The solid angle coverage is completed with forward copper/LAr and tungsten/LAr calorimeter modules optimized for electromagnetic and hadronic energy measurements, respectively.

The muon spectrometer (MS) comprises separate trigger and high-precision tracking chambers measuring the deflection of muons in a magnetic field generated by the superconducting air-core toroidal magnets. The field integral of the toroids ranges between 2.0 and 6.0 T m across most of the detector. Three layers of precision chambers, each consisting of layers of monitored drift tubes, cover the region $|\eta| < 2.7$, except in the innermost layer of the endcap region, where layers of small-strip thin-gap chambers and Micromegas chambers both provide precision tracking in the region $1.3 < |\eta| < 2.7$. The muon trigger system covers the range $|\eta| < 2.4$ with resistive-plate chambers in the barrel, thin-gap chambers in the endcap regions, and the aforementioned small-strip thin-gap chambers and Micromegas chambers in the innermost layer of the endcap. These replaced cathode-strip chambers that were used through Run 2.

The luminosity is measured mainly by the LUCID–2 detector that records Cherenkov light produced in the quartz windows of photomultipliers located close to the beampipe.

Events are selected by the first-level trigger system implemented in custom hardware, followed by selections made by algorithms implemented in software in the HLT [37,42]. The first-level trigger accepts events from the 40 MHz bunch crossings at a rate below 100 kHz, which the high-level trigger further reduces in order to record complete events to disk.

The Run 3 detector configuration benefits from several upgrades compared with that of Run 2 to maintain high detector performance at the higher pileup levels of Run 3. The improvements include a new innermost layer of the muon spectrometer in the endcap region, which provides higher redundancy and a large reduction in fake muon triggers. The trigger system also benefits from new LAr digital electronics with significantly increased granularity. Other updates and further details are provided in Ref. [41]. A software suite [43] is used in the data simulation, in the reconstruction and analysis of the real and simulated data, in the detector operations, and in the trigger and data acquisition systems of the experiment.

As described in more detail below, this analysis exploits some specialized capabilities of the ATLAS detector and its Trigger and Data Acquisition system. These include LRT (see Sec. II B), which is the ability to reconstruct tracks with a large impact parameter with respect to the PV, and the ability of the EM calorimeter to measure the flight direction and time-of-arrival of particles causing EM showers (see Sec. II C).

B. Large radius tracking

The standard ATLAS tracking algorithm is designed to reconstruct the trajectory of promptly produced charged particles. It is efficient out to a $|d_0|$ of 5 mm, limiting its usefulness for LLPs that decay into charged particles after traversing part of the detector. The LRT [44] is a configuration of the tracking algorithm designed to increase the tracking efficiency for decay products of LLPs. Figure 2(a) shows an example $|d_0|$ distribution, extending well past 5 mm, for several models in the EM-BDT search, which combines both standard and LRT tracking. For the offline reconstruction of data, it is implemented as a second pass, running on the remaining hits that were not used by the standard tracking, with a looser restriction on the impact parameters and other optimizations, e.g. in the seeding step. Large radius tracks are reconstructed out to a $|d_0|$ of 300 mm, the first layer of the SCT. Compared to previous searches during Run 2, the LRT configuration in the reconstruction software was improved to greatly reduce the number of incorrectly reconstructed tracks as well as to reduce the computation time, allowing LRT tracks to be reconstructed in all events. This improved reconstruction is used consistently for both the Run 2 and Run 3 data where the performance is similar since the inner detector geometry is the same for both runs. For the reconstruction of offline electrons and muons, described in Sec. IV, both standard and LRT tracks are used.

In Run 3, LRT is run in the HLT for the first time [37]. For signal-like electrons and muons, the LRT used in the

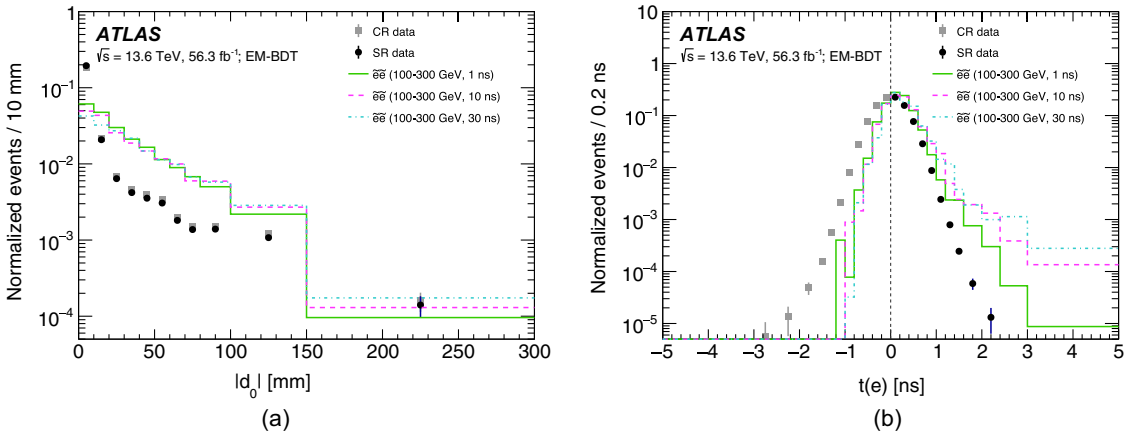

FIG. 2. Distributions of (a) the $|d_0|$ and (b) the LAr timing using the EM-BDT search regions with Run 3 data and selected signal samples with slepton masses of 100, 200, and 300 GeV. The LAr timing measurement was calibrated to zero for promptly produced particles traveling near the speed of light. The data events with negative times (gray squares) represent the signal-depleted control region (CR) used to determine the background estimate, while the data events with positive times (black circles) represent the signal region (SR) events on which the final search is performed. The SR data were blinded until the analysis strategy was finalized, and the data were unblinded to determine the results.

HLT is expected to be more than 80% efficient with respect to offline reconstruction for $|d_0| < 125$ mm. This is possible due to improvements in the LRT computation time, the HLT tracking algorithms, and the HLT computing resources. LRT for leptons in the trigger is implemented as a single pass, running on all hits in small regions around lepton candidates from the first-level trigger, with the same looser restrictions on impact parameters and similar optimizations as the offline reconstruction. This means the LRT-based lepton triggers do not use standard tracking. The same first-level hardware triggers for the primary prompt electron and muon triggers are used. The total trigger efficiency depends on the lepton flavor and kinematics [37]. For example, for mouns it drops from 90% at a small production radius to 60% at 300 mm.

C. Electromagnetic calorimeter timing and pointing measurements

Electrons from the decays of massive LLPs could reach the LAr calorimeter with a slight delay compared to prompt electrons. This delay arises mostly from the LLP time-of-flight, which corresponds to a relativistic speed ($\beta = v/c$) that can be substantially less than one.

In addition, the opening angle in the LLP decay causes the electron to be "non-pointing," arriving at the calorimeter from a direction that does not point directly back to the PV. This effect results in the geometrical path to the calorimeter being longer than that for a prompt electron from the PV, further increasing the delay in its arrival time. Figure 2(b) illustrates the delay in the timing distribution of several signal models in the EM-BDT SR.

As described in Refs. [38,39] and references therein, the fine segmentation of the LAr EM calorimeter can be used to measure the flight direction of a particle (electron or photon) that produces an EM shower, while its accordion structure and fast readout allows precise measurement of the particle's arrival time at the calorimeter. A line drawn through the centroids of the EM shower in the first two longitudinal layers is used to calculate the pointing value, defined as the difference between the position on the z-axis where the line crosses the beamline and the position of the PV. The resolution on the pointing measurement is ≈15 mm for an EM shower with an energy of ≈50–100 GeV in the barrel. The arrival time is determined using the energy deposit from the second-layer EM calorimeter cell with the maximum energy deposit among cells in the associated EM shower ($E_{\text{cell}}^{\text{max}}$). For an electron with an energy in the range of interest, this cell typically contains about 20%–50% of the total energy deposited in the EM shower. The timing resolution is approximately 200 ps for EM showers with $E_{\text{cell}}^{\text{max}}$ greater than 20 GeV and is dominated by the LHC beamspread.

III. DATA AND SIMULATION SAMPLES

Collision data collected by the ATLAS detector from the LHC's $\sqrt{s} = 13$ TeV pp Run 2 (2015–2018) and $\sqrt{s} = 13.6$ TeV pp Run 3 (2022–2023) are used, with luminosities corresponding to 140 fb^{-1} and 56.3 fb^{-1}, respectively, after applying detector conditions and data quality requirements [45]. The uncertainty in the Run 2 integrated luminosity is 0.83% [46], for 2022 it is 2.2% [47], and for 2023 it is 2.0% [48], following the methodology discussed in Ref. [46] and using the LUCID–2 detector [49] for the primary luminosity measurements complemented by measurements using the

inner detector and calorimeters. The ABCD high-p_T search uses the Run 2 and Run 3 datasets. The ABCD LRT and EM-BDT searches use only the Run 3 data. Run 2 data were reconstructed with a consistent software suite [43] as used for the Run 3 data to take advantage of developments, such as the improved LRT described in Sec. II B.

Data were collected with several unprescaled triggers [37,42] with signatures and thresholds that would accept events from displaced decays of leptons. Electron [50] and muon [51] triggers based on standard tracking [52] are efficient out to $|d_0|$ values of approximately 5 or 10 mm, respectively. Thus they are not optimal for saving events with LLPs of moderate lifetime. Photon triggers accept events with electrons, even if they are too displaced to reconstruct a track, but have higher energy thresholds than electron triggers. MS-only triggers accept events based on muon tracks in the MS, without the need for an inner-detector track; these also have higher thresholds and some have restrictions in η to additionally reduce the trigger rate. Thanks to the requirement of an inner detector track, LRT-based lepton triggers are able to save events with lower momentum thresholds of 30 and 20 GeV for electrons and muons, with $|d_0|$ thresholds of 3 and 2 mm, respectively. Table I lists the triggers used based on the analysis region and lepton topology.

For the baseline GMSB-motivated slepton signal model in Fig. 1, MC simulation events are used to determine the lepton selection criteria and estimate the sensitivity in a simplified GMSB SUSY model with light sleptons and a gravitino LSP with a mass much less than 1 GeV. The signal models are given by the slepton flavor, mass, and lifetime. For each slepton mass value, several slepton lifetimes were simulated, typically ranging from 1 ps to 30 ns. Since the distribution of particle flight distances follows an exponential distribution, it is possible to reweight the shape of that curve and thus generalize from the simulated samples to other lifetime values. Each event is assigned a weight according to a source signal lifetime, target signal lifetime, and the decay of the event in question.

For the dark sector model in Fig. 1(b), MC simulation is used to perform two scans of parameter space: varying the mass difference Δm and chargino mass for a fixed chargino lifetime of $\tau = 0.3$ ns, and varying the chargino lifetime and mass for a fixed $\Delta m = 40$ GeV. This choice was motivated by the analysis having the best expected sensitivity to the GMSB model for a lifetime of 0.3 ns, and a mass splitting of 40 GeV is the most favorable in terms of lepton p_T that is still consistent with the dark matter relic density. The W bosons are forced to decay into an electron or muon (no taus) with equal probability in the simulation.

Signal model MC simulation events with up to two additional partons at leading order are simulated using MADGRAPH5_aMC@NLO v2.6.1 [53] interfaced to PYTHIA 8.230 [54] with the A14 parameter set (tune) [55] along with the NNPDF2.3LO parton distribution function (PDF) set [56]. GEANT4 [57] is used to simulate the propagation and decay of the slepton, but without preserving information about its chirality. To model the impact of multiple interactions that occur in the same and neighboring bunch crossings (pileup), each hard-scattering event is overlaid [58] with simulated minimum bias events generated by EPOS 2.0.1.4 [59,60] with the EPOS LHC tune and PYTHIA8.307 [61] with the NNPDF2.3LO set of PDFs and

TABLE I. Summary of trigger thresholds used for the ABCD and EM-BDT analyses based on the object topology. Trigger objects are denoted as γ for photons, e for electrons, and μ for muons, preceded by the multiplicity and followed by the p_T threshold in GeV. "MS-only" indicates triggers that only rely on the muon spectrometer (MS), and not the inner detector. For example, $2\gamma 50$ means a trigger requiring the presence of two photons with $p_T > 50$ GeV. The $1\mu 60$ MS-only trigger has a restriction of $|\eta| < 1.05$. The large-radius tracking (LRT) electron (muon) trigger has a $|d_0| > 3(2)$ mm requirement. None of the triggers have an isolation requirement. Triggers listed with "Run 3 only" were only used for the corresponding analysis region to collect data in Run 3, otherwise they were also used for Run 2 data. "OR" indicates a logical OR of multiple triggers.

Topology	Trigger thresholds [GeV]
ABCD high-p_T	
`if` $\geq 1e, p_T > 160$ GeV	$1\gamma 140$
`else if` $\geq 2e, p_T > 60$ GeV	$2\gamma 50$
`else if` $\geq 1\mu, p_T > 60$ GeV, $\lvert\eta\rvert < 1.07$	$1\mu 60$ (MS-only)
`else if` $e\mu$ (Run 3 only)	$\gamma 40\mu 40$ (MS-only)
`else if` $\mu\mu$ (Run 3 only)	$2\mu 50$ (MS-only)
ABCD LRT	
$e, p_T > 31$ GeV (Run 3 only)	$1e30$ (LRT)
$\mu, p_T > 21$ GeV (Run 3 only)	$1\mu 20$ (LRT)
EM-BDT	
$= 1e, 0\gamma$ (Run 3 only)	$1e30$ (LRT) OR $1\gamma 140$
$\geq 2e$ OR $(1e, 1\gamma)$ (Run 3 only)	$1e30$ (LRT) OR $2\gamma 50$ OR $1\gamma 140$
$\geq 2\gamma$ (Run 3 only)	$2\gamma 50$ OR $1\gamma 140$

A3 tune [62]. The 13 TeV wino-like chargino-pair and slepton-pair production cross sections and uncertainties were calculated at next-to-leading-order (NLO) in α_s, with soft-gluon emission effects at next-to-leading-logarithm [63–70]. At 13.6 TeV, these were calculated at approximate next-to-next-to-leading-order in α_s matched with threshold resummation at the next-to-next-to-leading-logarithmic accuracy (aNNLO + NNLL) using an envelope of predictions with different factorization and renormalization scales and PDF sets [71]. The superpartners of the left- and right-handed leptons are assumed to have equal mass. The slepton-pair cross section for a single flavor of $\tilde{\ell}$ with mass 100 GeV (800 GeV) is 0.37 ± 0.01 pb (0.059 ± 0.004 fb) at 13 TeV and 0.41 ± 0.01 pb (0.069 ± 0.008 fb) at 13.6 TeV. The chargino-pair cross section for a mass of 300 GeV is 190 ± 13 fb at 13 TeV and 216 ± 9 fb at 13.6 TeV. A factor of 0.0642 is included to account for the branching ratio of the two W boson decays into electrons and muons, which accounts for decays via taus.

IV. OBJECT SELECTIONS AND EVENT PRESELECTIONS

The main objects used in this analysis are electrons and muons, including those produced in the decays of τ-leptons, and photons. Jets, including those from hadronically decaying τ-leptons, are also used in the procedure to remove ambiguities between nearby reconstructed objects ("overlap removal") and to construct the magnitude of the missing transverse momentum (E_T^{miss}), which is used in the EM-BDT analysis.

For electrons, muons, and photons, a baseline selection is used for the overlap removal procedure. For electrons and muons, additional kinematic requirements are imposed before separating events into the ABCD and EM-BDT regions; these are referred to as high-d_0 leptons in the paragraphs below. Analysis dependent selections are then applied to high-d_0 leptons to define signal leptons that are used to construct SRs, which are used to search for signal-like excesses above SM expectations. Table II summarizes the baseline and signal lepton selection requirements, with more details in the following text.

Electrons are reconstructed from ID tracks matched to clusters of energy deposited in the EM calorimeter. If a standard and large-radius track both point to the same EM cluster and lead to the reconstruction of a standard and LRT electron with the same cluster, the electron satisfying the stricter identification requirement is kept, and in case of a tie, the electron reconstructed with a standard track is kept. Baseline electrons must have $p_T > 10$ GeV, $|\eta| < 2.47$, and satisfy a modified version of the *VeryLoose* identification working point (WP) [72] that does not depend on $|d_0|$, $|d_0|$ significance, or the number of pixel hits, to avoid suppressing displaced electrons, referred to here as LLP VeryLoose. Figure 3(a) shows the efficiency of electrons

TABLE II. Overview of electron and muon baseline and signal selections. The signal selection is applied on top of the baseline selection. The ABCD identification and p_T requirements depend on the SR and on which triggers are used. $\Delta p_T/p_T = (p_T^{track} - p_T^e)/p_T^e$ is the relative difference between the track p_T and the calorimeter E_T. N_{miss} is the number of missing hits. The χ^2 variables are all reduced by the number of degrees of freedom (n.d.f.), and are for the ID track or CB track. N_{prec} is the number of precision layers, and N_ϕ is the number of ϕ layers. The TRT barrel selection is only applied for 2023 data.

Selection	Electrons		Muons
	Baseline		
p_T (GeV)	> 10		> 21
$\lvert d_0\rvert$ (mm)	< 300		$2 < \lvert d_0\rvert < 300$
$\lvert z_0\rvert$ (mm)	< 500		< 500
$\lvert\eta\rvert$	$\lvert\eta\rvert < 1.37$ OR $1.52 < \lvert\eta\rvert < 2.47$		< 2.5
Identification	LLP veryloose		LLP medium
	ABCD signal (LRT/high-p_T)	EM-BDT signal	ABCD signal (LRT/high-p_T)
Isolation	Tight_VarRad	Tight_VarRad	PFlow_Loose_VarRad
Identification	LLP loose /$\cdots$	LLP loose	$\cdots$
p_T (GeV)	$> 31/ > 65$	$\cdots$	$\cdots/ > 65$
$\lvert d_0\rvert$ (mm)	> 3	> 3	$\cdots/ > 3$
$(p_T^{track} - p_T^e)/p_T^e$	≥ -0.5	$\cdots$	$\cdots$
χ^2_{ID}/n.d.f.	< 2	$\cdots$	< 2
N_{miss}	≤ 1	$\cdots$	≤ 1
N_{prec}	$\cdots$	$\cdots$	≥ 3
χ^2_{CB}/n.d.f.	$\cdots$	$\cdots$	< 3
N_ϕ	$\cdots$	$\cdots$	> 0
Pass cosmic veto	$\cdots$	$\cdots$	True
Pass TRT barrel (2023)	True	True	True

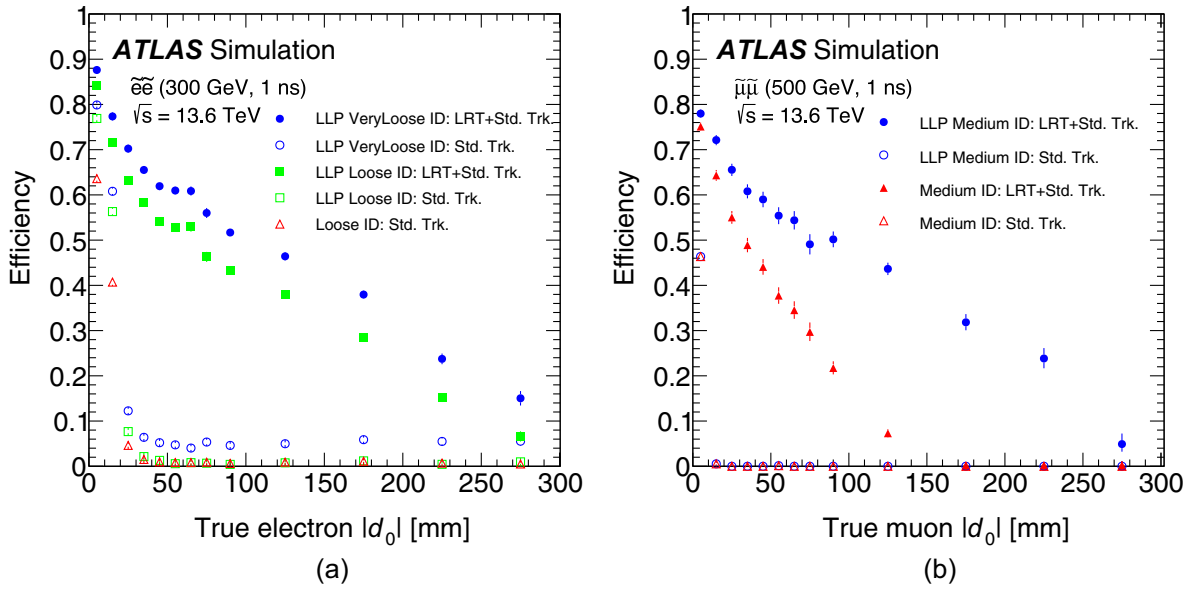

FIG. 3. Efficiency to reconstruct and identify (a) electrons and (b) muons using large-radius tracking (LRT) and standard tracking (Std. Trk.) with respect to generator-level leptons in simulated GMSB slepton signal models with a slepton lifetime of 1 ns and a selectron (smuon) mass of 300 (500) GeV. The efficiencies for the various LLP working points are shown as a function of the true transverse impact parameter $|d_0|$ of the daughter lepton.

from a selectron signal model to satisfy the standard and LLP electron identification WP as a function of the true lepton $|d_0|$ value.

High-d_0 electrons, for the purpose of analysis region definition, must additionally satisfy the object overlap removal, have $p_{\mathrm{T}} > 31$ GeV, $3 < |d_0| < 300$ mm, $|z_0| < 500$ mm, and fall outside of the EM calorimeter barrel-endcap transition region ($1.37 < |\eta| < 1.52$). The ABCD signal electron selection additionally requires that the electrons are isolated from nearby tracks and calorimeter energy deposits. The sum of the p_{T} of all prompt tracks within a cone, shrinking with p_{T} (max $\Delta R = 0.2$), and the E_{T} of all energy depositions within $\Delta R = 0.3$ of the electron must each be less than 6% of the electron p_{T} (Tight_VarRad). To suppress electrons from random overlaps of hadronic tracks and photon energy depositions, the relative difference between the electron track p_{T} measurement and that of the electron p_{T} measured when accounting for the calorimeter energy must satisfy $(p_{\mathrm{T}}^{\mathrm{track}} - p_{\mathrm{T}}^{e})/p_{\mathrm{T}}^{e} \equiv \Delta p_{\mathrm{T}} \geq -0.5$. To suppress combinatoric fake tracks, the ID track must have an χ^2 per degree of freedom (n.d.f.) satisfying $\chi^2_{\mathrm{ID}}/\mathrm{n.d.f.} < 2$, where χ^2 is the sum of the squares of the distances between each hit and the track position extrapolated to the given sensor divided by the resolution on this difference, and at most one missing cluster that is included in the track fit (track "hit") at a larger radius than the innermost hit. Signal electrons in regions triggered by the LRT trigger require the stricter LLP Loose identification WP to be consistent with the trigger, with the same modifications as above to the standard *Loose* WP [72]. The EM-BDT signal electron selection requires the baseline selection, $3 < |d_0| < 300$ mm, the same isolation criterion, and the same LLP Loose identification WP.

Muons are reconstructed from ID tracks matched to muon track segments. If a standard and LRT track both point to the same muon segment and lead to the reconstruction of a standard and LRT muon with the same segment, the duplication is resolved by keeping the muon with the smaller difference in η between the ID track and the muon track segment extrapolated to the PV. Baseline muons must have $p_{\mathrm{T}} > 21$ GeV, $|\eta| < 2.5$, and satisfy a modified version of the *Medium* identification WP [73] without requirements on the number of pixel and TRT hits, referred to here as LLP Medium; though, the standard tracks used to reconstruct muons still have a requirement of at least one pixel hit. Figure 3(b) shows the efficiency of muons from a smuon signal model to satisfy the standard and LLP muon medium identification WP as a function of the true lepton $|d_0|$ value.

High-d_0 muons must additionally satisfy the object overlap removal, $2 < |d_0| < 300$ mm, and $|z_0| < 500$ mm. Signal muons are required to additionally be isolated from nearby tracks and calorimeter energy depositions using an algorithm that exploits particle flow to associate tracks with their energy clusters [73]. The sum of the p_{T} of all prompt tracks within a cone, shrinking in p_{T} (max $\Delta R = 0.3$), of the muon is added to 40% of the sum of the E_{T} of energy depositions within $\Delta R = 0.2$ that are not matched to tracks, and the total is required to be less than 16% of the muon p_{T} (PFlow_Loose_VarRad). Several additional requirements are imposed to reject spurious muons from combinatoric fake tracks. Muons must be measured in at least three MS

precision tracking layers and have at least one high-precision ϕ measurement. The ID track must have $\chi^2_{\mathrm{ID}}/\mathrm{n.d.f.} < 2$ and at most one missing hit at a larger radius than the innermost hit, and the combined muon (CB) track must satisfy $\chi^2_{\mathrm{CB}}/\mathrm{n.d.f.} < 3$. To reject cosmic-ray muons, a cosmic muon veto is applied that is similar to the one used in the ATLAS Run 2 displaced leptons search [23] and originally developed in the ATLAS Run 2 search for a displaced vertex and a displaced muon [74]. A muon is tagged as originating from a cosmic-ray muon, and thus vetoed, if there are MS segments on the opposite side of the detector along its trajectory, within η and ϕ windows of $|\eta_\mu + \eta_{\mathrm{MS}}| < 0.01$ and $\pi - |\phi_\mu - \phi_{\mathrm{MS}}| < 0.08$, where the μ and MS subscripts refer to the reconstructed muon and MS segments, respectively. A geometric correction is applied to the η value used to take into account tracks that do not pass through the PV.

Photons are reconstructed from EM calorimeter depositions. Baseline photons must have $E_{\mathrm{T}} > 30$ GeV, fall within the barrel ($|\eta| < 1.37$) or endcap ($1.52 < |\eta| < 2.5$) regions, and satisfy the *Loose* photon identification WP [72]. Signal photons must also be isolated from nearby tracks and calorimeter depositions [72]. The sum of the p_{T} of all prompt tracks (E_{T} of all energy depositions) within $\Delta R = 0.2$ of the photon must be less than 5% (6.5%) of the photon E_{T}.

Jets are reconstructed with the particle-flow technique [75,76] using the anti-k_t algorithm with a radius parameter of 0.4 [77]. In this analysis, jets are only used for overlap removal, and for the EM-BDT search only, to evaluate the $E_{\mathrm{T}}^{\mathrm{miss}}$. Baseline jets must satisfy $p_{\mathrm{T}} > 20$ GeV and $|\eta| < 2.8$. To reject jets from pileup interactions, a jet vertex tagger algorithm employing a neural network is applied using a WP with an approximately fixed efficiency as a function of jet p_{T} [78].

The value of $E_{\mathrm{T}}^{\mathrm{miss}}$ is defined as the magnitude of the negative vector sum of the transverse momenta of all distinct reconstructed objects as well as tracks not associated with any reconstructed objects [78]. When calculating the value of $E_{\mathrm{T}}^{\mathrm{miss}}$, both prompt and displaced leptons are included.

The analysis requires one of the following three conditions to be true: at least one baseline electron, at least two baseline muons, or at least two baseline photons. Events must pass one of the triggers described in Sec. III, which depend on the final state and the p_{T} of the leptons and photons. During 2023, part of the TRT barrel was not in operation in a region defined by $-1.759 < \phi < -1.257$ and $|\eta| < 1.37$. Events with electrons or muons in this $\eta - \phi$ region are vetoed in 2023 data only.

Events are categorized into orthogonal ABCD high-p_{T}, ABCD LRT, and EM-BDT regions in cascading order based on the number of high-d_0 leptons, as defined above. If there are at least two such leptons with $p_{\mathrm{T}} > 65$ GeV, events fall into the ABCD high-p_{T} regions. Failing that, if events have at least two such leptons with $p_{\mathrm{T}} > 31(21)$ GeV for electrons (muons), events fall into the ABCD LRT regions. Remaining events fall into the EM-BDT regions. The flowchart in Fig. 4 illustrates the categorization of events. Additional selections, defined in

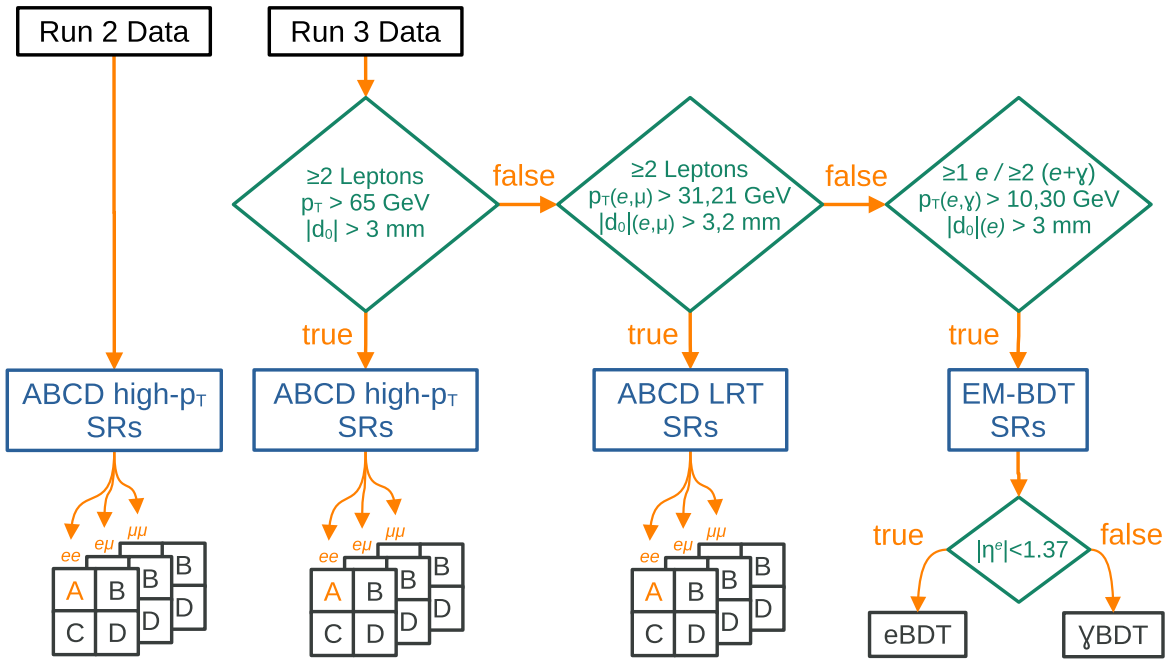

FIG. 4. Flowchart of the event categorization into the ABCD high-p_{T}, ABCD LRT, and EM-BDT SRs. The Run 2 and Run 3 ABCD high-p_{T} SRs are separate.

Secs. V and VI for the ABCD and EM-BDT approaches, respectively, are used to define SRs that are sensitive to BSM signals, control regions (CRs) that are used to estimate the backgrounds in the SRs, and validation regions (VRs) that are used to test the robustness of the background estimation methodology. The SRs, CRs, and VRs for each channel are mutually orthogonal.

V. ABCD ANALYSIS

The ABCD analysis defines SRs for three dilepton flavor combinations, ee, $\mu\mu$, and $e\mu$, using the flavors of the two leptons with the highest p_{T}. Backgrounds are estimated using two ABCD-based estimations, one for fake and heavy-flavor (FHF) leptons and one for cosmic-ray muons, which make use of leptons passing and failing certain quality criteria. These are estimated separately because, while they are uncorrelated with each other, different sets of background suppressing requirements need to be inverted to populate the background estimation regions. Cosmic-ray muons are only relevant for the $\mu\mu$ final state. Region A, shared for the FHF and cosmic-ray muon estimates, is the SR where both leptons pass all analysis requirements, regions B and C have one lepton passing the criteria and the other one failing them, and region D contains events where both leptons fail the criteria, which are different for the FHF and cosmic-ray muon estimates. When the criteria used on each lepton are uncorrelated, the estimate of the background in the SRs reduces to

$$N_A^{\mathrm{predicted}} = \frac{N_B^{\mathrm{FHF}} \times N_C^{\mathrm{FHF}}}{N_D^{\mathrm{FHF}}} + \frac{N_B^{\mathrm{Cosmics}} \times N_C^{\mathrm{Cosmics}}}{N_D^{\mathrm{Cosmics}}},$$

where $N_{B/C/D}^{\mathrm{FHF}}$ and $N_{B/C/D}^{\mathrm{Cosmics}}$ are the event yields in the various control regions for the FHF and cosmic-ray backgrounds, respectively, for a given lepton flavor combination. The B, C, and D regions for a given SR are included in the fits to determine the backgrounds for model-independent limits and BSM exclusions, as described further in Sec. VIII.

A. ABCD event selection

The selection of events for the ABCD analysis begins with the common preselection requirements described in Sec. IV. The ABCD search requires the presence of at least two signal leptons (e or μ) separated by $\Delta R(\ell_1, \ell_2) > 0.2$ and considers two orthogonal sets of SRs. The high-p_{T} SRs use a similar selection as the Run 2 search, relying on photon and MS-only muon triggers and requiring both leptons to have $p_{\mathrm{T}} > 65$ GeV and $|d_0| > 3$ mm. The Run 3 high-p_{T} SRs benefit from the addition of new photon plus MS-only and di-MS-only-muon triggers, listed in Table I. Separate SRs are defined for the ee, $\mu\mu$, and $e\mu$ events in Run 2 and Run 3, resulting in six orthogonal ABCD high-p_{T} SRs.

The ABCD LRT SRs use the novel LRT triggers that were introduced in Run 3 and require electrons (muons) with $p_{\mathrm{T}} > 31$ (21) GeV. The muon $|d_0|$ threshold is also reduced to 2 mm. Electrons are required to pass the stricter LLP Loose WP to be consistent with the LRT trigger. Events satisfying the high-p_{T} SR selection are vetoed. Three SRs exploiting the LRT triggers are defined for the ee, $\mu\mu$, and $e\mu$ events in Run 3 only, leading to a total of nine orthogonal SRs considered in the ABCD search. For the three $\mu\mu$ SRs, an additional cosmic-ray veto rejects events with back-to-back fully reconstructed muons, μ_1 and μ_2, with $|\eta(\mu_1) + \eta(\mu_2)| < 0.02$ and $\pi - |\phi(\mu_1) - \phi(\mu_2)| < 0.01$, taking advantage of the better angular resolution of fully reconstructed muons at the PV, compared to the extrapolated MS segments.

To maintain broad sensitivity to BSM physics scenarios besides the GMSB long-lived slepton and dark sector models considered in this paper, no additional kinematic selections are applied. Due to the low rates of displaced leptons in the data, these selection criteria are enough to reduce the expected background yields in all SRs to less than one event.

Example total acceptances, summing over the ABCD SRs lepton flavors, for the stau model with a 100 GeV mass and 0.01 ns lifetime in the high-p_{T} and LRT SRs are 0.001 and 0.012, respectively. For the smuon model with 800 GeV mass and 0.1 ns lifetime, the total acceptances are 0.19 and 0.06 for the high-p_{T} and LRT SRs, respectively.

B. ABCD background estimation

Two sources of background are considered in the ABCD analyses. The FHF lepton background contributes to all three lepton flavor channels and includes combinatoric fake tracks, random overlaps of hadronic tracks with EM clusters or MS tracks, photon conversions, and decays of heavy-flavor (HF) bottom and charm mesons. The cosmic-ray muon background contributes to $\mu\mu$ events only. Since these processes are not necessarily well-modeled in simulation, they are estimated from data CRs using ABCD methods that closely follow the methodology of the Run 2 ATLAS displaced leptons search [23]. The final background estimates and results for each SR are obtained from a simultaneous fit of the four ABCD regions that includes any signal contamination. The signal contamination is mostly less than 10% in the B and C regions for the FHF and always less than 1% in the denominator region D. It is only larger in a few B and C regions depending on the signal model. Thus any contamination would lead to a lightly overestimated background and a weaker analysis sensitivity. For the cosmic-ray muon estimation, the signal contamination is negligible in each region.

The background estimate for FHF leptons uses CRs in which some of the quality criteria for one lepton, the other lepton, or both, are inverted. A failing electron is one that

fails at least one of the requirements from Table II on Δp_{T}, ID track $\chi^2_{\mathrm{ID}}/\mathrm{n.d.f.}$, and the number of missing track hits, while satisfying all other ABCD signal electron requirements of Sec. IV. A failing muon is one that fails at least one of the requirements from Table II on the number of precision tracking layers, the presence of a high-precision ϕ measurement, ID track $\chi^2_{\mathrm{ID}}/\mathrm{n.d.f.}$, combined muon $\chi^2_{\mathrm{CB}}/\mathrm{n.d.f.}$, and the number of missing track hits, while satisfying all other ABCD signal muon requirements of Sec. IV. In the $\mu\mu$ high-p_{T} regions only, the observed yields in the ABCD CRs are too small to provide individual predictions for Run 2 and Run 3. Therefore the yields in the ABCD regions for these two datasets are combined and the predicted FHF background is scaled by the fractions of the total luminosity accounted for by each dataset, namely 0.71 for Run 2 and 0.29 for Run 3. The predicted SM background yields in each of the nine ABCD SRs is less than 0.2 events. As an example, for the high-p_{T} Run 3ee SR, the FHF B, C, and D region yields are 3, 6, and 278 respectively. This results in a predicted background of $3 \cdot 6/278 = 0.067^{+0.092}_{-0.041}$ assuming no signal contamination and ignoring the SR yields, which are included as a constraint in the fit for the final results.

This method assumes that the quality criteria of the two FHF leptons are uncorrelated with each other. The correlation coefficient, as measured in VRs, varies between -0.05 and -0.1. Two sets of VRs are defined to account for any systematic biases of the background estimation methodology, including potential correlations between the quality criteria of the leptons. The VR-fake regions are enriched in fake-lepton backgrounds by inverting the requirement on Δp_{T} for electrons and on the CB track $\chi^2_{\mathrm{CB}}/\mathrm{n.d.f.}$ requirement for muons. This makes these VRs a subset of region D, but orthogonal to regions A, B, and C. The VR-HF regions are enriched in heavy-flavor leptons by requiring at least one lepton to fail the isolation criteria. Some requirements are removed in order to increase the number of events in the heavy-flavor VRs: Δp_{T} in the ee and $e\mu$ channels; $\chi^2_{\mathrm{CB}}/\mathrm{n.d.f.}$ in the $\mu\mu$ channel; and N_{prec} and N_ϕ in the $e\mu$ channel. The observed yields in the nine VR-fake and VR-HF regions corresponding to the nine SRs are consistent with the background expectations obtained by performing the ABCD estimate in these VRs.

For cosmic-ray muons, the ABCD CRs are defined by inverting the MS quality requirements (number of precision tracking layers N_{prec}, number of high-precision ϕ measurements N_ϕ, or combined muon $\chi^2_{\mathrm{CB}}/\mathrm{n.d.f.}$) or by inverting the cosmic veto relying on the presence of the MS segments on the opposite side of the detector. The correlation coefficient between these quantities is -0.03, computed in events with two baseline muons. These are inverted for the muon in the top half of the detector, which is more likely to be misreconstructed than the muon in the bottom half since it travels in the opposite direction of particles that originate from the PV. For example, region B has a cosmic tagged top muon and region C has a top muon, failing at least one MS quality requirements. Applying the additional cosmic-ray veto on back-to-back fully reconstructed muons eliminates almost all of the events in these regions. Therefore the cosmic-ray muon background is estimated without this additional cosmic-ray veto applied and then scaled by the expected efficiency $T = (3.7 \pm 2.6) \times 10^{-3}$ for muons to survive the veto, evaluated using the events that fall in the superset of regions B, C, and D. The expected background yields are of the order 10^{-3} in the three $\mu\mu$ SRs.

This background method is validated in VRs enriched in cosmic-ray muons, in which the cosmic veto relying on the presence of MS segments on the opposite side of the detector as the bottom muon is replaced by the requirement that this muon has MS segments satisfying $|\eta_\mu + \eta_{\mathrm{MS}}| < 0.01$ and $\pi - |\phi_\mu - \phi_{\mathrm{MS}}| < 0.08$ but no such segments satisfying $|\eta_\mu + \eta_{\mathrm{MS}}| < 0.002$ and $\pi - |\phi_\mu - \phi_{\mathrm{MS}}| < 0.02$. To enrich the VR in cosmic-ray muons, the additional cosmic-ray veto based on the two fully reconstructed muons is not applied. The observed yields are consistent with the background expectations.

C. ABCD systematic uncertainties

While the sensitivity of the ABCD analysis is dominated by statistical uncertainties, systematic uncertainties are derived based on the agreement, or closure, of the VRs. Since these VRs, like the SRs, have limited numbers of events, the larger of the non-closure and the statistical uncertainty is used as the systematic uncertainty. Additional uncertainties common with the EM-BDT analysis are described in Sec. VII.

The systematic uncertainty in the FHF lepton background is based on the agreement between observed yields versus expected backgrounds in the VR-fake and VR-HF regions, testing the closure of the method in regions orthogonal to the SRs. For each region, the larger of two quantities is taken as the systematic uncertainty: the deviation from one of the ratio of the observed yield to the expected background, or the statistical uncertainty in the expected background. The values are extracted from VR-fake and VR-HF separately and then added in quadrature. Due to the small rate of fake muons, the $e\mu$ and $\mu^+\mu^-$ VRs all had less than five observed events. In all cases, the statistical uncertainty is equal to or larger than the non-closure. This results in positive uncertainties of 50%/190%/150% ($ee/e\mu/\mu\mu$) for the Run 2 high-p_{T} regions; 40%/160%/150% for the Run 3 high-p_{T} regions; and 130%/150%/240% for the Run 3 LRT regions.

Two sources of systematic uncertainty in the cosmic-ray muon background are considered. The first source is due to the assumption that the muon in the top half of the detector is the one that is mismeasured. The background is estimated by instead inverting the cosmic veto and/or MS quality variables (N_{prec}, N_ϕ, and $\chi^2_{\mathrm{CB}}/\mathrm{n.d.f.}$) of the bottom

muon and taking the relative difference with respect to the nominal result, resulting in uncertainties of 28%, 2%, and 41% in the Run 2 high-p_{T}, Run 2 high-p_{T}, and Run 3 LRT SRs, respectively. The cosmic-ray background is also estimated by inverting two of the three MS quality variables and taking the relative difference with respect to the nominal estimate. The largest deviation of the three pairs is used, resulting in uncertainties of 20%, 38%, and 82% in the Run 2 high-p_{T}, Run 2 high-p_{T}, and Run 3 LRT SRs, respectively.

VI. EM-BDT ANALYSIS

The EM-BDT analysis seeks to discriminate between displaced electrons and the background, which is dominated by prompt particles. In the interpretation of the results for the GMSB long-lived slepton model used as a benchmark (see the diagram in Fig. 1), the EM-BDT analysis is applied to the selectron and stau channels, since either can produce displaced electrons in the final state.

As an electron arising from the decay of a long-lived parent is both displaced and delayed, there exist significant correlations between many relevant observables, motivating the introduction of machine learning techniques in the development of a multivariate discriminant. An electron from an LLP decay that occurs too far into the detector may not have an identifiable track. In such a case, the electron is reconstructed as a photon, provided the decay is before the calorimeter. Two different BDTs are employed, each using variables that are verified with comparisons of $Z \to ee$ data and MC simulation to be reasonably well modeled. The "eBDT" seeks to identify displaced electrons from among those particles reconstructed as electrons, while the "γBDT" seeks to identify displaced electrons from among those particles initially reconstructed as photons. The γBDT extends the sensitivity of the analysis to events where the decay producing the electron occurs in front of the EM calorimeter but further from the beamline than the 300 mm limit where the LRT is applied; in such cases, it is still possible to identify the displaced electron from the EM calorimeter information only.

The discriminating variables for the eBDT include tracking information, EM calorimeter variables, and combinations of the ID and LAr measurements. The tracking variables include the track fit quality χ^2 value, the number of pixel hits on the track, the number of missing layers in the track, and the transverse and longitudinal impact parameters with respect to the PV position. The EM calorimeter variables include the LAr pointing measurement (z_{EM}), the absolute value of the LAr timing measurement, and two LAr shower shape variables, namely the fraction of the EM shower energy in the first and third longitudinal layers (f_1 and f_3, respectively). The combined variables include Δp_{T} and the difference between z_0 and z_{EM}; both of these combined variables are intended to help reject backgrounds from fake electrons. The background rejection of the eBDT is enough that the analysis can be performed with only one reconstructed electron in the event, thereby greatly extending the analysis sensitivity to longer slepton lifetime values, where only one selectron (or stau) has decayed before reaching the EM calorimeter. In events with more than one reconstructed electron, or with one electron and one or more photons, the eBDT is applied to the leading electron. Thus, the eBDT is an "object-level" discriminant, using only measurements of the electron itself and not of other properties of the event, and thereby functions as a "displaced electron tagger." This feature of the eBDT makes it rather model-independent.

The γBDT searches for displaced electrons reconstructed as photons. The lack of tracking information and higher background rates for photons than electrons makes a single photon region infeasible. Instead, the γBDT requires at least one additional electron or photon. The variables used are the pointing and timing measurements of the two objects, as well as the differences between them. In addition, the value of $E_{\mathrm{T}}^{\mathrm{miss}}$ in the event is used. This choice is motivated by the gravitinos produced in the baseline slepton model in order to extend the reach of the analysis to longer slepton lifetime values but does make the γBDT more model-dependent than the eBDT.

A. EM-BDT event selection

The selection of events for the EM-BDT analysis begins with the common preselection requirements described in Sec. IV. The EM-BDT event selection is made orthogonal to that of the ABCD analysis regions by vetoing dielectron events passing the ABCD p_{T} and $|d_0|$ requirements. The selected EM-BDT events are divided into several distinct final states, according to the multiplicity of reconstructed EM objects (electrons or photons) in the event. Each final state is selected by a set of triggers, as described in Table I.

The eBDT is used to analyze events with at least one electron in the barrel calorimeter ($|\eta| < 1.37$). These include single-electron events but also events with an electron in the barrel calorimeter plus either additional electrons or photons. In events with more than one reconstructed electron, the leading electron in the barrel is selected as the input object to the eBDT algorithm. The electron is required to have $E_{\mathrm{cell}}^{\mathrm{max}} > 5$ GeV to reduce the impact of noise on the calorimeter timing and an absolute value of its calorimeter time less than 12.5 ns to reject backgrounds from other bunch crossings.

Given the large backgrounds in the single-photon event samples as well as the lack of tracking information for photons, the γBDT is used to analyze only events with at least two reconstructed EM objects; the first must be a photon passing the baseline requirement, while the second can be another photon or an electron which fails the eBDT requirements. Electrons are treated as photons in this case and do not have the transverse impact parameter requirement in Table II. At least one EM object must be in the

barrel calorimeter ($|\eta| < 1.37$). Both EM objects are required to have $E_{\text{cell}}^{\text{max}} > 5$ GeV and an absolute value of its calorimeter time less than 12.5 ns. A requirement of $|z| < 2000$ mm for both EM objects eliminates beam-induced backgrounds that can fake the photon signature.

For a selectron with a mass of 200 GeV and a lifetime of 30 ns, total acceptances of the EM-BDT event selection are 0.0022 for the γBDT and 0.01 for the eBDT. The sum of these are two orders of a magnitude larger than the sum of the ABCD SR acceptances.

B. EM-BDT background estimation

The background in the EM-BDT analysis is dominated by prompt particles that are mismeasured or poorly reconstructed. Such effects cannot be sufficiently precisely simulated, and therefore the background estimation is necessarily entirely data-driven. The estimate is generated by dividing the data into three orthogonal regions: a CR, which can be used to estimate the background normalization and BDT distribution shape, a VR, which can be used to validate the background estimate before unblinding the SR data, and the SR, in which the search will ultimately be performed.

The EM-BDT analysis exploits the fact that, for prompt background, the distribution of the arrival time at the EM calorimeter should, due to resolution effects, be symmetric about zero, as seen in Fig. 2. In contrast, signal events should be delayed, and therefore have primarily positive arrival times. As a result, the CR can be defined for the eBDT (γBDT) by events where the leading electron has (both photons have) a negative time, while the SR is defined by events where the leading electron has (both photons have) a positive time. The VR is defined by kinematic selections that aim to achieve a dominance of background over signal by selecting events with enhanced SM W or Z boson production; the VR includes single-electron events with a transverse mass of the lepton and $E_{\text{T}}^{\text{miss}}$ system in the range from 60 to 100 GeV and dielectron events with a dielectron mass in the range from 80 to 100 GeV. To guarantee orthogonality among the three regions, the CR and SR definitions include vetoes of any events that fall within the VR selection.

For both the eBDT and the γBDT, the BDT is trained to separate the signal, as modeled with MC simulation, from the background, as modeled by the CR data. Signal models of various masses and lifetimes ≥ 1 ns were used for training in order to maximize the sensitivity to longer lifetimes. To make use of the entire sample of the MC simulation and the CR data, the signal sample and data used for training are split randomly into three "folds," and training is performed on each group individually. It is then required that the score assigned to a particular event during evaluation is determined using a fold other than the one assigned to that event in training. The final EM-BDT results for various slepton masses and lifetimes are obtained by signal-plus-background fits, including associated statistical and systematic uncertainties, of the unblinded SR data to the weighted sum of the CR-derived background template and signal template shape from MC simulation. The signal contamination in the CR is found to be less than one percent of the yield. Still, to account for signal contamination in the CR, particularly at low lifetimes where the signal has a similar shape in the CR and SR, the signal template in the fit is set to be the difference of the positive and negative timing BDT score distributions, i.e. the difference between the SR and CR templates. Before unblinding the SR data, the BDT distributions were validated by performing fits to the background-dominated VR.

The BDTs are defined such that their output values range from -1 to $+1$, with signal-like (background-like) events skewed toward positive (negative) BDT scores. The final statistical analysis uses a simultaneous fit to binned eBDT and γBDT distributions, where the normalization is allowed to float. Before unblinding, the binning used for the BDT scores was subject to an optimization procedure that sought to maximize the signal sensitivity. To ensure a non-zero background estimate could be made for each bin, the choice of bins was subject to the constraint that there exist at least one CR event in each bin. The eBDT and γBDT binnings were optimized separately. However, for both BDTs the very background-like events with BDT scores less than zero are not used in the fit, and the events with positive BDT scores are divided into five non-overlapping bins.

C. EM-BDT systematic uncertainties

While the sensitivity of the EM-BDT analysis is dominated by statistical uncertainties, several sources of systematic uncertainty are considered. The background normalization is determined in the fit, and therefore no corresponding systematic uncertainty is needed. However, systematic uncertainties that are considered can impact the results of the final fit by either impacting the shapes of the BDT score distribution of the signal or the background or by affecting only the signal normalization. Additional uncertainties common with the ABCD analysis are described in Sec. VII.

The largest systematic uncertainty in the shape of the background BDT distribution arises due to the assumption that the CR data, which has negative time values, describes accurately the expected background in the SR region, which has positive times. The systematic uncertainty in this assumption is determined by using the VR data, where the signal contribution is negligible and therefore the symmetry of the background around $t = 0$ ns can be tested quantitatively. Comparing the BDT distribution of the VR data with negative times with that of the VR data with positive times, the relative discrepancies increase monotonically toward the higher BDT score bins, and reach as high as 33% (84%) in the highest bin of the eBDT (γBDT)

score. These "non-closure" uncertainties are symmetrized about the central prediction and included as systematic uncertainties in the BDT background shape.

A systematic uncertainty in the shape of the signal BDT distribution arises due to uncertainties in the smearing of the time resolution. The MC simulation does not accurately describe the timing resolution in the data, and therefore the signal MC events are subjected to an additional smearing of the time. The smearing procedure consists of taking the raw time from the MC simulation, which already contains a model of the observed noise in the calorimeter, and adding additional correlated and uncorrelated components. The correlated component corresponds to the beam spread, and is therefore shared by all objects in the same event. The uncorrelated component is applied separately to each object and corresponds to different electronic and pileup noise assumptions and other global effects observed in comparisons between data and MC simulation. To determine an uncertainty in the signal BDT shape, the smearing is varied up and down within the experimental uncertainties, and the signal BDT shape is re-evaluated.

VII. COMMON SYSTEMATIC UNCERTAINTIES

Several sources of systematic uncertainties are evaluated for the prediction of signal model yields, both from the theoretical and experimental sides. The factorization and renormalization scales, α_S, parton distribution functions, and QCD radiation models are all varied to assess the impact on the simulated acceptance in the SRs. For the GMSB slepton model in the EM-BDT SR a 12% theory acceptance uncertainty is applied on the yield, while in the ABCD SRs the uncertainty varies between 10% and 30% in the excluded region. For the dark sector model, theory acceptance uncertainties in the yield in the ABCD SRs also vary between 10% and 30% in the excluded regions. The theory uncertainty in the total predicted cross section is not included as an additional uncertainty in the fit so that they are separated from experimental uncertainties and may easily be updating with future improvements to the predictions.

Experimental-based uncertainties in the modeling of leptons are determined in two parts. Electrons and muons are reconstructed with a track and calorimeter or MS information, respectively. These sub-detectors are sufficiently far from the PV relative to the displacements targeted in this search that the sub-detectors' performance, and simulation of said performance, should not differ by much from that for prompt leptons. Thus uncertainties in the tracking and calorimeter or MS information are separated in order to determine each in the most robust way. Additional uncertainties for displaced leptons are added to those derived for prompt leptons, which cover the calorimeter and MS portion of the leptons. Standard uncertainties in the modeling of photons are included; there are no additional displacement based uncertainties applied for photons other than that for the smearing of the time resolution described in Sec. VI C.

Uncertainties in reconstructed objects are propagated to the reconstruction of $E_{\mathrm{T}}^{\mathrm{miss}}$. Additional uncertainties in $E_{\mathrm{T}}^{\mathrm{miss}}$ come from varying the scale and resolution of the soft term, parallel and perpendicular to the hard term [78]. As $E_{\mathrm{T}}^{\mathrm{miss}}$ is used in selecting events with enhanced SM W production to define the EM-BDT VR, a systematic is assessed on the impact of $E_{\mathrm{T}}^{\mathrm{miss}}$-reconstruction uncertainties in the fitted EM-BDT score distributions. The migration of events from EM-BDT SRs to the EM-BDT VR was studied after redefining the VR using variations in $E_{\mathrm{T}}^{\mathrm{miss}}$. Based on this a 2% uncertainty in the signal yields in the EM-BDT SRs was assigned. For the γBDT, which uses $E_{\mathrm{T}}^{\mathrm{miss}}$ as an input variable, an additional uncertainty is evaluated by propagating the $E_{\mathrm{T}}^{\mathrm{miss}}$ systematic uncertainties into the γBDT score calculation and re-evaluating the γBDT shape. Uncertainties in $E_{\mathrm{T}}^{\mathrm{miss}}$ have no impact in the ABCD analysis since it is not used in the event selection.

The uncertainty in the modeling of LRT in offline reconstruction was determined from comparisons of data and MC simulation using K_S^0 vertices in Ref. [44]. These are parameterized in p_{T} and radius of the first hit on the track and vary from 0.3% to 16.8% per large-radius track.

Uncertainties in the simulated acceptance of the trigger for standard prompt leptons and photons are considered. Additional uncertainties in the LRT-based trigger acceptance are computed by comparing the trigger tracking efficiency with respect to offline tracks in data and MC simulation, as done in Ref. [37]. This amounts to an additional uncertainty of 11% for electrons and 2% for muons on top of the standard trigger uncertainties.

Standard corrections to the modeling of reconstruction, identification, and isolation requirements for leptons were computed with prompt $Z \to \ell\ell$ events using the same methods as described for electrons in Ref. [72] and muons in Ref. [73]. Uncertainties in the corrections for electrons are generally less than 11% for $p_{\mathrm{T}} > 30$ GeV; they rise to 70% for electrons with $p_{\mathrm{T}} < 20$ GeV. For muons the uncertainties in the corrections are generally less than 3%. An additional uncertainty in electron identification as a function of $|d_0|$ is assessed by comparing the relative loss in efficiency between the VeryLoose and Loose WPs of signal MC simulation; this amounts to an uncertainty of 16% per electron. For muons, the MS is sufficiently far away from the PV, and their identification does not make use of a likelihood discriminant. Thus, no additional displacement-based uncertainty is applied.

Part of the uncertainties in the ABCD background predictions come from the propagation of statistical uncertainties in the yield in each region. These range from plus 0.003–0.4 events on a predicted central value of less than one event in each SR, see Table III. The negative variation is capped so that the expected yield is not negative. The other set of uncertainties are those described in Sec. V C on

TABLE III. Expected and observed yields in the signal regions and model-independent upper limits derived using pseudo-experiments. Left to right: total expected background after a background-only fit, with the combined statistical and systematic uncertainties; number of events observed in data; and the 95% confidence level (CL) upper limits on the visible cross section ($\langle A\epsilon\sigma\rangle^{95}_{\text{obs}}$) and on the number of signal events (S^{95}_{obs}). The sixth column (S^{95}_{exp}) shows the expected 95% CL upper limit on the number of signal events, given the expected number (and $\pm 1\sigma$ excursions of the expectation) of background events. The last two columns indicate the confidence level of the background-only hypothesis (CL_b) and discovery p-value with the corresponding Gaussian significance [$Z(s=0)$]. CL_b provides a measure of compatibility of the observed data with the signal strength hypothesis at the 95% CL limit relative to fluctuations of the background, and $p(s=0)$ measures compatibility of the observed data with the background-only hypothesis relative to fluctuations of the background. The p-value is capped at 0.5.

Signal region	Total Bkg.	N_{obs}	$\langle A\epsilon\sigma\rangle^{95}_{\text{obs}}$ [fb]	S^{95}_{obs}	S^{95}_{exp}	CL_b	$p(s=0)$ (Z)
ee high-p_T (Run 2)	0.031, 0.031	0	0.02	3.0	$3.0^{+0.0}_{-0.0}$	0.46	0.5 (0)
ee high-p_T (Run 3)	0.06, 0.05	0	0.05	3.0	$3.0^{+0.0}_{-0.1}$	0.45	0.5 (0)
ee LRT	$0.0016^{+0.0029}_{-0.0016}$	1	0.07	4.1	$3.0^{+0.0}_{-0.1}$	0.97	0.01 (2.2)
$\mu\mu$ high-p_T (Run 2)	$0.02^{+0.22}_{-0.02}$	0	0.02	3.0	$3.0^{+0.0}_{-0.0}$	0.49	0.5 (0)
$\mu\mu$ high-p_T (Run 3)	$0.01^{+0.11}_{-0.01}$	0	0.05	3.0	$3.0^{+0.0}_{-0.0}$	0.48	0.5 (0)
$\mu\mu$ LRT	$0.02^{+0.04}_{-0.02}$	0	0.05	3.0	$3.0^{+0.0}_{-0.0}$	0.49	0.5 (0)
$e\mu$ high-p_T (Run 2)	$0.0016^{+0.0033}_{-0.0016}$	0	0.02	3.0	$3.0^{+0.0}_{-0.1}$	0.50	0.5 (0)
$e\mu$ high-p_T (Run 3)	$0.004^{+0.010}_{-0.004}$	0	0.05	3.0	$3.0^{+0.0}_{-0.0}$	0.50	0.5 (0)
$e\mu$ LRT	$0.2^{+0.4}_{-0.2}$	0	0.05	3.0	$3.0^{+0.1}_{-0.1}$	0.45	0.5 (0)
EM-BDT	$1.0^{+2.3}_{-0.9}$	3	0.13	7.1	$5.7^{+1.9}_{-0.8}$	0.77	0.2 (0.9)

the FHF and cosmics muon background predictions. The uncertainty on the FHF prediction ranges from 30% to 210%. The uncertainties on the cosmics muon background prediction, 2%–81%, have no impact on the analysis as the prediction is of the order 10^{-3}. The results in the ABCD SRs are dominated by Poisson statistical uncertainty on the yield. The dominant uncertainty in the signal prediction in the ABCD SRs depends on the region and signal model. Typical ranges for uncertainties are: 11%–40% for the number of MC simulation events, 25% for the signal theory acceptance, 10%–40% for the uncertainty in LRT, 1%–15% for muon modeling, and 20%–30% for electron modeling.

The uncertainty in the BDT backgrounds are dominated by the shape uncertainties, except for the most sensitive bin where the number of CR events is low and the statistical uncertainty is large. The dominant uncertainties for the eBDT are the electron modeling at 21%, the theory acceptance uncertainty at 12%, and the statistical uncertainty in the number of simulated events in the most sensitive bins at 7%. The dominant uncertainties for the γBDT are the signal acceptance uncertainty of 12%, and the statistical uncertainty in the number of simulated events in the two most sensitive bins at 11% and 4%. For both the ABCD and EM-BDT regions, the uncertainty in the

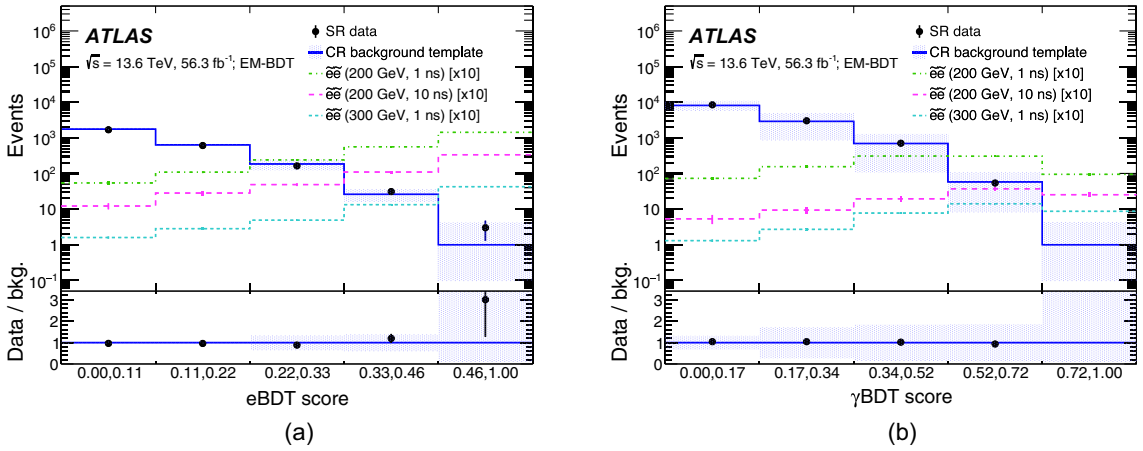

FIG. 5. BDT score distributions for (a) the eBDT and (b) the γBDT comparing the expected yields from the control region to the observed data. Selectron pair-production models with a mass of 300 GeV and a lifetime of 1 ns and a mass of 200 GeV with a lifetime of 1 ns or 10 ns are overlaid with 10 times the expected yield. The lower panel is the ratio of the observed data over the expected background.

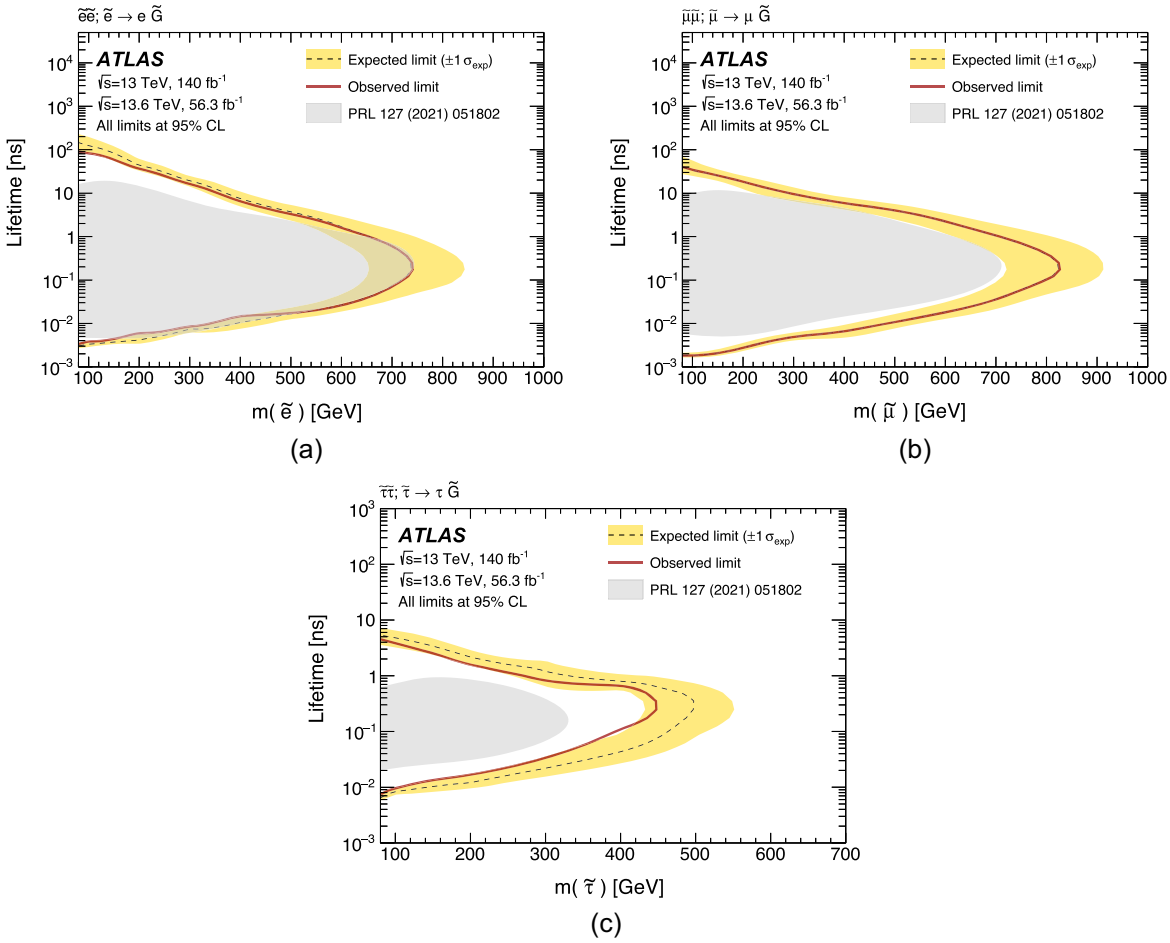

FIG. 6. Expected and observed 95% CL exclusion contours for (a) the selectron, (b) smuon, (c) and stau models. The selectron and stau limits are computed using both the ABCD and EM-BDT regions, while the smuon limits are from the ABCD regions only. The dashed line indicates the expected limit, and the surrounding band shows the 1σ variation of the expected limit due to uncertainties in the background prediction and experimental uncertainties in the signal modeling. The gray shaded area illustrates the observed exclusion obtained in the prior ATLAS Run 2 analysis [23].

lifetime reweighting, discussed in the next section, may be the dominant uncertainty when used.

VIII. RESULTS

Each of the orthogonal ABCD signal regions is used individually to compare the observed data yield with the expected background, the results of which are used as "discovery regions" to set model-independent limits on the production of displaced leptons; for the ABCD high-p_{T} analyses, these are quoted separately for the Run 2 and Run 3 data, due to the different center-of-mass energies, resulting in a total of nine orthogonal ABCD discovery regions. An EM-BDT discovery region is defined as the most signal-like bin of the eBDT distribution (eBDT score > 0.46) and is used to set model-independent limits on the production of displaced electrons. All model-independent limits are derived using pseudo-experiments. Model-dependent limits on the long-lived slepton model are obtained by performing a simultaneous fit to the eBDT and γBDT distributions, as well as the nine ABCD SRs. Only the ABCD SRs are used for the dark sector model. The EM-BDT SRs would be sensitive to some semi-hadronic decays, but the MC simulation only includes decays to two leptons; thus it was not included for limit setting.

Only one event is observed among the nine orthogonal ABCD signal regions, namely in the SRee-LRT region. The observed and expected yields in the orthogonal ABCD signal regions are presented in Table III. Corresponding model-independent upper limits on the visible BSM cross sections, the observed and expected limits on the number of non-SM events, and the p-values and corresponding local Z scores are also shown. The one event observed in the SRee-LRT region, compared to the background expectation of $0.0016^{+0.0029}_{-0.0016}$ events, corresponds to a local significance of 2.2σ.

The observed BDT distributions in the SRs of the eBDT and γBDT analyses are shown in Fig. 5. Shown superimposed are the background shapes as determined using the

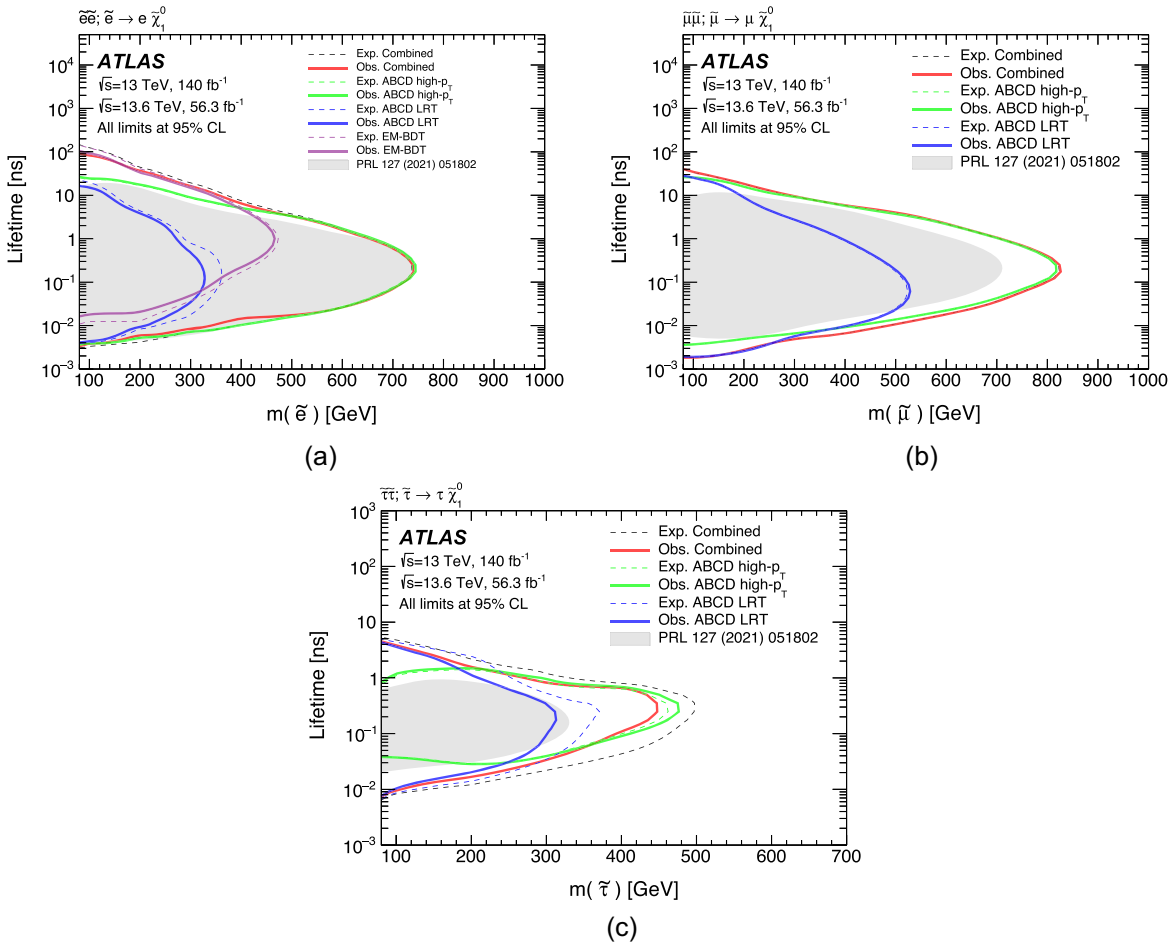

FIG. 7. Comparison of expected and observed 95% CL exclusion contours for (a) the selectron, (b) smuon, and (c) stau models for subsets of the analysis regions ABCD high-p_{T}, ABCD LRT, and EM-BDT. For the stau model, the EM-BDT SRs do not exclude any points by themselves. The dashed lines indicate the expected limits. The gray shaded area illustrates the observed exclusion obtained in the prior ATLAS Run 2 analysis [23].

CR data and example GMSB signal models with selectrons. The lower panels in the figures show the bin-by-bin ratios of the data divided by the background and illustrate that the observed SR data are consistent with the background expectation. Defining the EM-BDT discovery region as the most signal-like bin of the eBDT yields a background expectation of one event. The uncertainty in this background estimate is dominated by the statistical uncertainty resulting from the fact that it is determined from a single CR event in this bin of the eBDT, plus a systematic uncertainty of ± 0.33 from the other sources of uncertainty described previously. A total of 3 events are observed in the EM-BDT discovery region, corresponding to a local significance of 0.9σ; this result is included as the last row of Table III.

The combined ABCD and EM-BDT results are used to set exclusion contours on the GMSB stau and selectron models in the two-dimensional plane of slepton lifetime versus slepton mass. Only the ABCD results are used for the smuon and dark sector models. The combination is obtained by simultaneously fitting all included regions, using a single fit parameter to describe the signal strength. Thus the 13.6 to 13 TeV cross section ratio is taken from the theoretical prediction. To improve the interpolation between generated signal models with different lifetimes, a reweighting procedure is used to estimate the signal acceptances for lifetimes that were not included in the MC sample described in Sec. III and corresponding uncertainties in the signal yields are included in the fit. A 20% signal normalization uncertainty was assessed for reweighting to lifetimes up to 100 ns, increasing to 50% for reweighting to even higher lifetimes, where the uncertainties are based on comparing reweighted samples to simulated samples with the same lifetime.

The 95% CL exclusion contours for long-lived selectrons, smuons, and staus are shown in Fig. 6. Results from the prior Run 2 analysis [23] are also included. The excluded regions from the current analysis extend to significantly higher slepton masses and much higher slepton lifetimes. For example, selectrons with a mass of

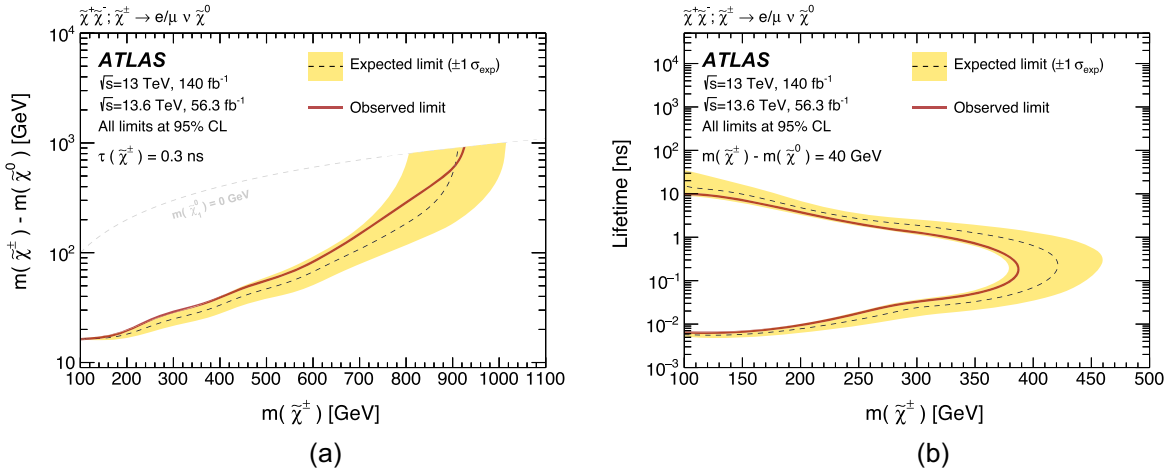

FIG. 8. Expected and observed 95% CL exclusion contours for the dark sector model with the (a) fixed lifetime and (b) fixed mass splitting. The dashed line indicates the expected limit, and the surrounding band shows the 1σ variation of the expected limit due to uncertainties in the background prediction and experimental uncertainties in the signal modeling.

150 GeV are excluded for lifetime values ranging from 4 ps to 60 ns, while selectrons, smuons, and staus with a lifetime of 0.3 ns are excluded up to 740, 830, and 440 GeV, respectively. The improvement in sensitivity for long lifetimes for selectrons with lower masses is due to the EM-BDT and new LRT-based triggers. For smuons, in addition to the LRT-based triggers, the improved sensitivity is due to better trigger acceptance for muons in the forward region. The sensitivity to stau models benefits from all of the improvements above and especially from the new LRT triggers since the leptons tend to have lower p_{T}. This is illustrated in Fig. 7, which overlays the exclusion contours for the ABCD high-p_{T}, ABCD LRT, and EM-BDT SRs. The difference between the expected and observed exclusion contours is due to the observed events in the ee LRT and EM-BDT SRs. Thus the combined observed limit, including the observed events, can be worse than the standalone high-p_{T} limit where no events were observed. The difference between the expected and observed exclusion contours for the stau model comes from the observed event in the ABCD LRT region as the EM-BDT sensitivity is sub-dominant for the mixed flavor final-state from the staus. All models benefit at high masses from the additional Run 3 data.

The 95% CL exclusion contours for the dark sector model are shown in Fig. 8. For a lifetime of $\tau = 0.3$ ns, mass differences down to $\Delta m = 16$ GeV are excluded for a chargino mass of 100 GeV, and charginos with masses up to 900 GeV are excluded for large values of Δm. For a mass difference of $\Delta m = 40$ GeV, charginos with masses up to 380 GeV are excluded, and chargino lifetimes of $0.006 < \tau < 10$ ns for a chargino mass of 100 GeV are

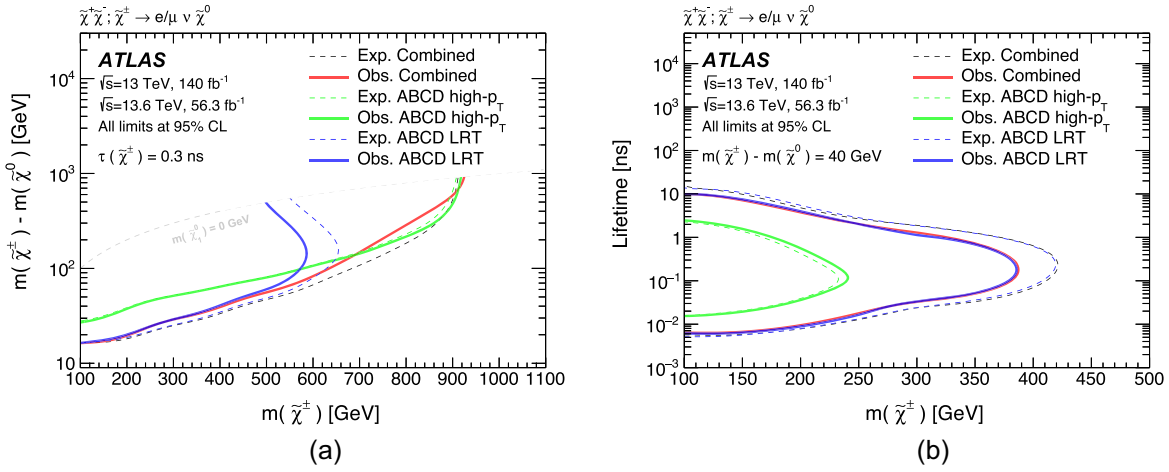

FIG. 9. Comparison of expected and observed 95% CL exclusion contours for the dark sector model with the (a) fixed-lifetime and (b) fixed-mass-splitting for subsets of the analysis regions ABCD high-p_{T} and ABCD LRT. The dashed lines indicate the expected limits.

excluded. Similar to the exclusion contour overlays for the slepton models, Fig. 9 illustrates the sensitivity to the chargino models for the ABCD high-p_{T} SRs at larger masses and sensitivity of the ABCD LRT SRs to the theoretically preferred small-mass-splittings between 10 and 40 GeV [35].

IX. CONCLUSION

A search for BSM physics using 56.3 fb^{-1} of proton-proton collision data collected by the ATLAS detector at the LHC during 2022–2023 with $\sqrt{s} = 13.6$ TeV, combined with the full Run 2 dataset in some regions, was presented. The analysis focuses on the signature of displaced electrons or muons, consistent with the decay of a long-lived BSM particle. The event selection exploits new Run 3 triggers that employ LRT for sensitivity to lower momentum final state particles. Two orthogonal approaches are used, one focusing on dilepton events and another using LAr measurements and multivariate techniques for expanded sensitivity to single-electron and photon-reconstructed events.

The observed event yields in the various signal regions are consistent with the SM background expectations. The results are therefore used to set model-independent limits on the production of displaced electrons and muons. The combined analysis results are interpreted with two models. The first is a GMSB model with pair-produced long-lived sleptons that decay into the lepton of the same flavor and a nearly massless gravitino, providing exclusion contours that extend significantly beyond previous results. For example, 95% CL exclusions are obtained for selectrons with a mass of 150 GeV and lifetime values ranging from 4 ps to 60 ns, and selectrons, smuons, and staus with a 0.3 ns lifetime are excluded up to masses of 740, 830, and 440 GeV, respectively. The second model is pair-produced dark charginos decaying into a W boson and neutralino, where small mass splittings of 10–40 GeV result in a dark matter relic density consistent with observations. Similarly, 95% CL are set for charginos with masses up to 380 GeV for a mass difference with the neutralino of 40 GeV, and mass differences down to 17 GeV are excluded for dark charginos with a 100 GeV mass.

ACKNOWLEDGMENTS

We thank CERN for the very successful operation of the LHC and its injectors, as well as the support staff at CERN and at our institutions worldwide without whom ATLAS could not be operated efficiently. The crucial computing support from all WLCG partners is acknowledged gratefully, in particular from CERN, the ATLAS Tier-1 facilities at TRIUMF/SFU (Canada), NDGF (Denmark, Norway, Sweden), CC-IN2P3 (France), KIT/GridKA (Germany), INFN-CNAF (Italy), NL-T1 (Netherlands), PIC (Spain), RAL (UK) and BNL (USA), the Tier-2 facilities worldwide and large non-WLCG resource providers. Major contributors of computing resources are listed in Ref. [79]. We gratefully acknowledge the support of ANPCyT, Argentina; YerPhI, Armenia; ARC, Australia; BMWFW and FWF, Austria; ANAS, Azerbaijan; CNPq and FAPESP, Brazil; NSERC, NRC and CFI, Canada; CERN; ANID, Chile; CAS, MOST and NSFC, China; Minciencias, Colombia; MEYS CR, Czech Republic; DNRF and DNSRC, Denmark; IN2P3-CNRS and CEA-DRF/IRFU, France; SRNSFG, Georgia; BMBF, HGF and MPG, Germany; GSRI, Greece; RGC and Hong Kong SAR, China; ISF and Benoziyo Center, Israel; INFN, Italy; MEXT and JSPS, Japan; CNRST, Morocco; NWO, Netherlands; RCN, Norway; MNiSW, Poland; FCT, Portugal; MNE/IFA, Romania; MSTDI, Serbia; MSSR, Slovakia; ARIS and MVZI, Slovenia; DSI/NRF, South Africa; MICIU/AEI, Spain; SRC and Wallenberg Foundation, Sweden; SERI, SNSF and Cantons of Bern and Geneva, Switzerland; NSTC, Taipei; TENMAK, Türkiye; STFC/UKRI, United Kingdom; DOE and NSF, United States of America. Individual groups and members have received support from BCKDF, CANARIE, CRC and DRAC, Canada; CERN-CZ, FORTE and PRIMUS, Czech Republic; COST, ERC, ERDF, Horizon 2020, ICSC-NextGenerationEU and Marie Skłodowska-Curie Actions, European Union; Investissements d'Avenir Labex, Investissements d'Avenir Idex and ANR, France; DFG and AvH Foundation, Germany; Herakleitos, Thales and Aristeia programmes co-financed by EU-ESF and the Greek NSRF, Greece; BSF-NSF and MINERVA, Israel; NCN and NAWA, Poland; La Caixa Banking Foundation, CERCA Programme Generalitat de Catalunya and PROMETEO and GenT Programmes Generalitat Valenciana, Spain; Göran Gustafssons Stiftelse, Sweden; The Royal Society and Leverhulme Trust, United Kingdom. In addition, individual members wish to acknowledge support from Armenia: Yerevan Physics Institute (FAPERJ); CERN: European Organization for Nuclear Research (CERN PJAS); Chile: Agencia Nacional de Investigación y Desarrollo (Grants No. FONDECYT 1230812, No. FONDECYT 1230987, No. FONDECYT 1240864); China: Chinese Ministry of Science and Technology (Grants No. MOST-2023YFA1605700, No. MOST-2023YFA1609300), National Natural Science Foundation of China (Grants No. NSFC-12175119, No. NSFC-12275265, No. NSFC-12075060); Czech Republic: Czech Science Foundation (Grant No. GAC–24-11373S), Ministry of Education Youth and Sports (Grants No. ERC-CZ-LL2327, No. FORTE CZ.02.01.01/00/22_008/0004632), PRIMUS Research Programme (Grant No. PRIMUS/21/SCI/017); EU: H2020 European Research Council (Grant No. ERC-101002463); European Union: European Research Council (Grants No. ERC-948254, No. ERC-101089007), Horizon 2020 Framework Programme (Grant

No. MUCCA–CHIST-ERA-19-XAI-00), European Union, Future Artificial Intelligence Research (FAIR-NextGenerationEU Grant No. PE00000013), Italian Center for High Performance Computing, Big Data and Quantum Computing (ICSC, NextGenerationEU); France: Agence Nationale de la Recherche (Grants No. ANR-20-CE31-0013, No. ANR-21-CE31-0013, No. ANR-21-CE31-0022, No. ANR-22-EDIR-0002), Investissements d'Avenir Labex (Grant No. ANR-11-LABX-0012); Germany: Baden-Württemberg Stiftung (BW Stiftung-Postdoc Eliteprogramme), Deutsche Forschungsgemeinschaft (Grants No. DFG-469666862, No. DFG-CR 312/5-2); Italy: Istituto Nazionale di Fisica Nucleare (ICSC, NextGenerationEU), Ministero dell'Università e della Ricerca (NextGenEU Grant No. I53D23000820006 M4C2.1.1); Japan: Japan Society for the Promotion of Science (Grants No. JSPS KAKENHI JP22H01227, No. JSPS KAKENHI JP22H04944, No. JSPS KAKENHI JP22KK0227, No. JSPS KAKENHI JP23KK0245); Netherlands: Netherlands Organisation for Scientific Research (Grant No. NWO Veni 2020–VI.Veni.202.179); Norway: Research Council of Norway (Grant No. RCN-314472); Poland: Ministry of Science and Higher Education (IDUB AGH, POB8, D4 no 9722), Polish National Agency for Academic Exchange (Grant No. PPN/PPO/2020/1/00002/U/00001), Polish National Science Centre (Grants No. NCN 2021/42/E/ST2/00350, No. NCN OPUS nr 2022/47/B/ST2/03059, No. NCN UMO-2019/34/E/ST2/00393, No. NCN & H2020 MSCA 945339, No. UMO-2020/37/B/ST2/01043, No. UMO-2021/40/C/ST2/00187, No. UMO-2022/47/O/ST2/00148, UMO-2023/49/B/ST2/04085, No. UMO-2023/51/B/ST2/00920); Portugal: Foundation for Science and Technology (FCT); Slovenia: Slovenian Research Agency (ARIS Grant No. J1-3010); Spain: Generalitat Valenciana (Artemisa, FEDER, IDIFEDER/2018/048), Ministry of Science and Innovation (MCIN & NextGenEU Grants No. PCI2022-135018-2, MICIN & FEDER No. PID2021-125273NB, No. RYC2019-028510-I, No. RYC2020-030254-I, No. RYC2021-031273-I, No. RYC2022-038164-I); Sweden: Carl Trygger Foundation Grant No. CTS-22:2312), Swedish Research Council (Grants No. VR 2023-04654, No. VR 2018-00482, No. VR 2021-03651, No. VR 2022-03845, No. VR 2022-04683, No. VR 2023-03403), Knut and Alice Wallenberg Foundation (Grants No. KAW 2018.0458, No. KAW 2019.0447, No. KAW 2022.0358); Switzerland: Swiss National Science Foundation (Grant No. SNSF–PCEFP2_194658); United Kingdom: Leverhulme Trust (Grant No. RPG-2020-004), Royal Society (Grant No. NIF-R1-231091); United States of America: U.S. Department of Energy (Grant No. ECA DE-AC02-76SF00515), Neubauer Family Foundation.

DATA AVAILABILITY

The data that support the findings of this article are not publicly available upon publication because it is not technically feasible and/or the cost of preparing, depositing, and hosting the data would be prohibitive within the terms of this research project. The data are available from the authors upon reasonable request.

[1] G. R. Farrar and P. Fayet, Phenomenology of the production, decay, and detection of new hadronic states associated with supersymmetry, Phys. Lett. **76B**, 575 (1978).
[2] Y. Golfand and E. Likhtman, Extension of the algebra of poincare group generators and violation of P invariance, Pis'ma Zh. Eksp. Teor. Fiz. **13**, 452 (1971) [JETP Lett. **13**, 323 (1971)].
[3] D. Volkov and V. Akulov, Is the neutrino a goldstone particle?, Phys. Lett. **46B**, 109 (1973).
[4] J. Wess and B. Zumino, Supergauge transformations in four dimensions, Nucl. Phys. **B70**, 39 (1974).
[5] J. Wess and B. Zumino, Supergauge invariant extension of quantum electrodynamics, Nucl. Phys. **B78**, 1 (1974).
[6] S. Ferrara and B. Zumino, Supergauge invariant Yang-Mills theories, Nucl. Phys. **B79**, 413 (1974).
[7] A. Salam and J. Strathdee, Super-symmetry and non-Abelian gauges, Phys. Lett. **51B**, 353 (1974).
[8] R. Barbier *et al.*, R-parity-violating supersymmetry, Phys. Rep. **420**, 1 (2005).
[9] B. C. Allanach, M. A. Bernhardt, H. K. Dreiner, C. H. Kom, and P. Richardson, Mass spectrum in R-parity violating minimal supergravity and benchmark points, Phys. Rev. D **75**, 035002 (2007).
[10] G. Giudice and A. Romanino, Split supersymmetry, Nucl. Phys. **B699**, 65 (2004); **B706**, 487(E) (2005).
[11] N. Arkani-Hamed and S. Dimopoulos, Supersymmetric unification without low energy supersymmetry and signatures for fine-tuning at the LHC, J. High Energy Phys. 06 (2005) 073.
[12] M. Dine and W. Fischler, A phenomenological model of particle physics based on supersymmetry, Phys. Lett. **110B**, 227 (1982).
[13] L. Alvarez-Gaumé, M. Claudson, and M. B. Wise, Low-energy supersymmetry, Nucl. Phys. **B207**, 96 (1982).
[14] C. R. Nappi and B. A. Ovrut, Supersymmetric extension of the $SU(3) \times SU(2) \times U(1)$ model, Phys. Lett. **113B**, 175 (1982).
[15] T. Appelquist, H.-C. Cheng, and B. A. Dobrescu, Bounds on universal extra dimensions, Phys. Rev. D **64**, 035002 (2001).

[16] H.-C. Cheng, K. T. Matchev, and M. Schmaltz, Bosonic supersymmetry? Getting fooled at the CERN LHC, Phys. Rev. D **66**, 056006 (2002).

[17] M. J. Strassler, Possible effects of a hidden valley on supersymmetric phenomenology, arXiv:hep-ph/0607160.

[18] L. Evans and P. Bryant, LHC machine, J. Instrum. **3**, S08001 (2008).

[19] J. Alwall, M.-P. Le, M. Lisanti, and J. G. Wacker, Searching for directly decaying gluinos at the Tevatron, Phys. Lett. B **666**, 34 (2008).

[20] J. Alwall, P. C. Schuster, and N. Toro, Simplified models for a first characterization of new physics at the LHC, Phys. Rev. D **79**, 075020 (2009).

[21] D. Alves *et al.*, Simplified models for LHC new physics searches, J. Phys. G **39**, 105005 (2012).

[22] J. A. Evans and J. Shelton, Long-lived staus and displaced leptons at the LHC, J. High Energy Phys. 04 (2016) 056.

[23] ATLAS Collaboration, Search for displaced leptons in $\sqrt{s} = 13$ TeV pp collisions with the ATLAS detector, Phys. Rev. Lett. **127**, 051802 (2021).

[24] ALEPH Collaboration, Search for gauge mediated SUSY breaking topologies in ee collisions at centre-of-mass energies up to 209 GeV, Eur. Phys. J. C **25**, 339 (2002).

[25] OPAL Collaboration, Searches for gauge-mediated supersymmetry breaking topologies in e^+e^- collisions at centre-of-mass energies up to $\sqrt{s} = 209$ GeV, Eur. Phys. J. C **46**, 307 (2006).

[26] DELPHI Collaboration, Searches for supersymmetric particles in e^+e^- collisions up to 208 GeV and interpretation of the results within the MSSM, Eur. Phys. J. C **31**, 421 (2003).

[27] DELPHI Collaboration, Search for supersymmetric particles in light gravitino scenarios and sleptons NLSP, Eur. Phys. J. C **27**, 153 (2003).

[28] LEPSUSYWG, ALEPH, DELPHI, L3, and OPAL Experiments Collaborations, Combined LEP GMSB Stau/Smuon/Selectron Results, 189–208 GeV, Report No. LEPSUSYWG/02-09.2, 2002, http://lepsusy.web.cern.ch/lepsusy/www/gmsb_summer02/lepgmsb.html.

[29] CMS Collaboration, Search for long-lived particles decaying to leptons with large impact parameter in proton–proton collisions at $\sqrt{s} = 13$ TeV, Eur. Phys. J. C **82**, 153 (2022).

[30] ATLAS Collaboration, Search for pairs of muons with small displacements in pp collisions at $\sqrt{s} = 13$ TeV with the ATLAS detector, Phys. Lett. B **846**, 138172 (2023).

[31] ATLAS Collaboration, Search for long-lived charginos based on a disappearing-track signature using 136 fb^{-1} of pp collisions at $\sqrt{s} = 13$ TeV with the ATLAS detector, Eur. Phys. J. C **82**, 606 (2022).

[32] A. Hayrapetyan *et al.*, Search for supersymmetry in final states with disappearing tracks in proton-proton collisions at $\sqrt{s} = 13$ TeV, Phys. Rev. D **109**, 072007 (2024).

[33] ATLAS Collaboration, Search for heavy, long-lived, charged particles with large ionisation energy loss in pp collisions at $\sqrt{s} = 13$ TeV using the ATLAS experiment and the full Run 2 dataset, J. High Energy Phys. 06 (2023) 158.

[34] A. Filimonova and S. Westhoff, Long live the Higgs portal!, J. High Energy Phys. 02 (2019) 140.

[35] F. Blekman, N. Desai, A. Filimonova, A. R. Sahasransu, and S. Westhoff, Soft displaced leptons at the LHC, J. High Energy Phys. 11 (2020) 112.

[36] ATLAS Collaboration, Software performance of the ATLAS track reconstruction for LHC run 3, Comput. Software Big Sci. **8**, 9 (2023).

[37] ATLAS Collaboration, The ATLAS trigger system for LHC Run 3 and trigger performance in 2022, J. Instrum. **19**, P06029 (2024).

[38] ATLAS Collaboration, Search in diphoton and dielectron final states for displaced production of Higgs or Z bosons with the ATLAS detector in $\sqrt{s} = 13$ TeV pp collisions, Phys. Rev. D **108**, 012012 (2023).

[39] ATLAS Collaboration, Search for displaced photons produced in exotic decays of the Higgs boson using 13 TeV pp collisions with the ATLAS detector, Phys. Rev. D **108**, 032016 (2023).

[40] ATLAS Collaboration, The ATLAS experiment at the CERN large hadron collider, J. Instrum. **3**, S08003 (2008).

[41] ATLAS Collaboration, The ATLAS experiment at the CERN large hadron collider: A description of the detector configuration for Run 3, J. Instrum. **19**, P05063 (2024).

[42] ATLAS Collaboration, Performance of the ATLAS trigger system in 2015, Eur. Phys. J. C **77**, 317 (2017).

[43] ATLAS Collaboration, Software and computing for Run 3 of the ATLAS experiment at the LHC, Eur. Phys. J. C **85**, 234 (2025).

[44] ATLAS Collaboration, Performance of the reconstruction of large impact parameter tracks in the inner detector of ATLAS, Eur. Phys. J. C **83**, 1081 (2023).

[45] ATLAS Collaboration, ATLAS data quality operations and performance for 2015–2018 data-taking, J. Instrum. **15**, P04003 (2020).

[46] ATLAS Collaboration, Luminosity determination in pp collisions at $\sqrt{s} = 13$ TeV using the ATLAS detector at the LHC, Eur. Phys. J. C **83**, 982 (2023).

[47] ATLAS Collaboration, Preliminary analysis of the luminosity calibration of the ATLAS 13.6 TeV data recorded in 2022, Report No. ATL-DAPR-PUB-2023-001, 2023, https://cds.cern.ch/record/2853525.

[48] ATLAS Collaboration, Preliminary analysis of the luminosity calibration for the ATLAS 13.6 TeV data recorded in 2023, Report No. ATL-DAPR-PUB-2024-001, 2024, https://cds.cern.ch/record/2900949.

[49] G. Avoni *et al.*, The new LUCID-2 detector for luminosity measurement and monitoring in ATLAS, J. Instrum. **13**, P07017 (2018).

[50] ATLAS Collaboration, Performance of electron and photon triggers in ATLAS during LHC Run 2, Eur. Phys. J. C **80**, 47 (2020).

[51] ATLAS Collaboration, Performance of the ATLAS muon triggers in Run 2, J. Instrum. **15**, P09015 (2020).

[52] ATLAS Collaboration, The ATLAS inner detector trigger performance in pp collisions at 13 TeV during LHC Run 2, Eur. Phys. J. C **82**, 206 (2022).

[53] J. Alwall, R. Frederix, S. Frixione, V. Hirschi, F. Maltoni, O. Mattelaer, H.-S. Shao, T. Stelzer, P. Torrielli, and M. Zaro, The automated computation of tree-level and next-to-leading

order differential cross sections, and their matching to parton shower simulations, J. High Energy Phys. 07 (2014) 079.
[54] T. Sjöstrand, S. Ask, J. R. Christiansen, R. Corke, N. Desai, P. Ilten, S. Mrenna, S. Prestel, C. O. Rasmussen, and P. Z. Skands, An introduction to PYTHIA 8.2, Comput. Phys. Commun. **191**, 159 (2015).
[55] ATLAS Collaboration, ATLAS PYTHIA 8 tunes to 7 TeV data, Report No. ATL-PHYS-PUB-2014-021, 2014, https://cds.cern.ch/record/1966419.
[56] R. D. Ball *et al.* (NNPDF Collaboration), Parton distributions with LHC data, Nucl. Phys. **B867**, 244 (2013).
[57] S. Agostinelli *et al.*, Geant4—a simulation toolkit, Nucl. Instrum. Methods Phys. Res., Sect. A **506**, 250 (2003).
[58] ATLAS Collaboration, Emulating the impact of additional proton–proton interactions in the ATLAS simulation by presampling sets of inelastic Monte Carlo events, Comput. Software Big Sci. **6**, 3 (2022).
[59] S. Porteboeuf, T. Pierog, and K. Werner, Producing hard processes regarding the complete event: The EPOS event generator, *Proceedings of the 45th Rencontres de Moriond on QCD and High Energy Interactions, Gioi Publishers* (2010), p. 135, arXiv:1006.2967.
[60] T. Pierog, I. Karpenko, J. M. Katzy, E. Yatsenko, and K. Werner, EPOS LHC: Test of collective hadronization with data measured at the CERN large hadron collider, Phys. Rev. C **92**, 034906 (2015).
[61] C. Bierlich *et al.*, A comprehensive guide to the physics and usage of PYTHIA 8.3, SciPost Phys. Codebases 8 (2022).
[62] ATLAS Collaboration, The PYTHIA 8 A3 tune description of ATLAS minimum bias and inelastic measurements incorporating the Donnachie–Landshoff diffractive model, Report No. ATL-PHYS-PUB-2016-017, 2016, https://cds.cern.ch/record/2206965.
[63] W. Beenakker, M. Klasen, M. Krämer, T. Plehn, M. Spira, and P. M. Zerwas, Production of charginos, neutralinos, and sleptons at hadron colliders, Phys. Rev. Lett. **83**, 3780 (1999); **100**, 029901(E) (2008).
[64] J. Debove, B. Fuks, and M. Klasen, Threshold resummation for gaugino pair production at hadron colliders, Nucl. Phys. **B842**, 51 (2011).
[65] B. Fuks, M. Klasen, D. R. Lamprea, and M. Rothering, Gaugino production in proton-proton collisions at a center-of-mass energy of 8 TeV, J. High Energy Phys. 10 (2012) 081.
[66] B. Fuks, M. Klasen, D. R. Lamprea, and M. Rothering, Precision predictions for electroweak superpartner production at hadron colliders with resummino, Eur. Phys. J. C **73**, 2480 (2013).
[67] J. Fiaschi and M. Klasen, Neutralino-chargino pair production at NLO + NLL with resummation-improved parton density functions for LHC Run II, Phys. Rev. D **98**, 055014 (2018).
[68] G. Bozzi, B. Fuks, and M. Klasen, Threshold resummation for slepton-pair production at hadron colliders, Nucl. Phys. **B777**, 157 (2007).
[69] B. Fuks, M. Klasen, D. R. Lamprea, and M. Rothering, Revisiting slepton pair production at the large hadron collider, J. High Energy Phys. 01 (2014) 168.
[70] J. Fiaschi and M. Klasen, Slepton pair production at the LHC in NLO + NLL with resummation-improved parton densities, J. High Energy Phys. 03 (2018) 094.
[71] J. Fiaschi, B. Fuks, M. Klasen, and A. Neuwirth, Electroweak superpartner production at 13.6 Tev with Resummino, Eur. Phys. J. C **83**, 707 (2023).
[72] ATLAS Collaboration, Electron and photon performance measurements with the ATLAS detector using the 2015–2017 LHC proton-proton collision data, J. Instrum. **14**, P12006 (2019).
[73] ATLAS Collaboration, Muon reconstruction and identification efficiency in ATLAS using the full Run 2 pp collision data set at $\sqrt{s} = 13$ TeV, Eur. Phys. J. C **81**, 578 (2021).
[74] ATLAS Collaboration, Search for long-lived, massive particles in events with a displaced vertex and a muon with large impact parameter in pp collisions at $\sqrt{s} = 13$ TeV with the ATLAS detector, Phys. Rev. D **102**, 032006 (2020).
[75] ATLAS Collaboration, Jet reconstruction and performance using particle flow with the ATLAS detector, Eur. Phys. J. C **77**, 466 (2017).
[76] M. Cacciari, G. P. Salam, and G. Soyez, FastJet user manual, Eur. Phys. J. C **72**, 1896 (2012).
[77] M. Cacciari, G. P. Salam, and G. Soyez, The anti-k_t jet clustering algorithm, J. High Energy Phys. 04 (2008) 063.
[78] ATLAS Collaboration, The performance of missing transverse momentum reconstruction and its significance with the ATLAS detector using 140 fb^{-1} of $\sqrt{s} = 13$ TeV pp collisions, arXiv:2402.05858.
[79] ATLAS Collaboration, ATLAS computing acknowledgements, Report No. ATL-SOFT-PUB-2025-001, 2025, https://cds.cern.ch/record/2922210.

G. Aad,[105] E. Aakvaag,[17] B. Abbott,[124] S. Abdelhameed,[120a] K. Abeling,[57] N. J. Abicht,[51] S. H. Abidi,[30] M. Aboelela,[46] A. Aboulhorma,[36e] H. Abramowicz,[156] H. Abreu,[155] Y. Abulaiti,[121] B. S. Acharya,[71a,71b,b] A. Ackermann,[65a] C. Adam Bourdarios,[4] L. Adamczyk,[88a] S. V. Addepalli,[27] M. J. Addison,[104] J. Adelman,[119] A. Adiguzel,[22c] T. Adye,[138] A. A. Affolder,[140] Y. Afik,[41] M. N. Agaras,[13] A. Aggarwal,[103] C. Agheorghiesei,[28c] F. Ahmadov,[40,c] S. Ahuja,[98] X. Ai,[64e] G. Aielli,[78a,78b] A. Aikot,[168] M. Ait Tamlihat,[36e] B. Aitbenchikh,[36a] M. Akbiyik,[103] T. P. A. Åkesson,[101] A. V. Akimov,[150] D. Akiyama,[173] N. N. Akolkar,[25] S. Aktas,[22a] K. Al Khoury,[43] G. L. Alberghi,[24b] J. Albert,[170] P. Albicocco,[55] G. L. Albouy,[62] S. Alderweireldt,[54] Z. L. Alegria,[125] M. Aleksa,[37] I. N. Aleksandrov,[40] C. Alexa,[28b] T. Alexopoulos,[10] F. Alfonsi,[24b] M. Algren,[58] M. Alhroob,[172] B. Ali,[136] H. M. J. Ali,[94,d] S. Ali,[32] S. W. Alibocus,[95] M. Aliev,[34c] G. Alimonti,[73a]

W. Alkakhi,[57] C. Allaire,[68] B. M. M. Allbrooke,[151] J. S. Allen,[104] J. F. Allen,[54] C. A. Allendes Flores,[141f] P. P. Allport,[21] A. Aloisio,[74a,74b] F. Alonso,[93] C. Alpigiani,[143] Z. M. K. Alsolami,[94] M. Alvarez Estevez,[102] A. Alvarez Fernandez,[103] M. Alves Cardoso,[58] M. G. Alviggi,[74a,74b] M. Aly,[104] Y. Amaral Coutinho,[85b] A. Ambler,[107] C. Amelung,[37] M. Amerl,[104] C. G. Ames,[112] D. Amidei,[109] B. Amini,[56] K. Amirie,[159] S. P. Amor Dos Santos,[134a] K. R. Amos,[168] D. Amperiadou,[157] S. An,[86] V. Ananiev,[129] C. Anastopoulos,[144] T. Andeen,[11] J. K. Anders,[37] A. C. Anderson,[61] S. Y. Andrean,[49a,49b] A. Andreazza,[73a,73b] S. Angelidakis,[9] A. Angerami,[43] A. V. Anisenkov,[39] A. Annovi,[76a] C. Antel,[58] E. Antipov,[150] M. Antonelli,[55] F. Anulli,[77a] M. Aoki,[86] T. Aoki,[158] M. A. Aparo,[151] L. Aperio Bella,[50] C. Appelt,[156] A. Apyan,[27] S. J. Arbiol Val,[89] C. Arcangeletti,[55] A. T. H. Arce,[53] J-F. Arguin,[111] S. Argyropoulos,[157] J.-H. Arling,[50] O. Arnaez,[4] H. Arnold,[150] G. Artoni,[77a,77b] H. Asada,[114] K. Asai,[122] S. Asai,[158] N. A. Asbah,[37] R. A. Ashby Pickering,[172] K. Assamagan,[30] R. Astalos,[29a] K. S. V. Astrand,[101] S. Atashi,[163] R. J. Atkin,[34a] M. Atkinson,[167] H. Atmani,[36f] P. A. Atmasiddha,[132] K. Augsten,[136] A. D. Auriol,[21] V. A. Austrup,[104] G. Avolio,[37] K. Axiotis,[58] G. Azuelos,[111,e] D. Babal,[29b] H. Bachacou,[139] K. Bachas,[157,f] A. Bachiu,[35] E. Bachmann,[52] A. Badea,[41] T. M. Baer,[109] P. Bagnaia,[77a,77b] M. Bahmani,[19] D. Bahner,[56] K. Bai,[127] J. T. Baines,[138] L. Baines,[97] O. K. Baker,[177] E. Bakos,[16] D. Bakshi Gupta,[8] L. E. Balabram Filho,[85b] V. Balakrishnan,[124] R. Balasubramanian,[4] E. M. Baldin,[39] P. Balek,[88a] E. Ballabene,[24b,24a] F. Balli,[139] L. M. Baltes,[65a] W. K. Balunas,[33] J. Balz,[103] I. Bamwidhi,[120b] E. Banas,[89] M. Bandieramonte,[133] A. Bandyopadhyay,[25] S. Bansal,[25] L. Barak,[156] M. Barakat,[50] E. L. Barberio,[108] D. Barberis,[59b,59a] M. Barbero,[105] M. Z. Barel,[118] T. Barillari,[113] M-S. Barisits,[37] T. Barklow,[148] P. Baron,[126] D. A. Baron Moreno,[104] A. Baroncelli,[64a] A. J. Barr,[130] J. D. Barr,[99] F. Barreiro,[102] J. Barreiro Guimarães da Costa,[14] M. G. Barros Teixeira,[134a] S. Barsov,[39] F. Bartels,[65a] R. Bartoldus,[148] A. E. Barton,[94] P. Bartos,[29a] A. Basan,[103] M. Baselga,[51] A. Bassalat,[68,g] M. J. Basso,[160a] S. Bataju,[46] R. Bate,[169] R. L. Bates,[61] S. Batlamous,[102] B. Batool,[146] M. Battaglia,[140] D. Battulga,[19] M. Bauce,[77a,77b] M. Bauer,[81] P. Bauer,[25] L. T. Bazzano Hurrell,[31] J. B. Beacham,[53] T. Beau,[131] J. Y. Beaucamp,[93] P. H. Beauchemin,[162] P. Bechtle,[25] H. P. Beck,[20,h] K. Becker,[172] A. J. Beddall,[84] V. A. Bednyakov,[40] C. P. Bee,[150] L. J. Beemster,[16] T. A. Beermann,[37] M. Begalli,[85d] M. Begel,[30] A. Behera,[150] J. K. Behr,[50] J. F. Beirer,[37] F. Beisiegel,[25] M. Belfkir,[120b] G. Bella,[156] L. Bellagamba,[24b] A. Bellerive,[35] P. Bellos,[21] K. Beloborodov,[39] D. Benchekroun,[36a] F. Bendebba,[36a] Y. Benhammou,[156] K. C. Benkendorfer,[63] L. Beresford,[50] M. Beretta,[55] E. Bergeaas Kuutmann,[166] N. Berger,[4] B. Bergmann,[136] J. Beringer,[18a] G. Bernardi,[5] C. Bernius,[148] F. U. Bernlochner,[25] F. Bernon,[37] A. Berrocal Guardia,[13] T. Berry,[98] P. Berta,[137] A. Berthold,[52] S. Bethke,[113] A. Betti,[77a,77b] A. J. Bevan,[97] N. K. Bhalla,[56] S. Bhatta,[150] D. S. Bhattacharya,[171] P. Bhattarai,[148] Z. M. Bhatti,[121] K. D. Bhide,[56] V. S. Bhopatkar,[125] R. M. Bianchi,[133] G. Bianco,[24b,24a] O. Biebel,[112] R. Bielski,[127] M. Biglietti,[79a] C. S. Billingsley,[46] Y. Bimgdi,[36f] M. Bindi,[57] A. Bingham,[176] A. Bingul,[22b] C. Bini,[77a,77b] G. A. Bird,[33] M. Birman,[174] M. Biros,[137] S. Biryukov,[151] T. Bisanz,[51] E. Bisceglie,[45b,45a] J. P. Biswal,[138] D. Biswas,[146] I. Bloch,[50] A. Blue,[61] U. Blumenschein,[97] J. Blumenthal,[103] V. S. Bobrovnikov,[39] M. Boehler,[56] B. Boehm,[171] D. Bogavac,[37] A. G. Bogdanchikov,[39] L. S. Boggia,[131] C. Bohm,[49a] V. Boisvert,[98] P. Bokan,[37] T. Bold,[88a] M. Bomben,[5] M. Bona,[97] M. Boonekamp,[139] A. G. Borbély,[61] I. S. Bordulev,[39] G. Borissov,[94] D. Bortoletto,[130] D. Boscherini,[24b] M. Bosman,[13] K. Bouaouda,[36a] N. Bouchhar,[168] L. Boudet,[4] J. Boudreau,[133] E. V. Bouhova-Thacker,[94] D. Boumediene,[42] R. Bouquet,[59b,59a] A. Boveia,[123] J. Boyd,[37] D. Boye,[30] P. R. Boyella,[167] I. R. Boyko,[40] L. Bozianu,[58] J. Bracinik,[21] N. Brahimi,[4] G. Brandt,[176] O. Brandt,[33] F. Braren,[50] B. Brau,[106] J. E. Brau,[127] R. Brener,[174] L. Brenner,[118] R. Brenner,[166] M. Bressan,[43] S. Bressler,[174] G. Brianti,[80a,80b] D. Britton,[61] D. Britzger,[113] I. Brock,[25] R. Brock,[110] G. Brooijmans,[43] A. J. Brooks,[70] E. M. Brooks,[160b] E. Brost,[30] L. M. Brown,[170,160a] L. E. Bruce,[63] T. L. Bruckler,[130] P. A. Bruckman de Renstrom,[89] B. Brüers,[50] A. Bruni,[24b] G. Bruni,[24b] D. Brunner,[49a,49b] M. Bruschi,[24b] N. Bruscino,[77a,77b] T. Buanes,[17] Q. Buat,[143] D. Buchin,[113] A. G. Buckley,[61] O. Bulekov,[39] B. A. Bullard,[148] S. Burdin,[95] C. D. Burgard,[51] A. M. Burger,[37] B. Burghgrave,[8] O. Burlayenko,[56] J. Burleson,[167] J. T. P. Burr,[33] J. C. Burzynski,[147] E. L. Busch,[43] V. Büscher,[103] P. J. Bussey,[61] J. M. Butler,[26] C. M. Buttar,[61] J. M. Butterworth,[99] W. Buttinger,[138] C. J. Buxo Vazquez,[110] A. R. Buzykaev,[39] S. Cabrera Urbán,[168] L. Cadamuro,[68] D. Caforio,[60] H. Cai,[133] Y. Cai,[14,115c] Y. Cai,[115a] V. M. M. Cairo,[37] O. Cakir,[3a] N. Calace,[37] P. Calafiura,[18a] G. Calderini,[131] P. Calfayan,[35] G. Callea,[61] L. P. Caloba,[85b] D. Calvet,[42] S. Calvet,[42]

M. Calvetti,[76a,76b] R. Camacho Toro,[131] S. Camarda,[37] D. Camarero Munoz,[27] P. Camarri,[78a,78b] M. T. Camerlingo,[74a,74b] D. Cameron,[37] C. Camincher,[170] M. Campanelli,[99] A. Camplani,[44] V. Canale,[74a,74b] A. C. Canbay,[3a] E. Canonero,[98] J. Cantero,[168] Y. Cao,[167] F. Capocasa,[27] M. Capua,[45b,45a] A. Carbone,[73a,73b] R. Cardarelli,[78a] J. C. J. Cardenas,[8] G. Carducci,[45b,45a] T. Carli,[37] G. Carlino,[74a] J. I. Carlotto,[13] B. T. Carlson,[133,i] E. M. Carlson,[170,160a] J. Carmignani,[95] L. Carminati,[73a,73b] A. Carnelli,[139] M. Carnesale,[37] S. Caron,[117] E. Carquin,[141f] I. B. Carr,[108] S. Carrá,[73a] G. Carratta,[24b,24a] A. M. Carroll,[127] M. P. Casado,[13,j] M. Caspar,[50] F. L. Castillo,[4] L. Castillo Garcia,[13] V. Castillo Gimenez,[168] N. F. Castro,[134a,134e] A. Catinaccio,[37] J. R. Catmore,[129] T. Cavaliere,[4] V. Cavaliere,[30] L. J. Caviedes Betancourt,[23b] Y. C. Cekmecelioglu,[50] E. Celebi,[84] S. Cella,[37] V. Cepaitis,[58] K. Cerny,[126] A. S. Cerqueira,[85a] A. Cerri,[151] L. Cerrito,[78a,78b] F. Cerutti,[18a] B. Cervato,[146] A. Cervelli,[24b] G. Cesarini,[55] S. A. Cetin,[84] D. Chakraborty,[119] J. Chan,[18a] W. Y. Chan,[158] J. D. Chapman,[33] E. Chapon,[139] B. Chargeishvili,[154b] D. G. Charlton,[21] M. Chatterjee,[20] C. Chauhan,[137] Y. Che,[115a] S. Chekanov,[6] S. V. Chekulaev,[160a] G. A. Chelkov,[40,k] A. Chen,[109] B. Chen,[156] B. Chen,[170] H. Chen,[115a] H. Chen,[30] J. Chen,[64c] J. Chen,[147] M. Chen,[130] S. Chen,[90] S. J. Chen,[115a] X. Chen,[64c] X. Chen,[15,l] Y. Chen,[64a] C. L. Cheng,[175] H. C. Cheng,[66a] S. Cheong,[148] A. Cheplakov,[40] E. Cheremushkina,[50] E. Cherepanova,[118] R. Cherkaoui El Moursli,[36e] E. Cheu,[7] K. Cheung,[67] L. Chevalier,[139] V. Chiarella,[55] G. Chiarelli,[76a] N. Chiedde,[105] G. Chiodini,[72a] A. S. Chisholm,[21] A. Chitan,[28b] M. Chitishvili,[168] M. V. Chizhov,[40,m] K. Choi,[11] Y. Chou,[143] E. Y. S. Chow,[117] K. L. Chu,[174] M. C. Chu,[66a] X. Chu,[14,115c] Z. Chubinidze,[55] J. Chudoba,[135] J. J. Chwastowski,[89] D. Cieri,[113] K. M. Ciesla,[88a] V. Cindro,[96] A. Ciocio,[18a] F. Cirotto,[74a,74b] Z. H. Citron,[174] M. Citterio,[73a] D. A. Ciubotaru,[28b] A. Clark,[58] P. J. Clark,[54] N. Clarke Hall,[99] C. Clarry,[159] J. M. Clavijo Columbie,[50] S. E. Clawson,[50] C. Clement,[49a,49b] Y. Coadou,[105] M. Cobal,[71a,71c] A. Coccaro,[59b] R. F. Coelho Barrue,[134a] R. Coelho Lopes De Sa,[106] S. Coelli,[73a] L. S. Colangeli,[159] B. Cole,[43] J. Collot,[62] P. Conde Muiño,[134a,134g] M. P. Connell,[34c] S. H. Connell,[34c] E. I. Conroy,[130] F. Conventi,[74a,n] H. G. Cooke,[21] A. M. Cooper-Sarkar,[130] F. A. Corchia,[24b,24a] A. Cordeiro Oudot Choi,[131] L. D. Corpe,[42] M. Corradi,[77a,77b] F. Corriveau,[107,o] A. Cortes-Gonzalez,[19] M. J. Costa,[168] F. Costanza,[4] D. Costanzo,[144] B. M. Cote,[123] J. Couthures,[4] G. Cowan,[98] K. Cranmer,[175] L. Cremer,[51] D. Cremonini,[24b,24a] S. Crépé-Renaudin,[62] F. Crescioli,[131] M. Cristinziani,[146] M. Cristoforetti,[80a,80b] V. Croft,[118] J. E. Crosby,[125] G. Crosetti,[45b,45a] A. Cueto,[102] H. Cui,[99] Z. Cui,[7] W. R. Cunningham,[61] F. Curcio,[168] J. R. Curran,[54] P. Czodrowski,[37] M. J. Da Cunha Sargedas De Sousa,[59b,59a] J. V. Da Fonseca Pinto,[85b] C. Da Via,[104] W. Dabrowski,[88a] T. Dado,[37] S. Dahbi,[153] T. Dai,[109] D. Dal Santo,[20] C. Dallapiccola,[106] M. Dam,[44] G. D'amen,[30] V. D'Amico,[112] J. Damp,[103] J. R. Dandoy,[35] D. Dannheim,[37] M. Danninger,[147] V. Dao,[150] G. Darbo,[59b] S. J. Das,[30] F. Dattola,[50] S. D'Auria,[73a,73b] A. D'Avanzo,[74a,74b] C. David,[34a] T. Davidek,[137] I. Dawson,[97] H. A. Day-hall,[136] K. De,[8] R. De Asmundis,[74a] N. De Biase,[50] S. De Castro,[24b,24a] N. De Groot,[117] P. de Jong,[118] H. De la Torre,[119] A. De Maria,[115a] A. De Salvo,[77a] U. De Sanctis,[78a,78b] F. De Santis,[72a,72b] A. De Santo,[151] J. B. De Vivie De Regie,[62] J. Debevc,[96] D. V. Dedovich,[40] J. Degens,[95] A. M. Deiana,[46] F. Del Corso,[24b,24a] J. Del Peso,[102] L. Delagrange,[131] F. Deliot,[139] C. M. Delitzsch,[51] M. Della Pietra,[74a,74b] D. Della Volpe,[58] A. Dell'Acqua,[37] L. Dell'Asta,[73a,73b] M. Delmastro,[4] C. C. Delogu,[103] P. A. Delsart,[62] S. Demers,[177] M. Demichev,[40] S. P. Denisov,[39] L. D'Eramo,[42] D. Derendarz,[89] F. Derue,[131] P. Dervan,[95] K. Desch,[25] C. Deutsch,[25] F. A. Di Bello,[59b,59a] A. Di Ciaccio,[78a,78b] L. Di Ciaccio,[4] A. Di Domenico,[77a,77b] C. Di Donato,[74a,74b] A. Di Girolamo,[37] G. Di Gregorio,[37] A. Di Luca,[80a,80b] B. Di Micco,[79a,79b] R. Di Nardo,[79a,79b] K. F. Di Petrillo,[41] M. Diamantopoulou,[35] F. A. Dias,[118] T. Dias Do Vale,[147] M. A. Diaz,[141a,141b] A. R. Didenko,[40] M. Didenko,[168] E. B. Diehl,[109] S. Díez Cornell,[50] C. Diez Pardos,[146] C. Dimitriadi,[166] A. Dimitrievska,[21] J. Dingfelder,[25] T. Dingley,[130] I-M. Dinu,[28b] S. J. Dittmeier,[65b] F. Dittus,[37] M. Divisek,[137] B. Dixit,[95] F. Djama,[105] T. Djobava,[154b] C. Doglioni,[104,101] A. Dohnalova,[29a] J. Dolejsi,[137] Z. Dolezal,[137] K. Domijan,[88a] K. M. Dona,[41] M. Donadelli,[85d] B. Dong,[110] J. Donini,[42] A. D'Onofrio,[74a,74b] M. D'Onofrio,[95] J. Dopke,[138] A. Doria,[74a] N. Dos Santos Fernandes,[134a] P. Dougan,[104] M. T. Dova,[93] A. T. Doyle,[61] M. A. Draguet,[130] M. P. Drescher,[57] E. Dreyer,[174] I. Drivas-koulouris,[10] M. Drnevich,[121] M. Drozdova,[58] D. Du,[64a] T. A. du Pree,[118] F. Dubinin,[39] M. Dubovsky,[29a] E. Duchovni,[174] G. Duckeck,[112] O. A. Ducu,[28b] D. Duda,[54] A. Dudarev,[37] E. R. Duden,[27] M. D'uffizi,[104] L. Duflot,[68] M. Dührssen,[37] I. Duminica,[28g] A. E. Dumitriu,[28b] M. Dunford,[65a] S. Dungs,[51] K. Dunne,[49a,49b] A. Duperrin,[105] H. Duran Yildiz,[3a] M. Düren,[60] A. Durglishvili,[154b]

D. Duvnjak,[35] B. L. Dwyer,[119] G. I. Dyckes,[18a] M. Dyndal,[88a] B. S. Dziedzic,[37] Z. O. Earnshaw,[151] G. H. Eberwein,[130] B. Eckerova,[29a] S. Eggebrecht,[57] E. Egidio Purcino De Souza,[85e] L. F. Ehrke,[58] G. Eigen,[17] K. Einsweiler,[18a] T. Ekelof,[166] P. A. Ekman,[101] S. El Farkh,[36b] Y. El Ghazali,[64a] H. El Jarrari,[37] A. El Moussaouy,[36a] V. Ellajosyula,[166] M. Ellert,[166] F. Ellinghaus,[176] N. Ellis,[37] J. Elmsheuser,[30] M. Elsawy,[120a] M. Elsing,[37] D. Emeliyanov,[138] Y. Enari,[86] I. Ene,[18a] S. Epari,[13] P. A. Erland,[89] D. Ernani Martins Neto,[89] M. Errenst,[176] M. Escalier,[68] C. Escobar,[168] E. Etzion,[156] G. Evans,[134a,134b] H. Evans,[70] L. S. Evans,[98] A. Ezhilov,[39] S. Ezzarqtouni,[36a] F. Fabbri,[24b,24a] L. Fabbri,[24b,24a] G. Facini,[99] V. Fadeyev,[140] R. M. Fakhrutdinov,[39] D. Fakoudis,[103] S. Falciano,[77a] L. F. Falda Ulhoa Coelho,[37] F. Fallavollita,[113] G. Falsetti,[45b,45a] J. Faltova,[137] C. Fan,[167] K. Y. Fan,[66b] Y. Fan,[14] Y. Fang,[14,115c] M. Fanti,[73a,73b] M. Faraj,[71a,71b] Z. Farazpay,[100] A. Farbin,[8] A. Farilla,[79a] T. Farooque,[110] S. M. Farrington,[138,54] F. Fassi,[36e] D. Fassouliotis,[9] M. Faucci Giannelli,[78a,78b] W. J. Fawcett,[33] L. Fayard,[68] P. Federic,[137] P. Federicova,[135] O. L. Fedin,[39,k] M. Feickert,[175] L. Feligioni,[105] D. E. Fellers,[127] C. Feng,[64b] Z. Feng,[118] M. J. Fenton,[163] L. Ferencz,[50] R. A. M. Ferguson,[94] S. I. Fernandez Luengo,[141f] P. Fernandez Martinez,[69] M. J. V. Fernoux,[105] J. Ferrando,[94] A. Ferrari,[166] P. Ferrari,[118,117] R. Ferrari,[75a] D. Ferrere,[58] C. Ferretti,[109] D. Fiacco,[77a,77b] F. Fiedler,[103] P. Fiedler,[136] S. Filimonov,[39] A. Filipčič,[96] E. K. Filmer,[160a] F. Filthaut,[117] M. C. N. Fiolhais,[134a,134c,p] L. Fiorini,[168] W. C. Fisher,[110] T. Fitschen,[104] P. M. Fitzhugh,[139] I. Fleck,[146] P. Fleischmann,[109] T. Flick,[176] M. Flores,[34d,q] L. R. Flores Castillo,[66a] L. Flores Sanz De Acedo,[37] F. M. Follega,[80a,80b] N. Fomin,[33] J. H. Foo,[159] A. Formica,[139] A. C. Forti,[104] E. Fortin,[37] A. W. Fortman,[18a] M. G. Foti,[18a] L. Fountas,[9,r] D. Fournier,[68] H. Fox,[94] P. Francavilla,[76a,76b] S. Francescato,[63] S. Franchellucci,[58] M. Franchini,[24b,24a] S. Franchino,[65a] D. Francis,[37] L. Franco,[117] V. Franco Lima,[37] L. Franconi,[50] M. Franklin,[63] G. Frattari,[27] Y. Y. Frid,[156] J. Friend,[61] N. Fritzsche,[37] A. Froch,[56] D. Froidevaux,[37] J. A. Frost,[130] Y. Fu,[64a] S. Fuenzalida Garrido,[141f] M. Fujimoto,[105] K. Y. Fung,[66a] E. Furtado De Simas Filho,[85e] M. Furukawa,[158] J. Fuster,[168] A. Gaa,[57] A. Gabrielli,[24b,24a] A. Gabrielli,[159] P. Gadow,[37] G. Gagliardi,[59b,59a] L. G. Gagnon,[18a] S. Gaid,[165] S. Galantzan,[156] J. Gallagher,[1] E. J. Gallas,[130] B. J. Gallop,[138] K. K. Gan,[123] S. Ganguly,[158] Y. Gao,[54] F. M. Garay Walls,[141a,141b] B. Garcia,[30] C. García,[168] A. Garcia Alonso,[118] A. G. Garcia Caffaro,[177] J. E. García Navarro,[168] M. Garcia-Sciveres,[18a] G. L. Gardner,[132] R. W. Gardner,[41] N. Garelli,[162] D. Garg,[82] R. B. Garg,[148] J. M. Gargan,[54] C. A. Garner,[159] C. M. Garvey,[34a] V. K. Gassmann,[162] G. Gaudio,[75a] V. Gautam,[13] P. Gauzzi,[77a,77b] J. Gavranovic,[96] I. L. Gavrilenko,[39] A. Gavrilyuk,[39] C. Gay,[169] G. Gaycken,[127] E. N. Gazis,[10] A. A. Geanta,[28b] C. M. Gee,[140] A. Gekow,[123] C. Gemme,[59b] M. H. Genest,[62] A. D. Gentry,[116] S. George,[98] W. F. George,[21] T. Geralis,[48] P. Gessinger-Befurt,[37] M. E. Geyik,[176] M. Ghani,[172] K. Ghorbanian,[97] A. Ghosal,[146] A. Ghosh,[163] A. Ghosh,[7] B. Giacobbe,[24b] S. Giagu,[77a,77b] T. Giani,[118] A. Giannini,[64a] S. M. Gibson,[98] M. Gignac,[140] D. T. Gil,[88b] A. K. Gilbert,[88a] B. J. Gilbert,[43] D. Gillberg,[35] G. Gilles,[118] L. Ginabat,[131] D. M. Gingrich,[2,e] M. P. Giordani,[71a,71c] P. F. Giraud,[139] G. Giugliarelli,[71a,71c] D. Giugni,[73a] F. Giuli,[78a,78b] I. Gkialas,[9,r] L. K. Gladilin,[39] C. Glasman,[102] G. R. Gledhill,[127] G. Glemža,[50] M. Glisic,[127] I. Gnesi,[45b] Y. Go,[30] M. Goblirsch-Kolb,[37] B. Gocke,[51] D. Godin,[111] B. Gokturk,[22a] S. Goldfarb,[108] T. Golling,[58] M. G. D. Gololo,[34g] D. Golubkov,[39] J. P. Gombas,[110] A. Gomes,[134a,134b] G. Gomes Da Silva,[146] A. J. Gomez Delegido,[168] R. Gonçalo,[134a] L. Gonella,[21] A. Gongadze,[154c] F. Gonnella,[21] J. L. Gonski,[148] R. Y. González Andana,[54] S. González de la Hoz,[168] R. Gonzalez Lopez,[95] C. Gonzalez Renteria,[18a] M. V. Gonzalez Rodrigues,[50] R. Gonzalez Suarez,[166] S. Gonzalez-Sevilla,[58] L. Goossens,[37] B. Gorini,[37] E. Gorini,[72a,72b] A. Gorišek,[96] T. C. Gosart,[132] A. T. Goshaw,[53] M. I. Gostkin,[40] S. Goswami,[125] C. A. Gottardo,[37] S. A. Gotz,[112] M. Gouighri,[36b] V. Goumarre,[50] A. G. Goussiou,[143] N. Govender,[34c] R. P. Grabarczyk,[130] I. Grabowska-Bold,[88a] K. Graham,[35] E. Gramstad,[129] S. Grancagnolo,[72a,72b] C. M. Grant,[1,139] P. M. Gravila,[28f] F. G. Gravili,[72a,72b] H. M. Gray,[18a] M. Greco,[72a,72b] M. J. Green,[1] C. Grefe,[25] A. S. Grefsrud,[17] I. M. Gregor,[50] K. T. Greif,[163] P. Grenier,[148] S. G. Grewe,[113] A. A. Grillo,[140] K. Grimm,[32] S. Grinstein,[13,s] J.-F. Grivaz,[68] E. Gross,[174] J. Grosse-Knetter,[57] L. Guan,[109] J. G. R. Guerrero Rojas,[168] G. Guerrieri,[37] R. Gugel,[103] J. A. M. Guhit,[109] A. Guida,[19] E. Guilloton,[172] S. Guindon,[37] F. Guo,[14,115c] J. Guo,[64c] L. Guo,[50] L. Guo,[14] Y. Guo,[109] A. Gupta,[51] R. Gupta,[133] S. Gurbuz,[25] S. S. Gurdasani,[56] G. Gustavino,[77a,77b] P. Gutierrez,[124] L. F. Gutierrez Zagazeta,[132] M. Gutsche,[52] C. Gutschow,[99] C. Gwenlan,[130] C. B. Gwilliam,[95] E. S. Haaland,[129] A. Haas,[121] M. Habedank,[61] C. Haber,[18a] H. K. Hadavand,[8] A. Hadef,[52] A. I. Hagan,[94] J. J. Hahn,[146]

E. H. Haines,[99] M. Haleem,[171] J. Haley,[125] G. D. Hallewell,[105] L. Halser,[20] K. Hamano,[170] M. Hamer,[25] E. J. Hampshire,[98] J. Han,[64b] L. Han,[115a] L. Han,[64a] S. Han,[18a] Y. F. Han,[159] K. Hanagaki,[86] M. Hance,[140] D. A. Hangal,[43] H. Hanif,[147] M. D. Hank,[132] J. B. Hansen,[44] P. H. Hansen,[44] D. Harada,[58] T. Harenberg,[176] S. Harkusha,[178] M. L. Harris,[106] Y. T. Harris,[25] J. Harrison,[13] N. M. Harrison,[123] P. F. Harrison,[172] N. M. Hartman,[113] N. M. Hartmann,[112] R. Z. Hasan,[98,138] Y. Hasegawa,[145] F. Haslbeck,[130] S. Hassan,[17] R. Hauser,[110] C. M. Hawkes,[21] R. J. Hawkings,[37] Y. Hayashi,[158] D. Hayden,[110] C. Hayes,[109] R. L. Hayes,[118] C. P. Hays,[130] J. M. Hays,[97] H. S. Hayward,[95] F. He,[64a] M. He,[14,115c] Y. He,[50] Y. He,[99] N. B. Heatley,[97] V. Hedberg,[101] A. L. Heggelund,[129] N. D. Hehir,[97,a] C. Heidegger,[56] K. K. Heidegger,[56] J. Heilman,[35] S. Heim,[50] T. Heim,[18a] J. G. Heinlein,[132] J. J. Heinrich,[127] L. Heinrich,[113,t] J. Hejbal,[135] A. Held,[175] S. Hellesund,[17] C. M. Helling,[169] S. Hellman,[49a,49b] R. C. W. Henderson,[94] L. Henkelmann,[33] A. M. Henriques Correia,[37] H. Herde,[101] Y. Hernández Jiménez,[150] L. M. Herrmann,[25] T. Herrmann,[52] G. Herten,[56] R. Hertenberger,[112] L. Hervas,[37] M. E. Hesping,[103] N. P. Hessey,[160a] J. Hessler,[113] M. Hidaoui,[36b] N. Hidic,[137] E. Hill,[159] S. J. Hillier,[21] J. R. Hinds,[110] F. Hinterkeuser,[25] M. Hirose,[128] S. Hirose,[161] D. Hirschbuehl,[176] T. G. Hitchings,[104] B. Hiti,[96] J. Hobbs,[150] R. Hobincu,[28e] N. Hod,[174] M. C. Hodgkinson,[144] B. H. Hodkinson,[130] A. Hoecker,[37] D. D. Hofer,[109] J. Hofer,[168] T. Holm,[25] M. Holzbock,[37] L. B. A. H. Hommels,[33] B. P. Honan,[104] J. J. Hong,[70] J. Hong,[64c] T. M. Hong,[133] B. H. Hooberman,[167] W. H. Hopkins,[6] M. C. Hoppesch,[167] Y. Horii,[114] M. E. Horstmann,[113] S. Hou,[153] M. R. Housenga,[167] A. S. Howard,[96] J. Howarth,[61] J. Hoya,[6] M. Hrabovsky,[126] A. Hrynevich,[50] T. Hryn'ova,[4] P. J. Hsu,[67] S.-C. Hsu,[143] T. Hsu,[68] M. Hu,[18a] Q. Hu,[64a] S. Huang,[33] X. Huang,[14,115c] Y. Huang,[144] Y. Huang,[103] Y. Huang,[14] Z. Huang,[104] Z. Hubacek,[136] M. Huebner,[25] F. Huegging,[25] T. B. Huffman,[130] M. Hufnagel Maranha De Faria,[85a] C. A. Hugli,[50] M. Huhtinen,[37] S. K. Huiberts,[17] R. Hulsken,[107] N. Huseynov,[12,u] J. Huston,[110] J. Huth,[63] R. Hyneman,[148] G. Iacobucci,[58] G. Iakovidis,[30] L. Iconomidou-Fayard,[68] J. P. Iddon,[37] P. Iengo,[74a,74b] R. Iguchi,[158] Y. Iiyama,[158] T. Iizawa,[130] Y. Ikegami,[86] N. Ilic,[159] H. Imam,[85c] G. Inacio Goncalves,[85d] T. Ingebretsen Carlson,[49a,49b] J. M. Inglis,[97] G. Introzzi,[75a,75b] M. Iodice,[79a] V. Ippolito,[77a,77b] R. K. Irwin,[95] M. Ishino,[158] W. Islam,[175] C. Issever,[19] S. Istin,[22a,v] H. Ito,[173] R. Iuppa,[80a,80b] A. Ivina,[174] J. M. Izen,[47] V. Izzo,[74a] P. Jacka,[135] P. Jackson,[1] C. S. Jagfeld,[112] G. Jain,[160a] P. Jain,[50] K. Jakobs,[56] T. Jakoubek,[174] J. Jamieson,[61] W. Jang,[158] M. Javurkova,[106] P. Jawahar,[104] L. Jeanty,[127] J. Jejelava,[154a,w] P. Jenni,[56,x] C. E. Jessiman,[35] C. Jia,[64b] H. Jia,[169] J. Jia,[150] X. Jia,[14,115c] Z. Jia,[115a] C. Jiang,[54] S. Jiggins,[50] J. Jimenez Pena,[13] S. Jin,[115a] A. Jinaru,[28b] O. Jinnouchi,[142] P. Johansson,[144] K. A. Johns,[7] J. W. Johnson,[140] F. A. Jolly,[50] D. M. Jones,[151] E. Jones,[50] K. S. Jones,[8] P. Jones,[33] R. W. L. Jones,[94] T. J. Jones,[95] H. L. Joos,[57,37] R. Joshi,[123] J. Jovicevic,[16] X. Ju,[18a] J. J. Junggeburth,[37] T. Junkermann,[65a] A. Juste Rozas,[13,s] M. K. Juzek,[89] S. Kabana,[141e] A. Kaczmarska,[89] M. Kado,[113] H. Kagan,[123] M. Kagan,[148] A. Kahn,[132] C. Kahra,[103] T. Kaji,[158] E. Kajomovitz,[155] N. Kakati,[174] I. Kalaitzidou,[56] C. W. Kalderon,[30] N. J. Kang,[140] D. Kar,[34g] K. Karava,[130] M. J. Kareem,[160b] E. Karentzos,[25] O. Karkout,[118] S. N. Karpov,[40] Z. M. Karpova,[40] V. Kartvelishvili,[94] A. N. Karyukhin,[39] E. Kasimi,[157] J. Katzy,[50] S. Kaur,[35] K. Kawade,[145] M. P. Kawale,[124] C. Kawamoto,[90] T. Kawamoto,[64a] E. F. Kay,[37] F. I. Kaya,[162] S. Kazakos,[110] V. F. Kazanin,[39] Y. Ke,[150] J. M. Keaveney,[34a] R. Keeler,[170] G. V. Kehris,[63] J. S. Keller,[35] J. J. Kempster,[151] O. Kepka,[135] B. P. Kerridge,[138] S. Kersten,[176] B. P. Kerševan,[96] L. Keszeghova,[29a] S. Ketabchi Haghighat,[159] R. A. Khan,[133] A. Khanov,[125] A. G. Kharlamov,[39] T. Kharlamova,[39] E. E. Khoda,[143] M. Kholodenko,[134a] T. J. Khoo,[19] G. Khoriauli,[171] J. Khubua,[154b,a] Y. A. R. Khwaira,[131] B. Kibirige,[34g] D. Kim,[6] D. W. Kim,[49a,49b] Y. K. Kim,[41] N. Kimura,[99] M. K. Kingston,[57] A. Kirchhoff,[57] C. Kirfel,[25] F. Kirfel,[25] J. Kirk,[138] A. E. Kiryunin,[113] S. Kita,[161] C. Kitsaki,[10] O. Kivernyk,[25] M. Klassen,[162] C. Klein,[35] L. Klein,[171] M. H. Klein,[46] S. B. Klein,[58] U. Klein,[95] A. Klimentov,[30] T. Klioutchnikova,[37] P. Kluit,[118] S. Kluth,[113] E. Kneringer,[81] T. M. Knight,[159] A. Knue,[51] M. Kobel,[52] D. Kobylianskii,[174] S. F. Koch,[130] M. Kocian,[148] P. Kodyš,[137] D. M. Koeck,[127] P. T. Koenig,[25] T. Koffas,[35] O. Kolay,[52] I. Koletsou,[4] T. Komarek,[89] K. Köneke,[56] A. X. Y. Kong,[1] T. Kono,[122] N. Konstantinidis,[99] P. Kontaxakis,[58] B. Konya,[101] R. Kopeliansky,[43] S. Koperny,[88a] K. Korcyl,[89] K. Kordas,[157,y] A. Korn,[99] S. Korn,[57] I. Korolkov,[13] N. Korotkova,[39] B. Kortman,[118] O. Kortner,[113] S. Kortner,[113] W. H. Kostecka,[119] V. V. Kostyukhin,[146] A. Kotsokechagia,[37] A. Kotwal,[53] A. Koulouris,[37] A. Kourkoumeli-Charalampidi,[75a,75b] C. Kourkoumelis,[9] E. Kourlitis,[113] O. Kovanda,[127] R. Kowalewski,[170] W. Kozanecki,[127] A. S. Kozhin,[39]

V. A. Kramarenko,[39] G. Kramberger,[96] P. Kramer,[25] M. W. Krasny,[131] A. Krasznahorkay,[37] A. C. Kraus,[119] J. W. Kraus,[176] J. A. Kremer,[50] T. Kresse,[52] L. Kretschmann,[176] J. Kretzschmar,[95] K. Kreul,[19] P. Krieger,[159] K. Krizka,[21] K. Kroeninger,[51] H. Kroha,[113] J. Kroll,[135] J. Kroll,[132] K. S. Krowpman,[110] U. Kruchonak,[40] H. Krüger,[25] N. Krumnack,[83] M. C. Kruse,[53] O. Kuchinskaia,[39] S. Kuday,[3a] S. Kuehn,[37] R. Kuesters,[56] T. Kuhl,[50] V. Kukhtin,[40] Y. Kulchitsky,[40] S. Kuleshov,[141d,141b] M. Kumar,[34g] N. Kumari,[50] P. Kumari,[160b] A. Kupco,[135] T. Kupfer,[51] A. Kupich,[39] O. Kuprash,[56] H. Kurashige,[87] L. L. Kurchaninov,[160a] O. Kurdysh,[68] Y. A. Kurochkin,[38] A. Kurova,[39] M. Kuze,[142] A. K. Kvam,[106] J. Kvita,[126] T. Kwan,[107] N. G. Kyriacou,[109] L. A. O. Laatu,[105] C. Lacasta,[168] F. Lacava,[77a,77b] H. Lacker,[19] D. Lacour,[131] N. N. Lad,[99] E. Ladygin,[40] A. Lafarge,[42] B. Laforge,[131] T. Lagouri,[177] F. Z. Lahbabi,[36a] S. Lai,[57] J. E. Lambert,[170] S. Lammers,[70] W. Lampl,[7] C. Lampoudis,[157,y] G. Lamprinoudis,[103] A. N. Lancaster,[119] E. Lançon,[30] U. Landgraf,[56] M. P. J. Landon,[97] V. S. Lang,[56] O. K. B. Langrekken,[129] A. J. Lankford,[163] F. Lanni,[37] K. Lantzsch,[25] A. Lanza,[75a] M. Lanzac Berrocal,[168] J. F. Laporte,[139] T. Lari,[73a] F. Lasagni Manghi,[24b] M. Lassnig,[37] V. Latonova,[135] A. Laurier,[155] S. D. Lawlor,[144] Z. Lawrence,[104] R. Lazaridou,[172] M. Lazzaroni,[73a,73b] B. Le,[104] H. D. M. Le,[110] E. M. Le Boulicaut,[177] L. T. Le Pottier,[18a] B. Leban,[24b,24a] A. Lebedev,[83] M. LeBlanc,[104] F. Ledroit-Guillon,[62] S. C. Lee,[153] S. Lee,[49a,49b] T. F. Lee,[95] L. L. Leeuw,[34c] M. Lefebvre,[170] C. Leggett,[18a] G. Lehmann Miotto,[37] M. Leigh,[58] W. A. Leight,[106] W. Leinonen,[117] A. Leisos,[157,z] M. A. L. Leite,[85c] C. E. Leitgeb,[19] R. Leitner,[137] K. J. C. Leney,[46] T. Lenz,[25] S. Leone,[76a] C. Leonidopoulos,[54] A. Leopold,[149] R. Les,[110] C. G. Lester,[33] M. Levchenko,[39] J. Levêque,[4] L. J. Levinson,[174] G. Levrini,[24b,24a] M. P. Lewicki,[89] C. Lewis,[143] D. J. Lewis,[4] L. Lewitt,[144] A. Li,[30] B. Li,[64b] C. Li,[64a] C-Q. Li,[113] H. Li,[64a] H. Li,[64b] H. Li,[115a] H. Li,[15] H. Li,[64b] J. Li,[64c] K. Li,[14] L. Li,[64c] M. Li,[14,115c] S. Li,[14,115c] S. Li,[64d,64c,aa] T. Li,[5] X. Li,[107] Z. Li,[158] Z. Li,[14,115c] Z. Li,[64a] S. Liang,[14,115c] Z. Liang,[14] M. Liberatore,[139] B. Liberti,[78a] K. Lie,[66c] J. Lieber Marin,[85e] H. Lien,[70] H. Lin,[109] K. Lin,[110] L. Linden,[112] R. E. Lindley,[7] J. H. Lindon,[2] J. Ling,[63] E. Lipeles,[132] A. Lipniacka,[17] A. Lister,[169] J. D. Little,[70] B. Liu,[14] B. X. Liu,[115b] D. Liu,[64d,64c] E. H. L. Liu,[21] J. B. Liu,[64a] J. K. K. Liu,[33] K. Liu,[64d] K. Liu,[64d,64c] M. Liu,[64a] M. Y. Liu,[64a] P. Liu,[14] Q. Liu,[64d,143,64c] X. Liu,[64a] X. Liu,[64b] Y. Liu,[115b,115c] Y. L. Liu,[64b] Y. W. Liu,[64a] S. L. Lloyd,[97] E. M. Lobodzinska,[50] P. Loch,[7] E. Lodhi,[159] T. Lohse,[19] K. Lohwasser,[144] E. Loiacono,[50] J. D. Lomas,[21] J. D. Long,[43] I. Longarini,[163] R. Longo,[167] I. Lopez Paz,[69] A. Lopez Solis,[50] N. A. Lopez-canelas,[7] N. Lorenzo Martinez,[4] A. M. Lory,[112] M. Losada,[120a] G. Löschcke Centeno,[151] O. Loseva,[39] X. Lou,[49a,49b] X. Lou,[14,115c] A. Lounis,[68] P. A. Love,[94] G. Lu,[14,115c] M. Lu,[68] S. Lu,[132] Y. J. Lu,[67] H. J. Lubatti,[143] C. Luci,[77a,77b] F. L. Lucio Alves,[115a] F. Luehring,[70] O. Lukianchuk,[68] B. S. Lunday,[132] O. Lundberg,[149] B. Lund-Jensen,[149,a] N. A. Luongo,[6] M. S. Lutz,[37] A. B. Lux,[26] D. Lynn,[30] R. Lysak,[135] E. Lytken,[101] V. Lyubushkin,[40] T. Lyubushkina,[40] M. M. Lyukova,[150] M. Firdaus M. Soberi,[54] H. Ma,[30] K. Ma,[64a] L. L. Ma,[64b] W. Ma,[64a] Y. Ma,[125] J. C. MacDonald,[103] P. C. Machado De Abreu Farias,[85e] R. Madar,[42] T. Madula,[99] J. Maeda,[87] T. Maeno,[30] H. Maguire,[144] V. Maiboroda,[139] A. Maio,[134a,134b,134d] K. Maj,[88a] O. Majersky,[50] S. Majewski,[127] N. Makovec,[68] V. Maksimovic,[16] B. Malaescu,[131] Pa. Malecki,[89] V. P. Maleev,[39] F. Malek,[62,bb] M. Mali,[96] D. Malito,[98] U. Mallik,[82,a] S. Maltezos,[10] S. Malyukov,[40] J. Mamuzic,[13] G. Mancini,[55] M. N. Mancini,[27] G. Manco,[75a,75b] J. P. Mandalia,[97] S. S. Mandarry,[151] I. Mandić,[96] L. Manhaes de Andrade Filho,[85a] I. M. Maniatis,[174] J. Manjarres Ramos,[92] D. C. Mankad,[174] A. Mann,[112] S. Manzoni,[37] L. Mao,[64c] X. Mapekula,[34c] A. Marantis,[157,z] G. Marchiori,[5] M. Marcisovsky,[135] C. Marcon,[73a] M. Marinescu,[21] S. Marium,[50] M. Marjanovic,[124] A. Markhoos,[56] M. Markovitch,[68] M. K. Maroun,[106] E. J. Marshall,[94] Z. Marshall,[18a] S. Marti-Garcia,[168] J. Martin,[99] T. A. Martin,[138] V. J. Martin,[54] B. Martin dit Latour,[17] L. Martinelli,[77a,77b] M. Martinez,[13,s] P. Martinez Agullo,[168] V. I. Martinez Outschoorn,[106] P. Martinez Suarez,[13] S. Martin-Haugh,[138] G. Martinovicova,[137] V. S. Martoiu,[28b] A. C. Martyniuk,[99] A. Marzin,[37] D. Mascione,[80a,80b] L. Masetti,[103] J. Masik,[104] A. L. Maslennikov,[39] S. L. Mason,[43] P. Massarotti,[74a,74b] P. Mastrandrea,[76a,76b] A. Mastroberardino,[45b,45a] T. Masubuchi,[128] T. T. Mathew,[127] T. Mathisen,[166] J. Matousek,[137] D. M. Mattern,[51] J. Maurer,[28b] T. Maurin,[61] A. J. Maury,[68] B. Maček,[96] D. A. Maximov,[39] A. E. May,[104] R. Mazini,[34g] I. Maznas,[119] M. Mazza,[110] S. M. Mazza,[140] E. Mazzeo,[73a,73b] J. P. Mc Gowan,[170] S. P. Mc Kee,[109] C. A. Mc Lean,[6] C. C. McCracken,[169] E. F. McDonald,[108] A. E. McDougall,[118] J. A. Mcfayden,[151] R. P. McGovern,[132] R. P. Mckenzie,[34g] T. C. Mclachlan,[50] D. J. Mclaughlin,[99] S. J. McMahon,[138]

C. M. Mcpartland,[95] R. A. McPherson,[170,o] S. Mehlhase,[112] A. Mehta,[95] D. Melini,[168] B. R. Mellado Garcia,[34g] A. H. Melo,[57] F. Meloni,[50] A. M. Mendes Jacques Da Costa,[104] H. Y. Meng,[159] L. Meng,[94] S. Menke,[113] M. Mentink,[37] E. Meoni,[45b,45a] G. Mercado,[119] S. Merianos,[157] C. Merlassino,[71a,71c] L. Merola,[74a,74b] C. Meroni,[73a,73b] J. Metcalfe,[6] A. S. Mete,[6] E. Meuser,[103] C. Meyer,[70] J-P. Meyer,[139] R. P. Middleton,[138] L. Mijović,[54] G. Mikenberg,[174] M. Mikestikova,[135] M. Mikuž,[96] H. Mildner,[103] A. Milic,[37] D. W. Miller,[41] E. H. Miller,[148] L. S. Miller,[35] A. Milov,[174] D. A. Milstead,[49a,49b] T. Min,[115a] A. A. Minaenko,[39] I. A. Minashvili,[154b] A. I. Mincer,[121] B. Mindur,[88a] M. Mineev,[40] Y. Mino,[90] L. M. Mir,[13] M. Miralles Lopez,[61] M. Mironova,[18a] M. C. Missio,[117] A. Mitra,[172] V. A. Mitsou,[168] Y. Mitsumori,[114] O. Miu,[159] P. S. Miyagawa,[97] T. Mkrtchyan,[65a] M. Mlinarevic,[99] T. Mlinarevic,[99] M. Mlynarikova,[37] S. Mobius,[20] P. Mogg,[112] M. H. Mohamed Farook,[116] A. F. Mohammed,[14,115c] S. Mohapatra,[43] G. Mokgatitswane,[34g] L. Moleri,[174] B. Mondal,[146] S. Mondal,[136] K. Mönig,[50] E. Monnier,[105] L. Monsonis Romero,[168] J. Montejo Berlingen,[13] A. Montella,[49a,49b] M. Montella,[123] F. Montereali,[79a,79b] F. Monticelli,[93] S. Monzani,[71a,71c] A. Morancho Tarda,[44] N. Morange,[68] A. L. Moreira De Carvalho,[50] M. Moreno Llácer,[168] C. Moreno Martinez,[58] J. M. Moreno Perez,[23b] P. Morettini,[59b] S. Morgenstern,[37] M. Morii,[63] M. Morinaga,[158] M. Moritsu,[91] F. Morodei,[77a,77b] P. Moschovakos,[37] B. Moser,[130] M. Mosidze,[154b] T. Moskalets,[46] P. Moskvitina,[117] J. Moss,[32,cc] P. Moszkowicz,[88a] A. Moussa,[36d] Y. Moyal,[174] E. J. W. Moyse,[106] O. Mtintsilana,[34g] S. Muanza,[105] J. Mueller,[133] D. Muenstermann,[94] R. Müller,[37] G. A. Mullier,[166] A. J. Mullin,[33] J. J. Mullin,[132] A. E. Mulski,[63] D. P. Mungo,[159] D. Munoz Perez,[168] F. J. Munoz Sanchez,[104] M. Murin,[104] W. J. Murray,[172,138] M. Muškinja,[96] C. Mwewa,[30] A. G. Myagkov,[39,k] A. J. Myers,[8] G. Myers,[109] M. Myska,[136] B. P. Nachman,[18a] K. Nagai,[130] K. Nagano,[86] R. Nagasaka,[158] J. L. Nagle,[30,dd] E. Nagy,[105] A. M. Nairz,[37] Y. Nakahama,[86] K. Nakamura,[86] K. Nakkalil,[5] H. Nanjo,[128] E. A. Narayanan,[46] I. Naryshkin,[39] L. Nasella,[73a,73b] S. Nasri,[120b] C. Nass,[25] G. Navarro,[23a] J. Navarro-Gonzalez,[168] R. Nayak,[156] A. Nayaz,[19] P. Y. Nechaeva,[39] S. Nechaeva,[24b,24a] F. Nechansky,[135] L. Nedic,[130] T. J. Neep,[21] A. Negri,[75a,75b] M. Negrini,[24b] C. Nellist,[118] C. Nelson,[107] K. Nelson,[109] S. Nemecek,[135] M. Nessi,[37,ee] M. S. Neubauer,[167] F. Neuhaus,[103] J. Neundorf,[50] J. Newell,[95] P. R. Newman,[21] C. W. Ng,[133] Y. W. Y. Ng,[50] B. Ngair,[120a] H. D. N. Nguyen,[111] R. B. Nickerson,[130] R. Nicolaidou,[139] J. Nielsen,[140] M. Niemeyer,[57] J. Niermann,[57] N. Nikiforou,[37] V. Nikolaenko,[39,k] I. Nikolic-Audit,[131] K. Nikolopoulos,[21] P. Nilsson,[30] I. Ninca,[50] G. Ninio,[156] A. Nisati,[77a] N. Nishu,[2] R. Nisius,[113] N. Nitika,[71a,71c] J-E. Nitschke,[52] E. K. Nkadimeng,[34g] T. Nobe,[158] T. Nommensen,[152] M. B. Norfolk,[144] B. J. Norman,[35] M. Noury,[36a] J. Novak,[96] T. Novak,[96] L. Novotny,[136] R. Novotny,[116] L. Nozka,[126] K. Ntekas,[163] N. M. J. Nunes De Moura Junior,[85b] J. Ocariz,[131] A. Ochi,[87] I. Ochoa,[134a] S. Oerdek,[50,ff] J. T. Offermann,[41] A. Ogrodnik,[137] A. Oh,[104] C. C. Ohm,[149] H. Oide,[86] R. Oishi,[158] M. L. Ojeda,[37] Y. Okumura,[158] L. F. Oleiro Seabra,[134a] I. Oleksiyuk,[58] S. A. Olivares Pino,[141d] G. Oliveira Correa,[13] D. Oliveira Damazio,[30] J. L. Oliver,[163] Ö. O. Öncel,[56] A. P. O'Neill,[20] A. Onofre,[134a,134e] P. U. E. Onyisi,[11] M. J. Oreglia,[41] D. Orestano,[79a,79b] N. Orlando,[13] R. S. Orr,[159] L. M. Osojnak,[132] R. Ospanov,[64a] Y. Osumi,[114] G. Otero y Garzon,[31] H. Otono,[91] P. S. Ott,[65a] G. J. Ottino,[18a] M. Ouchrif,[36d] F. Ould-Saada,[129] T. Ovsiannikova,[143] M. Owen,[61] R. E. Owen,[138] V. E. Ozcan,[22a] F. Ozturk,[89] N. Ozturk,[8] S. Ozturk,[84] H. A. Pacey,[130] A. Pacheco Pages,[13] C. Padilla Aranda,[13] G. Padovano,[77a,77b] S. Pagan Griso,[18a] G. Palacino,[70] A. Palazzo,[72a,72b] J. Pampel,[25] J. Pan,[177] T. Pan,[66a] D. K. Panchal,[11] C. E. Pandini,[118] J. G. Panduro Vazquez,[138] H. D. Pandya,[1] H. Pang,[15] P. Pani,[50] G. Panizzo,[71a,71c] L. Panwar,[131] L. Paolozzi,[58] S. Parajuli,[167] A. Paramonov,[6] C. Paraskevopoulos,[55] D. Paredes Hernandez,[66b] A. Pareti,[75a,75b] K. R. Park,[43] T. H. Park,[159] M. A. Parker,[33] F. Parodi,[59b,59a] V. A. Parrish,[54] J. A. Parsons,[43] U. Parzefall,[56] B. Pascual Dias,[111] L. Pascual Dominguez,[102] E. Pasqualucci,[77a] S. Passaggio,[59b] F. Pastore,[98] P. Patel,[89] U. M. Patel,[53] J. R. Pater,[104] T. Pauly,[37] F. Pauwels,[137] C. I. Pazos,[162] M. Pedersen,[129] R. Pedro,[134a] S. V. Peleganchuk,[39] O. Penc,[37] E. A. Pender,[54] S. Peng,[15] G. D. Penn,[177] K. E. Penski,[112] M. Penzin,[39] B. S. Peralva,[85d] A. P. Pereira Peixoto,[143] L. Pereira Sanchez,[148] D. V. Perepelitsa,[30,dd] G. Perera,[106] E. Perez Codina,[160a] M. Perganti,[10] H. Pernegger,[37] S. Perrella,[77a,77b] O. Perrin,[42] K. Peters,[50] R. F. Y. Peters,[104] B. A. Petersen,[37] T. C. Petersen,[44] E. Petit,[105] V. Petousis,[136] C. Petridou,[157,y] T. Petru,[137] A. Petrukhin,[146] M. Pettee,[18a] A. Petukhov,[39] K. Petukhova,[37] R. Pezoa,[141f] L. Pezzotti,[37] G. Pezzullo,[177] A. J. Pfleger,[37] T. M. Pham,[175] T. Pham,[108] P. W. Phillips,[138] G. Piacquadio,[150] E. Pianori,[18a] F. Piazza,[127] R. Piegaia,[31] D. Pietreanu,[28b]

A. D. Pilkington,[104] M. Pinamonti,[71a,71c] J. L. Pinfold,[2] B. C. Pinheiro Pereira,[134a] J. Pinol Bel,[13] A. E. Pinto Pinoargote,[139] L. Pintucci,[71a,71c] K. M. Piper,[151] A. Pirttikoski,[58] D. A. Pizzi,[35] L. Pizzimento,[66b] A. Pizzini,[118] M.-A. Pleier,[30] V. Pleskot,[137] E. Plotnikova,[40] G. Poddar,[97] R. Poettgen,[101] L. Poggioli,[131] S. Polacek,[137] G. Polesello,[75a] A. Poley,[147,160a] A. Polini,[24b] C. S. Pollard,[172] Z. B. Pollock,[123] E. Pompa Pacchi,[77a,77b] N. I. Pond,[99] D. Ponomarenko,[70] L. Pontecorvo,[37] S. Popa,[28a] G. A. Popeneciu,[28d] A. Poreba,[37] D. M. Portillo Quintero,[160a] S. Pospisil,[136] M. A. Postill,[144] P. Postolache,[28c] K. Potamianos,[172] P. A. Potepa,[88a] I. N. Potrap,[40] C. J. Potter,[33] H. Potti,[152] J. Poveda,[168] M. E. Pozo Astigarraga,[37] A. Prades Ibanez,[78a,78b] J. Pretel,[170] D. Price,[104] M. Primavera,[72a] L. Primomo,[71a,71c] M. A. Principe Martin,[102] R. Privara,[126] T. Procter,[61] M. L. Proffitt,[143] N. Proklova,[132] K. Prokofiev,[66c] G. Proto,[113] J. Proudfoot,[6] M. Przybycien,[88a] W. W. Przygoda,[88b] A. Psallidas,[48] J. E. Puddefoot,[144] D. Pudzha,[56] D. Pyatiizbyantseva,[39] J. Qian,[109] R. Qian,[110] D. Qichen,[104] Y. Qin,[13] T. Qiu,[54] A. Quadt,[57] M. Queitsch-Maitland,[104] G. Quetant,[58] R. P. Quinn,[169] G. Rabanal Bolanos,[63] D. Rafanoharana,[56] F. Raffaeli,[78a,78b] F. Ragusa,[73a,73b] J. L. Rainbolt,[41] J. A. Raine,[58] S. Rajagopalan,[30] E. Ramakoti,[39] L. Rambelli,[59b,59a] I. A. Ramirez-Berend,[35] K. Ran,[50,115c] D. S. Rankin,[132] N. P. Rapheeha,[34g] H. Rasheed,[28b] V. Raskina,[131] D. F. Rassloff,[65a] A. Rastogi,[18a] S. Rave,[103] S. Ravera,[59b,59a] B. Ravina,[57] I. Ravinovich,[174] M. Raymond,[37] A. L. Read,[129] N. P. Readioff,[144] D. M. Rebuzzi,[75a,75b] G. Redlinger,[30] A. S. Reed,[113] K. Reeves,[27] J. A. Reidelsturz,[176] D. Reikher,[127] A. Rej,[51] C. Rembser,[37] M. Renda,[28b] F. Renner,[50] A. G. Rennie,[163] A. L. Rescia,[50] S. Resconi,[73a] M. Ressegotti,[59b,59a] S. Rettie,[37] J. G. Reyes Rivera,[110] E. Reynolds,[18a] O. L. Rezanova,[39] P. Reznicek,[137] H. Riani,[36d] N. Ribaric,[53] E. Ricci,[80a,80b] R. Richter,[113] S. Richter,[49a,49b] E. Richter-Was,[88b] M. Ridel,[131] S. Ridouani,[36d] P. Rieck,[121] P. Riedler,[37] E. M. Riefel,[49a,49b] J. O. Rieger,[118] M. Rijssenbeek,[150] M. Rimoldi,[37] L. Rinaldi,[24b,24a] P. Rincke,[57] T. T. Rinn,[30] M. P. Rinnagel,[112] G. Ripellino,[166] I. Riu,[13] J. C. Rivera Vergara,[170] F. Rizatdinova,[125] E. Rizvi,[97] B. R. Roberts,[18a] S. S. Roberts,[140] S. H. Robertson,[107,o] D. Robinson,[33] M. Robles Manzano,[103] A. Robson,[61] A. Rocchi,[78a,78b] C. Roda,[76a,76b] S. Rodriguez Bosca,[37] Y. Rodriguez Garcia,[23a] A. M. Rodríguez Vera,[119] S. Roe,[37] J. T. Roemer,[37] A. R. Roepe-Gier,[140] O. Røhne,[129] R. A. Rojas,[37] C. P. A. Roland,[131] J. Roloff,[30] A. Romaniouk,[81] E. Romano,[75a,75b] M. Romano,[24b] A. C. Romero Hernandez,[167] N. Rompotis,[95] L. Roos,[131] S. Rosati,[77a] B. J. Rosser,[41] E. Rossi,[130] E. Rossi,[74a,74b] L. P. Rossi,[63] L. Rossini,[56] R. Rosten,[123] M. Rotaru,[28b] B. Rottler,[56] C. Rougier,[92] D. Rousseau,[68] D. Rousso,[50] A. Roy,[167] S. Roy-Garand,[159] A. Rozanov,[105] Z. M. A. Rozario,[61] Y. Rozen,[155] A. Rubio Jimenez,[168] V. H. Ruelas Rivera,[19] T. A. Ruggeri,[1] A. Ruggiero,[130] A. Ruiz-Martinez,[168] A. Rummler,[37] Z. Rurikova,[56] N. A. Rusakovich,[40] H. L. Russell,[170] G. Russo,[77a,77b] J. P. Rutherfoord,[7] S. Rutherford Colmenares,[33] M. Rybar,[137] E. B. Rye,[129] A. Ryzhov,[46] J. A. Sabater Iglesias,[58] H. F-W. Sadrozinski,[140] F. Safai Tehrani,[77a] B. Safarzadeh Samani,[138] S. Saha,[1] M. Sahinsoy,[84] A. Saibel,[168] M. Saimpert,[139] M. Saito,[158] T. Saito,[158] A. Sala,[73a,73b] D. Salamani,[37] A. Salnikov,[148] J. Salt,[168] A. Salvador Salas,[156] D. Salvatore,[45b,45a] F. Salvatore,[151] A. Salzburger,[37] D. Sammel,[56] E. Sampson,[94] D. Sampsonidis,[157,y] D. Sampsonidou,[127] J. Sánchez,[168] V. Sanchez Sebastian,[168] H. Sandaker,[129] C. O. Sander,[50] J. A. Sandesara,[106] M. Sandhoff,[176] C. Sandoval,[23b] L. Sanfilippo,[65a] D. P. C. Sankey,[138] T. Sano,[90] A. Sansoni,[55] L. Santi,[37,77b] C. Santoni,[42] H. Santos,[134a,134b] A. Santra,[174] E. Sanzani,[24b,24a] K. A. Saoucha,[165] J. G. Saraiva,[134a,134d] J. Sardain,[7] O. Sasaki,[86] K. Sato,[161] C. Sauer,[37] E. Sauvan,[4] P. Savard,[159,e] R. Sawada,[158] C. Sawyer,[138] L. Sawyer,[100] C. Sbarra,[24b] A. Sbrizzi,[24b,24a] T. Scanlon,[99] J. Schaarschmidt,[143] U. Schäfer,[103] A. C. Schaffer,[68,46] D. Schaile,[112] R. D. Schamberger,[150] C. Scharf,[19] M. M. Schefer,[20] V. A. Schegelsky,[39] D. Scheirich,[137] M. Schernau,[141e] C. Scheulen,[57] C. Schiavi,[59b,59a] M. Schioppa,[45b,45a] B. Schlag,[148] S. Schlenker,[37] J. Schmeing,[176] M. A. Schmidt,[176] K. Schmieden,[103] C. Schmitt,[103] N. Schmitt,[103] S. Schmitt,[50] L. Schoeffel,[139] A. Schoening,[65b] P. G. Scholer,[35] E. Schopf,[130] M. Schott,[25] J. Schovancova,[37] S. Schramm,[58] T. Schroer,[58] H-C. Schultz-Coulon,[65a] M. Schumacher,[56] B. A. Schumm,[140] Ph. Schune,[139] A. J. Schuy,[143] H. R. Schwartz,[140] A. Schwartzman,[148] T. A. Schwarz,[109] Ph. Schwemling,[139] R. Schwienhorst,[110] F. G. Sciacca,[20] A. Sciandra,[30] G. Sciolla,[27] F. Scuri,[76a] C. D. Sebastiani,[95] K. Sedlaczek,[119] S. C. Seidel,[116] A. Seiden,[140] B. D. Seidlitz,[43] C. Seitz,[50] J. M. Seixas,[85b] G. Sekhniaidze,[74a] L. Selem,[62] N. Semprini-Cesari,[24b,24a] D. Sengupta,[58] V. Senthilkumar,[168] L. Serin,[68] M. Sessa,[78a,78b] H. Severini,[124] F. Sforza,[59b,59a] A. Sfyrla,[58] Q. Sha,[14] E. Shabalina,[57] A. H. Shah,[33] R. Shaheen,[149] J. D. Shahinian,[132] D. Shaked Renous,[174] L. Y. Shan,[14] M. Shapiro,[18a] A. Sharma,[37] A. S. Sharma,[169] P. Sharma,[82] P. B. Shatalov,[39]

K. Shaw,[151] S. M. Shaw,[104] Q. Shen,[64c] D. J. Sheppard,[147] P. Sherwood,[99] L. Shi,[99] X. Shi,[14] S. Shimizu,[86] C. O. Shimmin,[177] I. P. J. Shipsey,[130,a] S. Shirabe,[91] M. Shiyakova,[40,gg] M. J. Shochet,[41] D. R. Shope,[129] B. Shrestha,[124] S. Shrestha,[123,hh] I. Shreyber,[39] M. J. Shroff,[170] P. Sicho,[135] A. M. Sickles,[167] E. Sideras Haddad,[34g,164] A. C. Sidley,[118] A. Sidoti,[24b] F. Siegert,[52] Dj. Sijacki,[16] F. Sili,[93] J. M. Silva,[54] I. Silva Ferreira,[85b] M. V. Silva Oliveira,[30] S. B. Silverstein,[49a] S. Simion,[68] R. Simoniello,[37] E. L. Simpson,[104] H. Simpson,[151] L. R. Simpson,[109] S. Simsek,[84] S. Sindhu,[57] P. Sinervo,[159] S. Singh,[30] S. Sinha,[50] S. Sinha,[104] M. Sioli,[24b,24a] I. Siral,[37] E. Sitnikova,[50] J. Sjölin,[49a,49b] A. Skaf,[57] E. Skorda,[21] P. Skubic,[124] M. Slawinska,[89] V. Smakhtin,[174] B. H. Smart,[138] S. Yu. Smirnov,[39] Y. Smirnov,[39] L. N. Smirnova,[39,k] O. Smirnova,[101] A. C. Smith,[43] D. R. Smith,[163] E. A. Smith,[41] J. L. Smith,[104] R. Smith,[148] H. Smitmanns,[103] M. Smizanska,[94] K. Smolek,[136] A. A. Snesarev,[39] H. L. Snoek,[118] S. Snyder,[30] R. Sobie,[170,o] A. Soffer,[156] C. A. Solans Sanchez,[37] E. Yu. Soldatov,[39] U. Soldevila,[168] A. A. Solodkov,[39] S. Solomon,[27] A. Soloshenko,[40] K. Solovieva,[56] O. V. Solovyanov,[42] P. Sommer,[52] A. Sonay,[13] W. Y. Song,[160b] A. Sopczak,[136] A. L. Sopio,[54] F. Sopkova,[29b] J. D. Sorenson,[116] I. R. Sotarriva Alvarez,[142] V. Sothilingam,[65a] O. J. Soto Sandoval,[141c,141b] S. Sottocornola,[70] R. Soualah,[165] Z. Soumaimi,[36e] D. South,[50] N. Soybelman,[174] S. Spagnolo,[72a,72b] M. Spalla,[113] D. Sperlich,[56] G. Spigo,[37] B. Spisso,[74a,74b] D. P. Spiteri,[61] M. Spousta,[137] E. J. Staats,[35] R. Stamen,[65a] A. Stampekis,[21] E. Stanecka,[89] W. Stanek-Maslouska,[50] M. V. Stange,[52] B. Stanislaus,[18a] M. M. Stanitzki,[50] B. Stapf,[50] E. A. Starchenko,[39] G. H. Stark,[140] J. Stark,[92] P. Staroba,[135] P. Starovoitov,[65a] S. Stärz,[107] R. Staszewski,[89] G. Stavropoulos,[48] A. Stefl,[37] P. Steinberg,[30] B. Stelzer,[147,160a] H. J. Stelzer,[133] O. Stelzer-Chilton,[160a] H. Stenzel,[60] T. J. Stevenson,[151] G. A. Stewart,[37] J. R. Stewart,[125] M. C. Stockton,[37] G. Stoicea,[28b] M. Stolarski,[134a] S. Stonjek,[113] A. Straessner,[52] J. Strandberg,[149] S. Strandberg,[49a,49b] M. Stratmann,[176] M. Strauss,[124] T. Strebler,[105] P. Strizenec,[29b] R. Ströhmer,[171] D. M. Strom,[127] R. Stroynowski,[46] A. Strubig,[49a,49b] S. A. Stucci,[30] B. Stugu,[17] J. Stupak,[124] N. A. Styles,[50] D. Su,[148] S. Su,[64a] W. Su,[64d] X. Su,[64a] D. Suchy,[29a] K. Sugizaki,[158] V. V. Sulin,[39] M. J. Sullivan,[95] D. M. S. Sultan,[130] L. Sultanaliyeva,[39] S. Sultansoy,[3b] T. Sumida,[90] H. Sun,[167] S. Sun,[175] O. Sunneborn Gudnadottir,[166] N. Sur,[105] M. R. Sutton,[151] H. Suzuki,[161] M. Svatos,[135] M. Swiatlowski,[160a] T. Swirski,[171] I. Sykora,[29a] M. Sykora,[137] T. Sykora,[137] D. Ta,[103] K. Tackmann,[50,ff] A. Taffard,[163] R. Tafirout,[160a] J. S. Tafoya Vargas,[68] Y. Takubo,[86] M. Talby,[105] A. A. Talyshev,[39] K. C. Tam,[66b] N. M. Tamir,[156] A. Tanaka,[158] J. Tanaka,[158] R. Tanaka,[68] M. Tanasini,[150] Z. Tao,[169] S. Tapia Araya,[141f] S. Tapprogge,[103] A. Tarek Abouelfadl Mohamed,[110] S. Tarem,[155] K. Tariq,[14] G. Tarna,[28b] G. F. Tartarelli,[73a] M. J. Tartarin,[92] P. Tas,[137] M. Tasevsky,[135] E. Tassi,[45b,45a] A. C. Tate,[167] G. Tateno,[158] Y. Tayalati,[36e,ii] G. N. Taylor,[108] W. Taylor,[160b] R. Teixeira De Lima,[148] P. Teixeira-Dias,[98] J. J. Teoh,[159] K. Terashi,[158] J. Terron,[102] S. Terzo,[13] M. Testa,[55] R. J. Teuscher,[159,o] A. Thaler,[81] O. Theiner,[58] T. Theveneaux-Pelzer,[105] O. Thielmann,[176] D. W. Thomas,[98] J. P. Thomas,[21] E. A. Thompson,[18a] P. D. Thompson,[21] E. Thomson,[132] R. E. Thornberry,[46] C. Tian,[64a] Y. Tian,[58] V. Tikhomirov,[39,k] Yu. A. Tikhonov,[39] S. Timoshenko,[39] D. Timoshyn,[137] E. X. L. Ting,[1] P. Tipton,[177] A. Tishelman-Charny,[30] S. H. Tlou,[34g] K. Todome,[142] S. Todorova-Nova,[137] S. Todt,[52] L. Toffolin,[71a,71c] M. Togawa,[86] J. Tojo,[91] S. Tokár,[29a] K. Tokushuku,[86] O. Toldaiev,[70] M. Tomoto,[86,114] L. Tompkins,[148,jj] K. W. Topolnicki,[88b] E. Torrence,[127] H. Torres,[92] E. Torró Pastor,[168] M. Toscani,[31] C. Tosciri,[41] M. Tost,[11] D. R. Tovey,[144] I. S. Trandafir,[28b] T. Trefzger,[171] A. Tricoli,[30] I. M. Trigger,[160a] S. Trincaz-Duvoid,[131] D. A. Trischuk,[27] B. Trocmé,[62] A. Tropina,[40] L. Truong,[34c] M. Trzebinski,[89] A. Trzupek,[89] F. Tsai,[150] M. Tsai,[109] A. Tsiamis,[157] P. V. Tsiareshka,[40] S. Tsigaridas,[160a] A. Tsirigotis,[157,z] V. Tsiskaridze,[159] E. G. Tskhadadze,[154a] M. Tsopoulou,[157] Y. Tsujikawa,[90] I. I. Tsukerman,[39] V. Tsulaia,[18a] S. Tsuno,[86] K. Tsuri,[122] D. Tsybychev,[150] Y. Tu,[66b] A. Tudorache,[28b] V. Tudorache,[28b] A. N. Tuna,[63] S. Turchikhin,[59b,59a] I. Turk Cakir,[3a] R. Turra,[73a] T. Turtuvshin,[40,kk] P. M. Tuts,[43] S. Tzamarias,[157,y] E. Tzovara,[103] F. Ukegawa,[161] P. A. Ulloa Poblete,[141c,141b] E. N. Umaka,[30] G. Unal,[37] A. Undrus,[30] G. Unel,[163] J. Urban,[29b] P. Urrejola,[141a] G. Usai,[8] R. Ushioda,[142] M. Usman,[111] F. Ustuner,[54] Z. Uysal,[84] V. Vacek,[136] B. Vachon,[107] T. Vafeiadis,[37] A. Vaitkus,[99] C. Valderanis,[112] E. Valdes Santurio,[49a,49b] M. Valente,[160a] S. Valentinetti,[24b,24a] A. Valero,[168] E. Valiente Moreno,[168] A. Vallier,[92] J. A. Valls Ferrer,[168] D. R. Van Arneman,[118] T. R. Van Daalen,[143] A. Van Der Graaf,[51] P. Van Gemmeren,[6] M. Van Rijnbach,[37] S. Van Stroud,[99] I. Van Vulpen,[118] P. Vana,[137] M. Vanadia,[78a,78b] U. M. Vande Voorde,[149] W. Vandelli,[37] E. R. Vandewall,[125] D. Vannicola,[156] L. Vannoli,[55]

R. Vari,[77a] E. W. Varnes,[7] C. Varni,[18b] T. Varol,[153] D. Varouchas,[68] L. Varriale,[168] K. E. Varvell,[152] M. E. Vasile,[28b] L. Vaslin,[86] A. Vasyukov,[40] L. M. Vaughan,[125] R. Vavricka,[103] T. Vazquez Schroeder,[37] J. Veatch,[32] V. Vecchio,[104] M. J. Veen,[106] I. Veliscek,[30] L. M. Veloce,[159] F. Veloso,[134a,134c] S. Veneziano,[77a] A. Ventura,[72a,72b] S. Ventura Gonzalez,[139] A. Verbytskyi,[113] M. Verducci,[76a,76b] C. Vergis,[97] M. Verissimo De Araujo,[85b] W. Verkerke,[118] J. C. Vermeulen,[118] C. Vernieri,[148] M. Vessella,[106] M. C. Vetterli,[147,e] A. Vgenopoulos,[103] N. Viaux Maira,[141f] T. Vickey,[144] O. E. Vickey Boeriu,[144] G. H. A. Viehhauser,[130] L. Vigani,[65b] M. Vigl,[113] M. Villa,[24b,24a] M. Villaplana Perez,[168] E. M. Villhauer,[54] E. Vilucchi,[55] M. G. Vincter,[35] A. Visibile,[118] C. Vittori,[37] I. Vivarelli,[24b,24a] E. Voevodina,[113] F. Vogel,[112] J. C. Voigt,[52] P. Vokac,[136] Yu. Volkotrub,[88b] E. Von Toerne,[25] B. Vormwald,[37] V. Vorobel,[137] K. Vorobev,[39] M. Vos,[168] K. Voss,[146] M. Vozak,[118] L. Vozdecky,[124] N. Vranjes,[16] M. Vranjes Milosavljevic,[16] M. Vreeswijk,[118] N. K. Vu,[64d,64c] R. Vuillermet,[37] O. Vujinovic,[103] I. Vukotic,[41] I. K. Vyas,[35] S. Wada,[161] C. Wagner,[148] J. M. Wagner,[18a] W. Wagner,[176] S. Wahdan,[176] H. Wahlberg,[93] C. H. Waits,[124] J. Walder,[138] R. Walker,[112] W. Walkowiak,[146] A. Wall,[132] E. J. Wallin,[101] T. Wamorkar,[6] A. Z. Wang,[140] C. Wang,[103] C. Wang,[11] H. Wang,[18a] J. Wang,[66c] P. Wang,[99] R. Wang,[63] R. Wang,[6] S. M. Wang,[153] S. Wang,[14] T. Wang,[64a] W. T. Wang,[82] W. Wang,[14] X. Wang,[115a] X. Wang,[167] X. Wang,[64c] Y. Wang,[64d] Y. Wang,[115a] Y. Wang,[64a] Z. Wang,[109] Z. Wang,[64d,53,64c] Z. Wang,[109] A. Warburton,[107] R. J. Ward,[21] N. Warrack,[61] S. Waterhouse,[98] A. T. Watson,[21] H. Watson,[54] M. F. Watson,[21] E. Watton,[61,138] G. Watts,[143] B. M. Waugh,[99] J. M. Webb,[56] C. Weber,[30] H. A. Weber,[19] M. S. Weber,[20] S. M. Weber,[65a] C. Wei,[64a] Y. Wei,[56] A. R. Weidberg,[130] E. J. Weik,[121] J. Weingarten,[51] C. Weiser,[56] C. J. Wells,[50] T. Wenaus,[30] B. Wendland,[51] T. Wengler,[37] N. S. Wenke,[113] N. Wermes,[25] M. Wessels,[65a] A. M. Wharton,[94] A. S. White,[63] A. White,[8] M. J. White,[1] D. Whiteson,[163] L. Wickremasinghe,[128] W. Wiedenmann,[175] M. Wielers,[138] C. Wiglesworth,[44] D. J. Wilbern,[124] H. G. Wilkens,[37] J. J. H. Wilkinson,[33] D. M. Williams,[43] H. H. Williams,[132] S. Williams,[33] S. Willocq,[106] B. J. Wilson,[104] P. J. Windischhofer,[41] F. I. Winkel,[31] F. Winklmeier,[127] B. T. Winter,[56] J. K. Winter,[104] M. Wittgen,[148] M. Wobisch,[100] T. Wojtkowski,[62] Z. Wolffs,[118] J. Wollrath,[37] M. W. Wolter,[89] H. Wolters,[134a,134c] M. C. Wong,[140] E. L. Woodward,[43] S. D. Worm,[50] B. K. Wosiek,[89] K. W. Woźniak,[89] S. Wozniewski,[57] K. Wraight,[61] C. Wu,[21] M. Wu,[115b] M. Wu,[117] S. L. Wu,[175] X. Wu,[58] Y. Wu,[64a] Z. Wu,[4] J. Wuerzinger,[113,t] T. R. Wyatt,[104] B. M. Wynne,[54] S. Xella,[44] L. Xia,[115a] M. Xia,[15] M. Xie,[64a] S. Xin,[14,115c] A. Xiong,[127] J. Xiong,[18a] D. Xu,[14] H. Xu,[64a] L. Xu,[64a] R. Xu,[132] T. Xu,[109] Y. Xu,[143] Z. Xu,[54] Z. Xu,[115a] B. Yabsley,[152] S. Yacoob,[34a] Y. Yamaguchi,[86] E. Yamashita,[158] H. Yamauchi,[161] T. Yamazaki,[18a] Y. Yamazaki,[87] S. Yan,[61] Z. Yan,[106] H. J. Yang,[64c,64d] H. T. Yang,[64a] S. Yang,[64a] T. Yang,[66c] X. Yang,[37] X. Yang,[14] Y. Yang,[46] Y. Yang,[64a] W-M. Yao,[18a] H. Ye,[115a] H. Ye,[57] J. Ye,[14] S. Ye,[30] X. Ye,[64a] Y. Yeh,[99] I. Yeletskikh,[40] B. Yeo,[18b] M. R. Yexley,[99] T. P. Yildirim,[130] P. Yin,[43] K. Yorita,[173] S. Younas,[28b] C. J. S. Young,[37] C. Young,[148] C. Yu,[14,115c] Y. Yu,[64a] J. Yuan,[14,115c] M. Yuan,[109] R. Yuan,[64d,64c] L. Yue,[99] M. Zaazoua,[64a] B. Zabinski,[89] E. Zaid,[54] Z. K. Zak,[89] T. Zakareishvili,[168] S. Zambito,[58] J. A. Zamora Saa,[141d,141b] J. Zang,[158] D. Zanzi,[56] O. Zaplatilek,[136] C. Zeitnitz,[176] H. Zeng,[14] J. C. Zeng,[167] D. T. Zenger Jr.,[27] O. Zenin,[39] T. Ženiš,[29a] S. Zenz,[97] S. Zerradi,[36a] D. Zerwas,[68] M. Zhai,[14,115c] D. F. Zhang,[144] J. Zhang,[64b] J. Zhang,[6] K. Zhang,[14,115c] L. Zhang,[64a] L. Zhang,[115a] P. Zhang,[14,115c] R. Zhang,[175] S. Zhang,[109] S. Zhang,[92] T. Zhang,[158] X. Zhang,[64c] Y. Zhang,[143] Y. Zhang,[99] Y. Zhang,[115a] Z. Zhang,[18a] Z. Zhang,[64b] Z. Zhang,[68] H. Zhao,[143] T. Zhao,[64b] Y. Zhao,[140] Z. Zhao,[64a] Z. Zhao,[64a] A. Zhemchugov,[40] J. Zheng,[115a] K. Zheng,[167] X. Zheng,[64a] Z. Zheng,[148] D. Zhong,[167] B. Zhou,[109] H. Zhou,[7] N. Zhou,[64c] Y. Zhou,[15] Y. Zhou,[115a] Y. Zhou,[7] C. G. Zhu,[64b] J. Zhu,[109] X. Zhu,[64d] Y. Zhu,[64c] Y. Zhu,[64a] X. Zhuang,[14] K. Zhukov,[70] N. I. Zimine,[40] J. Zinsser,[65b] M. Ziolkowski,[146] L. Živković,[16] A. Zoccoli,[24b,24a] K. Zoch,[63] T. G. Zorbas,[144] O. Zormpa,[48] W. Zou,[43] and L. Zwalinski[37]

(ATLAS Collaboration)

[1]*Department of Physics, University of Adelaide, Adelaide, Australia*
[2]*Department of Physics, University of Alberta, Edmonton, Alberta, Canada*
[3a]*Department of Physics, Ankara University, Ankara, Türkiye*
[3b]*Division of Physics, TOBB University of Economics and Technology, Ankara, Türkiye*
[4]*LAPP, Université Savoie Mont Blanc, CNRS/IN2P3, Annecy, France*

[5]*APC, Université Paris Cité, CNRS/IN2P3, Paris, France*
[6]*High Energy Physics Division, Argonne National Laboratory, Argonne, Illinois, USA*
[7]*Department of Physics, University of Arizona, Tucson, Arizona, USA*
[8]*Department of Physics, University of Texas at Arlington, Arlington, Texas, USA*
[9]*Physics Department, National and Kapodistrian University of Athens, Athens, Greece*
[10]*Physics Department, National Technical University of Athens, Zografou, Greece*
[11]*Department of Physics, University of Texas at Austin, Austin, Texas, USA*
[12]*Institute of Physics, Azerbaijan Academy of Sciences, Baku, Azerbaijan*
[13]*Institut de Física d'Altes Energies (IFAE), Barcelona Institute of Science and Technology, Barcelona, Spain*
[14]*Institute of High Energy Physics, Chinese Academy of Sciences, Beijing, China*
[15]*Physics Department, Tsinghua University, Beijing, China*
[16]*Institute of Physics, University of Belgrade, Belgrade, Serbia*
[17]*Department for Physics and Technology, University of Bergen, Bergen, Norway*
[18a]*Physics Division, Lawrence Berkeley National Laboratory, Berkeley, California, USA*
[18b]*University of California, Berkeley, California, USA*
[19]*Institut für Physik, Humboldt Universität zu Berlin, Berlin, Germany*
[20]*Albert Einstein Center for Fundamental Physics and Laboratory for High Energy Physics, University of Bern, Bern, Switzerland*
[21]*School of Physics and Astronomy, University of Birmingham, Birmingham, United Kingdom*
[22a]*Department of Physics, Bogazici University, Istanbul, Türkiye*
[22b]*Department of Physics Engineering, Gaziantep University, Gaziantep, Türkiye*
[22c]*Department of Physics, Istanbul University, Istanbul, Türkiye*
[23a]*Facultad de Ciencias y Centro de Investigaciónes, Universidad Antonio Nariño, Bogotá, Colombia*
[23b]*Departamento de Física, Universidad Nacional de Colombia, Bogotá, Colombia*
[24a]*Dipartimento di Fisica e Astronomia A. Righi, Università di Bologna, Bologna, Italy*
[24b]*INFN Sezione di Bologna, Bologna, Italy*
[25]*Physikalisches Institut, Universität Bonn, Bonn, Germany*
[26]*Department of Physics, Boston University, Boston, Massachusetts, USA*
[27]*Department of Physics, Brandeis University, Waltham, Massachusetts, USA*
[28a]*Transilvania University of Brasov, Brasov, Romania*
[28b]*Horia Hulubei National Institute of Physics and Nuclear Engineering, Bucharest, Romania*
[28c]*Department of Physics, Alexandru Ioan Cuza University of Iasi, Iasi, Romania*
[28d]*National Institute for Research and Development of Isotopic and Molecular Technologies, Physics Department, Cluj-Napoca, Romania*
[28e]*National University of Science and Technology Politechnica, Bucharest, Romania*
[28f]*West University in Timisoara, Timisoara, Romania*
[28g]*Faculty of Physics, University of Bucharest, Bucharest, Romania*
[29a]*Faculty of Mathematics, Physics and Informatics, Comenius University, Bratislava, Slovak Republic*
[29b]*Department of Subnuclear Physics, Institute of Experimental Physics of the Slovak Academy of Sciences, Kosice, Slovak Republic*
[30]*Physics Department, Brookhaven National Laboratory, Upton, New York, USA*
[31]*Universidad de Buenos Aires, Facultad de Ciencias Exactas y Naturales, Departamento de Física, y CONICET, Instituto de Física de Buenos Aires (IFIBA), Buenos Aires, Argentina*
[32]*California State University, Long Beach, California, USA*
[33]*Cavendish Laboratory, University of Cambridge, Cambridge, United Kingdom*
[34a]*Department of Physics, University of Cape Town, Cape Town, South Africa*
[34b]*iThemba Labs, Western Cape, South Africa*
[34c]*Department of Mechanical Engineering Science, University of Johannesburg, Johannesburg, South Africa*
[34d]*National Institute of Physics, University of the Philippines Diliman (Philippines), Quezon City, Philippines*
[34e]*University of South Africa, Department of Physics, Pretoria, South Africa*
[34f]*University of Zululand, KwaDlangezwa, South Africa*
[34g]*School of Physics, University of the Witwatersrand, Johannesburg, South Africa*
[35]*Department of Physics, Carleton University, Ottawa, Ontario, Canada*
[36a]*Faculté des Sciences Ain Chock, Université Hassan II de Casablanca, Casablanca, Morocco*
[36b]*Faculté des Sciences, Université Ibn-Tofail, Kénitra, Morocco*
[36c]*Faculté des Sciences Semlalia, Université Cadi Ayyad, LPHEA-Marrakech, Morocco*
[36d]*LPMR, Faculté des Sciences, Université Mohamed Premier, Oujda, Morocco*

[36e]*Faculté des sciences, Université Mohammed V, Rabat, Morocco*
[36f]*Institute of Applied Physics, Mohammed VI Polytechnic University, Ben Guerir, Morocco*
[37]*CERN, Geneva, Switzerland*
[38]*Affiliated with an institute formerly covered by a cooperation agreement with CERN*
[39]*Affiliated with an institute covered by a cooperation agreement with CERN*
[40]*Affiliated with an international laboratory covered by a cooperation agreement with CERN*
[41]*Enrico Fermi Institute, University of Chicago, Chicago, Illinois, USA*
[42]*LPC, Université Clermont Auvergne, CNRS/IN2P3, Clermont-Ferrand, France*
[43]*Nevis Laboratory, Columbia University, Irvington, New York, USA*
[44]*Niels Bohr Institute, University of Copenhagen, Copenhagen, Denmark*
[45a]*Dipartimento di Fisica, Università della Calabria, Rende, Italy*
[45b]*INFN Gruppo Collegato di Cosenza, Laboratori Nazionali di Frascati, Frascati, Italy*
[46]*Physics Department, Southern Methodist University, Dallas, Texas, USA*
[47]*Physics Department, University of Texas at Dallas, Richardson, Texas, USA*
[48]*National Centre for Scientific Research "Demokritos," Agia Paraskevi, Greece*
[49a]*Department of Physics, Stockholm University, Stockholm, Sweden*
[49b]*Oskar Klein Centre, Stockholm, Sweden*
[50]*Deutsches Elektronen-Synchrotron DESY, Hamburg and Zeuthen, Germany*
[51]*Fakultät Physik, Technische Universität Dortmund, Dortmund, Germany*
[52]*Institut für Kern- und Teilchenphysik, Technische Universität Dresden, Dresden, Germany*
[53]*Department of Physics, Duke University, Durham, North Carolina, USA*
[54]*SUPA—School of Physics and Astronomy, University of Edinburgh, Edinburgh, United Kingdom*
[55]*INFN e Laboratori Nazionali di Frascati, Frascati, Italy*
[56]*Physikalisches Institut, Albert-Ludwigs-Universität Freiburg, Freiburg, Germany*
[57]*II. Physikalisches Institut, Georg-August-Universität Göttingen, Göttingen, Germany*
[58]*Département de Physique Nucléaire et Corpusculaire, Université de Genève, Genève, Switzerland*
[59a]*Dipartimento di Fisica, Università di Genova, Genova, Italy*
[59b]*INFN Sezione di Genova, Genova, Italy*
[60]*II. Physikalisches Institut, Justus-Liebig-Universität Giessen, Giessen, Germany*
[61]*SUPA—School of Physics and Astronomy, University of Glasgow, Glasgow, United Kingdom*
[62]*LPSC, Université Grenoble Alpes, CNRS/IN2P3, Grenoble INP, Grenoble, France*
[63]*Laboratory for Particle Physics and Cosmology, Harvard University, Cambridge, Massachusetts, USA*
[64a]*Department of Modern Physics and State Key Laboratory of Particle Detection and Electronics, University of Science and Technology of China, Hefei, China*
[64b]*Institute of Frontier and Interdisciplinary Science and Key Laboratory of Particle Physics and Particle Irradiation (MOE), Shandong University, Qingdao, China*
[64c]*State Key Laboratory of Dark Matter Physics, School of Physics and Astronomy, Shanghai Jiao Tong University, Key Laboratory for Particle Astrophysics and Cosmology (MOE), SKLPPC, Shanghai, China*
[64d]*State Key Laboratory of Dark Matter Physics, Tsung-Dao Lee Institute, Shanghai Jiao Tong University, Shanghai, China*
[64e]*School of Physics, Zhengzhou University, Zhengzhou, China*
[65a]*Kirchhoff-Institut für Physik, Ruprecht-Karls-Universität Heidelberg, Heidelberg, Germany*
[65b]*Physikalisches Institut, Ruprecht-Karls-Universität Heidelberg, Heidelberg, Germany*
[66a]*Department of Physics, Chinese University of Hong Kong, Sha Tin, New Town, Hong Kong, China*
[66b]*Department of Physics, University of Hong Kong, Hong Kong, China*
[66c]*Department of Physics and Institute for Advanced Study, Hong Kong University of Science and Technology, Clear Water Bay, Kowloon, Hong Kong, China*
[67]*Department of Physics, National Tsing Hua University, Hsinchu, Taiwan*
[68]*IJCLab, Université Paris-Saclay, CNRS/IN2P3, 91405, Orsay, France*
[69]*Centro Nacional de Microelectrónica (IMB-CNM-CSIC), Barcelona, Spain*
[70]*Department of Physics, Indiana University, Bloomington, Indiana, USA*
[71a]*INFN Gruppo Collegato di Udine, Sezione di Trieste, Udine, Italy*
[71b]*ICTP, Trieste, Italy*
[71c]*Dipartimento Politecnico di Ingegneria e Architettura, Università di Udine, Udine, Italy*
[72a]*INFN Sezione di Lecce, Lecce, Italy*
[72b]*Dipartimento di Matematica e Fisica, Università del Salento, Lecce, Italy*
[73a]*INFN Sezione di Milano, Milano, Italy*
[73b]*Dipartimento di Fisica, Università di Milano, Milano, Italy*
[74a]*INFN Sezione di Napoli, Napoli, Italy*
[74b]*Dipartimento di Fisica, Università di Napoli, Napoli, Italy*

[75a]*INFN Sezione di Pavia, Pavia, Italy*
[75b]*Dipartimento di Fisica, Università di Pavia, Pavia, Italy*
[76a]*INFN Sezione di Pisa, Pisa, Italy*
[76b]*Dipartimento di Fisica E. Fermi, Università di Pisa, Pisa, Italy*
[77a]*INFN Sezione di Roma, Roma, Italy*
[77b]*Dipartimento di Fisica, Sapienza Università di Roma, Roma, Italy*
[78a]*INFN Sezione di Roma Tor Vergata, Roma, Italy*
[78b]*Dipartimento di Fisica, Università di Roma Tor Vergata, Roma, Italy*
[79a]*INFN Sezione di Roma Tre, Roma, Italy*
[79b]*Dipartimento di Matematica e Fisica, Università Roma Tre, Roma, Italy*
[80a]*INFN-TIFPA, Trento, Italy*
[80b]*Università degli Studi di Trento, Trento, Italy*
[81]*Universität Innsbruck, Department of Astro and Particle Physics, Innsbruck, Austria*
[82]*University of Iowa, Iowa City, Iowa, USA*
[83]*Department of Physics and Astronomy, Iowa State University, Ames, Iowa, USA*
[84]*Istinye University, Sariyer, Istanbul, Türkiye*
[85a]*Departamento de Engenharia Elétrica, Universidade Federal de Juiz de Fora (UFJF), Juiz de Fora, Brazil*
[85b]*Universidade Federal do Rio De Janeiro COPPE/EE/IF, Rio de Janeiro, Brazil*
[85c]*Instituto de Física, Universidade de São Paulo, São Paulo, Brazil*
[85d]*Rio de Janeiro State University, Rio de Janeiro, Brazil*
[85e]*Federal University of Bahia, Bahia, Brazil*
[86]*KEK, High Energy Accelerator Research Organization, Tsukuba, Japan*
[87]*Graduate School of Science, Kobe University, Kobe, Japan*
[88a]*AGH University of Krakow, Faculty of Physics and Applied Computer Science, Krakow, Poland*
[88b]*Marian Smoluchowski Institute of Physics, Jagiellonian University, Krakow, Poland*
[89]*Institute of Nuclear Physics Polish Academy of Sciences, Krakow, Poland*
[90]*Faculty of Science, Kyoto University, Kyoto, Japan*
[91]*Research Center for Advanced Particle Physics and Department of Physics, Kyushu University, Fukuoka, Japan*
[92]*L2IT, Université de Toulouse, CNRS/IN2P3, UPS, Toulouse, France*
[93]*Instituto de Física La Plata, Universidad Nacional de La Plata and CONICET, La Plata, Argentina*
[94]*Physics Department, Lancaster University, Lancaster, United Kingdom*
[95]*Oliver Lodge Laboratory, University of Liverpool, Liverpool, United Kingdom*
[96]*Department of Experimental Particle Physics, Jožef Stefan Institute and Department of Physics, University of Ljubljana, Ljubljana, Slovenia*
[97]*Department of Physics and Astronomy, Queen Mary University of London, London, United Kingdom*
[98]*Department of Physics, Royal Holloway University of London, Egham, United Kingdom*
[99]*Department of Physics and Astronomy, University College London, London, United Kingdom*
[100]*Louisiana Tech University, Ruston, Louisiana, USA*
[101]*Fysiska institutionen, Lunds universitet, Lund, Sweden*
[102]*Departamento de Física Teorica C-15 and CIAFF, Universidad Autónoma de Madrid, Madrid, Spain*
[103]*Institut für Physik, Universität Mainz, Mainz, Germany*
[104]*School of Physics and Astronomy, University of Manchester, Manchester, United Kingdom*
[105]*CPPM, Aix-Marseille Université, CNRS/IN2P3, Marseille, France*
[106]*Department of Physics, University of Massachusetts, Amherst, Massachusetts, USA*
[107]*Department of Physics, McGill University, Montreal, Quebec, Canada*
[108]*School of Physics, University of Melbourne, Victoria, Australia*
[109]*Department of Physics, University of Michigan, Ann Arbor, Michigan, USA*
[110]*Department of Physics and Astronomy, Michigan State University, East Lansing, Michigan, USA*
[111]*Group of Particle Physics, University of Montreal, Montreal, Quebec, Canada*
[112]*Fakultät für Physik, Ludwig-Maximilians-Universität München, München, Germany*
[113]*Max-Planck-Institut für Physik (Werner-Heisenberg-Institut), München, Germany*
[114]*Graduate School of Science and Kobayashi-Maskawa Institute, Nagoya University, Nagoya, Japan*
[115a]*Department of Physics, Nanjing University, Nanjing, China*
[115b]*School of Science, Shenzhen Campus of Sun Yat-sen University, Shenzhen, China*
[115c]*University of Chinese Academy of Science (UCAS), Beijing, China*
[116]*Department of Physics and Astronomy, University of New Mexico, Albuquerque, New Mexico, USA*
[117]*Institute for Mathematics, Astrophysics and Particle Physics, Radboud University/Nikhef, Nijmegen, Netherlands*

[118]*Nikhef National Institute for Subatomic Physics and University of Amsterdam, Amsterdam, Netherlands*
[119]*Department of Physics, Northern Illinois University, DeKalb, Illinois, USA*
[120a]*New York University Abu Dhabi, Abu Dhabi, United Arab Emirates*
[120b]*United Arab Emirates University, Al Ain, United Arab Emirates*
[121]*Department of Physics, New York University, New York, New York, USA*
[122]*Ochanomizu University, Otsuka, Bunkyo-ku, Tokyo, Japan*
[123]*Ohio State University, Columbus, Ohio, USA*
[124]*Homer L. Dodge Department of Physics and Astronomy, University of Oklahoma, Norman, Oklahoma, USA*
[125]*Department of Physics, Oklahoma State University, Stillwater, Oklahoma, USA*
[126]*Palacký University, Joint Laboratory of Optics, Olomouc, Czech Republic*
[127]*Institute for Fundamental Science, University of Oregon, Eugene, Oregon, USA*
[128]*Graduate School of Science, University of Osaka, Osaka, Japan*
[129]*Department of Physics, University of Oslo, Oslo, Norway*
[130]*Department of Physics, Oxford University, Oxford, United Kingdom*
[131]*LPNHE, Sorbonne Université, Université Paris Cité, CNRS/IN2P3, Paris, France*
[132]*Department of Physics, University of Pennsylvania, Philadelphia, Pennsylvania, USA*
[133]*Department of Physics and Astronomy, University of Pittsburgh, Pittsburgh, Pennsylvania, USA*
[134a]*Laboratório de Instrumentação e Física Experimental de Partículas—LIP, Lisboa, Portugal*
[134b]*Departamento de Física, Faculdade de Ciências, Universidade de Lisboa, Lisboa, Portugal*
[134c]*Departamento de Física, Universidade de Coimbra, Coimbra, Portugal*
[134d]*Centro de Física Nuclear da Universidade de Lisboa, Lisboa, Portugal*
[134e]*Departamento de Física, Escola de Ciências, Universidade do Minho, Braga, Portugal*
[134f]*Departamento de Física Teórica y del Cosmos, Universidad de Granada, Granada (Spain), Spain*
[134g]*Departamento de Física, Instituto Superior Técnico, Universidade de Lisboa, Lisboa, Portugal*
[135]*Institute of Physics of the Czech Academy of Sciences, Prague, Czech Republic*
[136]*Czech Technical University in Prague, Prague, Czech Republic*
[137]*Charles University, Faculty of Mathematics and Physics, Prague, Czech Republic*
[138]*Particle Physics Department, Rutherford Appleton Laboratory, Didcot, United Kingdom*
[139]*IRFU, CEA, Université Paris-Saclay, Gif-sur-Yvette, France*
[140]*Santa Cruz Institute for Particle Physics, University of California Santa Cruz, Santa Cruz, California, USA*
[141a]*Departamento de Física, Pontificia Universidad Católica de Chile, Santiago, Chile*
[141b]*Millennium Institute for Subatomic physics at high energy frontier (SAPHIR), Santiago, Chile*
[141c]*Instituto de Investigación Multidisciplinario en Ciencia y Tecnología, y Departamento de Física, Universidad de La Serena, La Serena, Chile*
[141d]*Universidad Andres Bello, Department of Physics, Santiago, Chile*
[141e]*Instituto de Alta Investigación, Universidad de Tarapacá, Arica, Chile*
[141f]*Departamento de Física, Universidad Técnica Federico Santa María, Valparaíso, Chile*
[142]*Department of Physics, Institute of Science, Tokyo, Japan*
[143]*Department of Physics, University of Washington, Seattle, Washington, USA*
[144]*Department of Physics and Astronomy, University of Sheffield, Sheffield, United Kingdom*
[145]*Department of Physics, Shinshu University, Nagano, Japan*
[146]*Department Physik, Universität Siegen, Siegen, Germany*
[147]*Department of Physics, Simon Fraser University, Burnaby, British ColumbiaBC, Canada*
[148]*SLAC National Accelerator Laboratory, Stanford, California, USA*
[149]*Department of Physics, Royal Institute of Technology, Stockholm, Sweden*
[150]*Departments of Physics and Astronomy, Stony Brook University, Stony Brook, New York, USA*
[151]*Department of Physics and Astronomy, University of Sussex, Brighton, United Kingdom*
[152]*School of Physics, University of Sydney, Sydney, Australia*
[153]*Institute of Physics, Academia Sinica, Taipei, Taiwan*
[154a]*E. Andronikashvili Institute of Physics, Iv. Javakhishvili Tbilisi State University, Tbilisi, Georgia*
[154b]*High Energy Physics Institute, Tbilisi State University, Tbilisi, Georgia*
[154c]*University of Georgia, Tbilisi, Georgia*
[155]*Department of Physics, Technion, Israel Institute of Technology, Haifa, Israel*
[156]*Raymond and Beverly Sackler School of Physics and Astronomy, Tel Aviv University, Tel Aviv, Israel*
[157]*Department of Physics, Aristotle University of Thessaloniki, Thessaloniki, Greece*
[158]*International Center for Elementary Particle Physics and Department of Physics, University of Tokyo, Tokyo, Japan*
[159]*Department of Physics, University of Toronto, Toronto, Ontario, Canada*

[160a]*TRIUMF, Vancouver, British Columbia, Canada*
[160b]*Department of Physics and Astronomy, York University, Toronto, Ontario, Canada*
[161]*Division of Physics and Tomonaga Center for the History of the Universe, Faculty of Pure and Applied Sciences, University of Tsukuba, Tsukuba, Japan*
[162]*Department of Physics and Astronomy, Tufts University, Medford, Massachusetts, USA*
[163]*Department of Physics and Astronomy, University of California Irvine, Irvine, California, USA*
[164]*University of West Attica, Athens, Greece*
[165]*University of Sharjah, Sharjah, United Arab Emirates*
[166]*Department of Physics and Astronomy, University of Uppsala, Uppsala, Sweden*
[167]*Department of Physics, University of Illinois, Urbana, Illinois, USA*
[168]*Instituto de Física Corpuscular (IFIC), Centro Mixto Universidad de Valencia—CSIC, Valencia, Spain*
[169]*Department of Physics, University of British Columbia, Vancouver, British Columbia, Canada*
[170]*Department of Physics and Astronomy, University of Victoria, Victoria, British Columbia, Canada*
[171]*Fakultät für Physik und Astronomie, Julius-Maximilians-Universität Würzburg, Würzburg, Germany*
[172]*Department of Physics, University of Warwick, Coventry, United Kingdom*
[173]*Waseda University, Tokyo, Japan*
[174]*Department of Particle Physics and Astrophysics, Weizmann Institute of Science, Rehovot, Israel*
[175]*Department of Physics, University of Wisconsin, Madison, Wisconsin, USA*
[176]*Fakultät für Mathematik und Naturwissenschaften, Fachgruppe Physik, Bergische Universität Wuppertal, Wuppertal, Germany*
[177]*Department of Physics, Yale University, New Haven, Connecticut, USA*
[178]*Yerevan Physics Institute, Yerevan, Armenia*

[a]Deceased.
[b]Also at Department of Physics, King's College London, London, United Kingdom.
[c]Also at Institute of Physics, Azerbaijan Academy of Sciences, Baku, Azerbaijan.
[d]Also at Imam Mohammad Ibn Saud Islamic University, Riyadh, Saudi Arabia.
[e]Also at TRIUMF, Vancouver, British Columbia, Canada.
[f]Also at Department of Physics, University of Thessaly, Lamia, Greece.
[g]Also at An-Najah National University, Nablus, Palestine.
[h]Also at Department of Physics, University of Fribourg, Fribourg, Switzerland.
[i]Also at Department of Physics, Westmont College, Santa Barbara, USA.
[j]Also at Departament de Fisica de la Universitat Autonoma de Barcelona, Barcelona, Spain.
[k]Also at Affiliated with an institute covered by a cooperation agreement with CERN.
[l]Also at The Collaborative Innovation Center of Quantum Matter (CICQM), Beijing, China.
[m]Also at Faculty of Physics, Sofia University, 'St. Kliment Ohridski', Sofia, Bulgaria.
[n]Also at Università di Napoli Parthenope, Napoli, Italy.
[o]Also at Institute of Particle Physics (IPP), Victoria, British Columbia, Canada.
[p]Also at Borough of Manhattan Community College, City University of New York, New York, New York, USA.
[q]Also at National Institute of Physics, University of the Philippines Diliman (Philippines), Quezon City, Philippines.
[r]Also at Department of Financial and Management Engineering, University of the Aegean, Chios, Greece.
[s]Also at Institucio Catalana de Recerca i Estudis Avancats, ICREA, Barcelona, Spain.
[t]Also at Technical University of Munich, Munich, Germany.
[u]Also at CMD-AC UNEC Research Center, Azerbaijan State University of Economics (UNEC), Baku, Azerbaijan.
[v]Also at Yeditepe University, Physics Department, Istanbul, Türkiye.
[w]Also at Institute of Theoretical Physics, Ilia State University, Tbilisi, Georgia.
[x]Also at CERN, Geneva, Switzerland.
[y]Also at Center for Interdisciplinary Research and Innovation (CIRI-AUTH), Thessaloniki, Greece.
[z]Also at Hellenic Open University, Patras, Greece.
[aa]Also at Center for High Energy Physics, Peking University, Peking, China.
[bb]Also at Department of Physics, Stellenbosch University, Stellenbosch, South Africa.
[cc]Also at Department of Physics, California State University, Sacramento, California, USA.
[dd]Also at University of Colorado Boulder, Department of Physics, Boulder, Colorado, USA.
[ee]Also at Département de Physique Nucléaire et Corpusculaire, Université de Genève, Genève, Switzerland.
[ff]Also at Institut für Experimentalphysik, Universität Hamburg, Hamburg, Germany.
[gg]Also at Institute for Nuclear Research and Nuclear Energy (INRNE) of the Bulgarian Academy of Sciences, Sofia, Bulgaria.
[hh]Also at Washington College, Chestertown, Maryland, USA.
[ii]Also at Institute of Applied Physics, Mohammed VI Polytechnic University, Ben Guerir, Morocco.
[jj]Also at Department of Physics, Stanford University, Stanford, California, USA.
[kk]Also at Institute of Physics and Technology, Mongolian Academy of Sciences, Ulaanbaatar, Mongolia.